Dynamic response of the southwestern Laurentide Ice Sheet during the last deglaciation

by

Sophie L. Norris

A thesis submitted in partial fulfillment of the requirements for the degree of

Doctor of Philosophy

Department of Earth and Atmospheric Sciences
University of Alberta

Abstract

This thesis utilises geomorphic mapping, cosmogenic nuclide dating, and numerical modelling, to reconstruct the timing and deglacial dynamics of the southwestern Laurentide Ice Sheet (SWLIS). A paucity of geomorphic data within the interior portions of the SWLIS is addressed through the mapping of a 150,000 km^2 region of northern Alberta and Saskatchewan. Multi-generation glacial landforms present a complex glacial geomorphic signal within the region, suggesting the SWLIS underwent several glaciodynamic shifts during the last deglaciation.

A new database of 26 ^{10}Be surface exposure ages from glacial erratics spanning a 1200 km transect across the SWLIS is then presented. This chronology is combined with pre-existing luminescence, ^{10}Be surface exposure ages, and 'high quality' minimum radiocarbon chronologies, exclusive of dates on bulk sediments, terrestrial shells, or mixed assemblages, to provide an updated chronology for the retreat of the SWLIS. These data indicate that initial detachment of the SWLIS from its convergence with the Cordilleran Ice Sheet occurred at ~15.0 ka BP, concurrent with, or possibly somewhat before the abrupt warming at the onset of the Bølling-Allerød, and retreated >1200 km to its Younger Dryas position in ≤ 2500 yrs.

Synthesis of pre-existing ice flow mapping and new surficial geomorphology, allows the identification of discrete ice flowsets, including those potentially formed by palaeo-ice streams. Reconciling these ice flow dynamics with the new chronology reveals a complex pattern of ice stream behaviour characterised by substantial flow switches and

reconfigurations. This reconstruction suggests the SWLIS underwent ice sheet scale reorganisation at least three times in ~2500 yrs. These rapid, decadal to centennial, changes in ice stream orientations demonstrate both, how ice streams can influence an ice sheet's broader response to external climate forcing, and how ice sheets, through changes to ice flow regime, are highly sensitive to rapid climate change.

The role of meltwater discharge from large proglacial lakes associated with rapid deglaciation is then examined. Geomorphic and sedimentological evidence from the Beaver River Spillway, eastern Alberta, provides a rarely preserved example of catastrophic meltwater drainage associated with deglaciation. Modelling results indicate peak discharge within Beaver River Spillway was approximately $14\,000$–$26\,000$ m³ s^{-1} and maintained a minimum flow duration of 3-5 days. This case study not only demonstrates the catastrophic nature of meltwater drainage from the SWLIS but also demonstrates the role of easily erodible glacial sediment as a control on meltwater channel evolution and morphology within the Canadian Prairies.

Preface

Chapter 2 of this thesis has been published as "Norris, Sophie L., Martin Margold, and Duane G. Froese. 2016. Glacial landforms of northwest Saskatchewan. *Journal of Maps,* 13 (2): 600-607." I was responsible for the geomorphic mapping and lead authorship of the manuscript. M Margold and D.G. Froese read and provided comments on the manuscript.

Chapter 3 of this thesis is in preparation for publication in Geology. I was responsible for sample collection, data analysis, and lead authorship of the manuscript. D.G. Froese and M. Margold were involved with concept development and manuscript composition. J.C. Gosse and A.J. Hidy were responsible for cosmogenic nuclide dating. Additional cosmogenic nuclide ages were provided by M. Margold. All co-authors read and provided comments on the manuscript.

Chapter 4: of this thesis is in preparation for publication in Quaternary Science Reviews. I was responsible for data compilation, interpretation, and lead authorship of the manuscript. D.G. Froese and M. Margold were involved with concept development and manuscript composition. All co-authors read and provided comments on the manuscript.

Chapter 5 of this thesis has been published as "Norris, S.L., Margold, M., Utting, D.J., & Froese, D.G. 2019. Geomorphic, sedimentary and hydraulic reconstruction of a glacial lake outburst flood in northern Alberta, Canada. *Boreas*, 48 (4): 1006-1018." I was responsible for modelling, data analysis, and lead authorship of the manuscript. Borehole data and imagery were provided by D.J. Utting. M. Margold and D.G. Froese were involved in concept formation and modelling interpretation. All co-authors read and provided comments on the manuscript.

The introductory statements in Chapter 1 and concluding analysis in Chapter 6 are my own original work.

Acknowledgements

Table of Contents

LIST OF TABLES

LIST OF FIGURES

CHAPTER 1: INTRODUCTION

The contribution of modern ice sheet mass loss to global sea-level rise has accelerated over recent decades, largely resulting from increased ice sheet thinning and enhanced ice-flow rates (Alley et al., 2005; Rignot et al., 2008, 2011). Ice sheet instability is of concern given the potential meltwater equivalent contribution of ice sheets in Greenland and Antarctica (Golledge et al., 2015; Ritz et al., 2015). However, limited observations spanning more than a few decades, mean the response of modern ice sheets to future climatic change over longer timescales remains uncertain. Reconstructing palaeo-ice sheet behaviour in response to past climatic fluctuations is therefore critical to assessing future changes to contemporary ice sheets (Alley and Bindschadler, 2001; Rignot and Thomas, 2002; Clark et al., 2009; Carlson and Clark, 2012).

Due to its complex and often well-preserved imprint, the Late Wisconsinan Laurentide Ice Sheet (LIS) has been recognised as valuable in accessing continental-scale ice sheet dynamics (Stokes et al., 2015; Margold et al., 2015, 2018). The stability of the LIS had a major impact on global sea level and climate, responding to and triggering abrupt, decadal to millennial changes to the ocean-atmospheric system (Tarasov and Peltier, 2005, Clark et al., 2001). A comprehensive reconstruction of the ice sheet's extent, dynamics and evolution are, therefore, critical to our understanding of its response to climate fluctuations (Clark et al., 2009; Carlson and Winsor, 2012; Carlson and Clark, 2012). Until recently, the majority of studies have focused on the highly dynamic marine terminating portion of the LIS where ice shelf break up, major meltwater routing and rapid deglaciation have been identified (e.g. Barber et al., 1999; Clark et al., 2001; Tarasov et al., 2012). In contrast, the response of the terrestrial terminating southwestern LIS (SWLIS) to past climate fluctuations, particularly during deglaciation remains understudied. The SWLIS encompassed ice flowing south from the Keewatin sector (Fig 1.1) and converged with the Cordilleran Ice Sheet to the west, extending into the northwestern United States (Dyke et al., 2003). New numerical modelling (Gregoire et al., 2012; Gregoire et al., 2016) and recent field evidence (Margold et al., 2019) have indicated down wasting of the convergence zone (recently termed a "saddle" see Gregoire et al . (2012)) that connected the SWLIS and Cordilleran Ice Sheet (CIS) was driven by rapid deglacial warming.
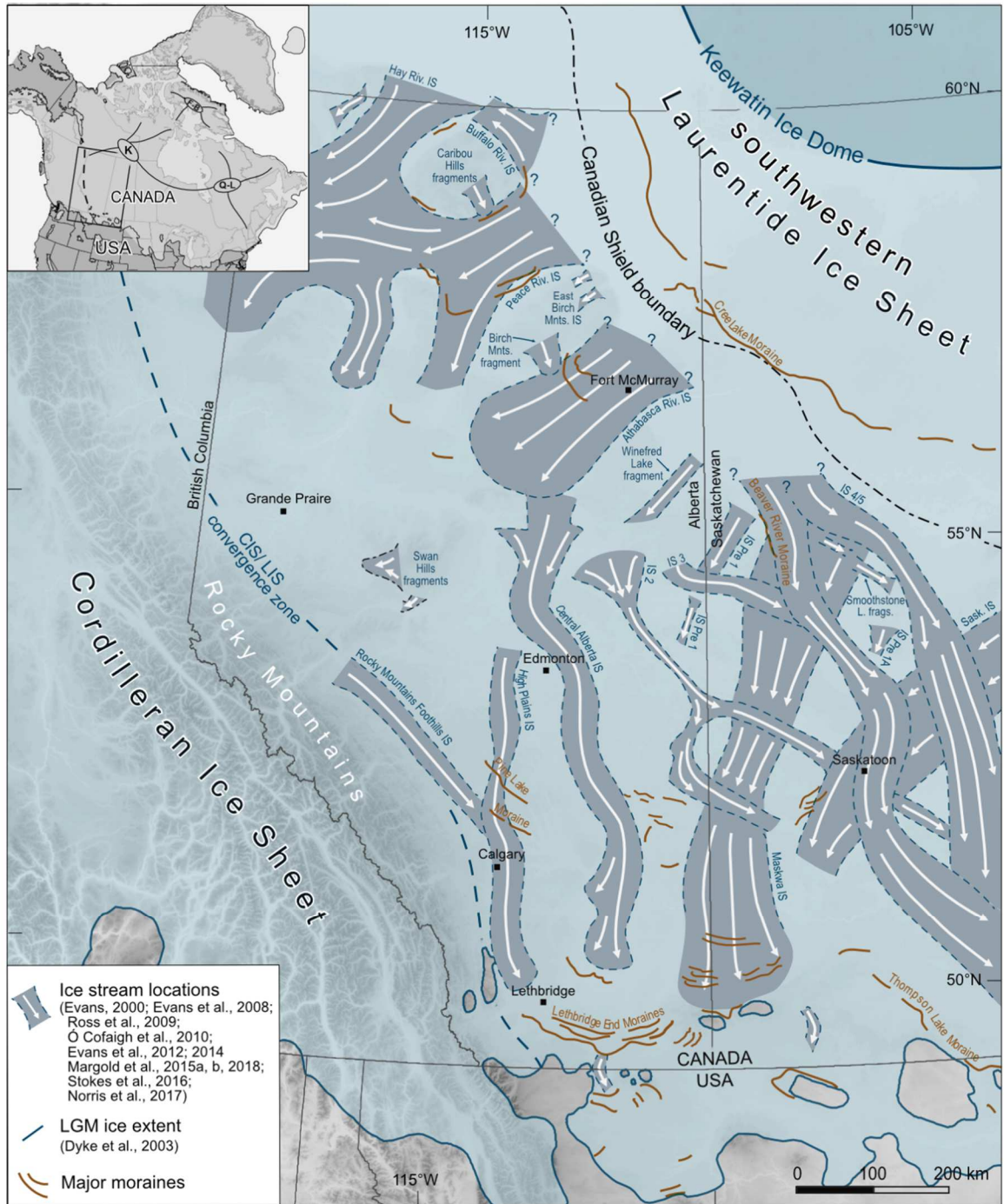
Figure 1.1: Regional ice flow configuration and extent of the southwestern sector of the Laurentide Ice Sheet. Previously identified ice stream locations and moraines summarised from; Evans, 2000; Evans et al., 2008; Ross et al., 2009; Ó Cofaigh et al., 2010; Evans et al., 2012, 2014; Atkinson et al., 2014; Margold et al., 2015a, b, 2018; Stokes et al., 2016.

Independently, multiple local and regional geomorphic and sedimentary investigations of portions of the SWLIS, have also highlighted the potential for major, potentially rapid, flow reorganisations during deglaciation (Ross et al., 2009; Ó Cofaigh et al., 2010; Atkinson et al., 2016). However, the connection between rapid down wasting of the CIS/LIS convergence zone and changing ice dynamics remains unexplored. Furthermore, an absence of chronological control in many regions and, large discrepancies between dating methods where they do exist, mean the ice sheet response following initial deglaciation is not well constrained.

To improve understanding of the behavior of the SWLIS the overarching objective of this thesis is to investigate its timing, dynamics and meltwater discharge during the last deglaciation.

In order to fulfill this aim, the following objectives will be to:
1) Map the glacial geomorphology of the interior SWLIS using a range of remote sensing products;
2) Constrain the timing and rate of deglaciation of the SWLIS by directly dating former ice margin positions using cosmogenic nuclide dating methods;
3) Use the geomorphic map produced in objective 1 in combination with pre-existing mapping within the peripherical regions of the SWLIS to identify the ice dynamics as discrete ice flowsets, including those potentially formed by palaeo-ice streams;
4) Embed identified ice flow dynamics into the deglaciation of the SWLIS using the ice margin chronology identified in objective 2 to provide a comprehensive reconstruction of the SWLIS; and
5) Establish the significance of deglacial meltwater drainage of the SWLIS through a case study of a large glacial lake outburst in northern Alberta.

These aims and objectives are addressed through four chapters: Chapter 2 is a detailed geomorphic review and mapping project for the interior portions of the SWLIS. This chapter provides the foundation to assess the timing and dynamics of deglaciation in the region. Chapter 3 presents a comprehensive chronological database encompassing 26 new

[10]Be surface exposure ages and integration with existing chronometers. Chapter 4 combines these data with regional geomorphic mapping to assess the deglacial behaviour of the SWLIS. Chapter 5 is a palaeohydrological reconstruction of the drainage of a large glacial lake outburst flood from the margin of the SWLIS. Collectively these papers lay out a new reconstruction of the deglaciation of the SWLIS, from initial deglaciation (~15ka) to Younger Dryas cooling (12.9 ka), summarized in Chapter 6 together with suggestions for future research directions.

1.1 Detailed chapter summaries

Chapter 2

A version of this chapter has been published as:

Norris, S. L., Margold, M., and Froese, D. G. (2017). Glacial landforms of northwest Saskatchewan. *Journal of Maps*, *13*(2), 600-607.

> *A comprehensive map of glacial landforms is presented for the area of northwest Saskatchewan, Canada. Remote sensing of 1-arc second (~30 m resolution) Shuttle Radar Topography Mission digital elevation models over an area of approximately 150,000 km² were used as the primary data source for landform identification. A total of 16,856 landforms were identified pertaining to Quaternary glacial and postglacial activity. Ten landform types were mapped: ice flow parallel lineations (flutings, drumlins, mega-scale glacial lineations, and crag-and-tail ridges), moraines (major and minor), ice-thrust ridges, crevasse-fill ridges, meltwater landforms (major and minor meltwater channels and eskers), palaeo-shorelines and dunes. Collectively, these landforms constitute a glacial and postglacial landform record, which exhibits a more complex pattern than previously recognised, with evidence of multiple cross-cutting ice flow directions. This geomorphological mapping of the regional landform record provides the prerequisite for future reconstructions of the glacial dynamics and chronology of northwest Saskatchewan.*

Chapter 3

A version of this chapter is in preparation for submission to Geology

The timing of Laurentide Ice Sheet deglaciation, along its southwestern margin, controls the evolution and drainage of large glacial lakes and has implications for the migration of early humans into the Americas. Accurate reconstruction of the ice sheet's retreat also constrains glacial isostatic adjustment models and is imperative for our understanding of ice sheet sensitivity to climate forcings. Despite its importance, much of the retreat history of the southwestern Laurentide Ice Sheet is poorly constrained by minimum limiting ^{14}C data. Here, we present a database of 24 ^{10}Be surface exposure ages from glacial erratics spanning southwestern Alberta to northwestern Saskatchewan, Canada. We combine these data with regional geomorphic mapping and pre-existing luminescence, ^{10}Be surface exposure ages, and 'high quality' minimum radiocarbon chronologies, exclusive of dates on bulk sediments, terrestrial shells or mixed assemblages, to provide an updated chronology for the retreat of the southwestern Laurentide Ice Sheet. Our compiled dataset of cosmogenic, luminescence, and minimum radiocarbon dates present a consistent retreat record. These data suggest that initial detachment of the southwestern Laurentide Ice Sheet from its convergence with the Cordilleran Ice Sheet occurred at ~15.0 ka BP, concurrent with, or possibly somewhat before the abrupt warming at the onset of the Bølling-Allerød, and retreated >1200 km to its Younger Dryas position in ≤ 2500 yrs.

Chapter 4

A version of this chapter is in preparation for submission to Quaternary Science Reviews

Recent ice margin chronology indicates the southwestern sector of the Laurentide Ice Sheet collapsed due to abrupt Bølling-Allerød warming. Here, we reconstruct the ice flow dynamics associated with this period of rapid climate change. Our reconstruction reveals rapid ice geometry changes including reorganisation of the ice drainage network. Initial westward flow, signifies maximum stage ice flow, unconstrained by topography. Following this, our reconstruction shows a major glaciodynamic shift characterised by topographically controlled south-eastward flow constrained by palaeo-valley systems. This is subsequently replaced by a second switch in flow orientation to the southwest corresponding with an increase in the influence of topography on streaming flow during ice retreat. We suggest the region underwent ice sheet scale reorganisation upwards of three times in ≤ 2500 yrs. These extremely rapid, decadal to centennial, changes in ice flow geometry demonstrate not only how ice streams can influence an ice sheets broader response to external climate forcing, but also how ice sheets, through changes to ice flow regime, are highly sensitive to rapid climate change.

Chapter 5

A version of this chapter has been published as:

Norris, S. L., Margold, M., Utting, D. J., & Froese, D. G. (2019). Geomorphic, sedimentary and hydraulic reconstruction of a glacial lake outburst flood in northern Alberta, Canada. *Boreas*, *48*(4), 1006-1018.

Glacial lake outburst floods occurred frequently during the last deglaciation of the Laurentide Ice Sheet. Within the Interior Plains, these floods carved large spillway systems; however, due to a lack of abundant sediment, deposits within prairie spillways are rarely preserved. Here, we present geomorphic and sedimentary evidence and hydraulic modelling of the eastern Beaver River Spillway, formed by the catastrophic drainage of the ice-dammed glacial Lake Algar, in north central Alberta. During this flood, coarse-grained sediment eroded from local till formed large pendant bars. Within the first ~50 km of the spillway (Reach 1), pendant bars contain downstream orientated foresets overlain by horizontally bedded coarser gravels. The remaining pendant bars (Reach 2), present downflow of a moraine barrier, differ, comprising massive, matrix-supported, inversely graded gravels capped by a boulder layer. We use a HEC-GeoRAS/HEC-RAS system in conjunction with palaeostage indicators to estimate the steady-state water surface elevation. Modelling results show that peak discharge within Reach 1 of the eastern Beaver River Spillway was approximately 14 000–21 000 $m^3 s^{-1}$. For Reach 2, 30 km downstream, the peak discharge was estimated at 23 000–40 000 $m^3 s^{-1}$ (nbulked 18 000–26 000 $m^3 s^{-1}$). The downstream discharge increase, consistent with the sedimentary change in pendant bar deposits, is attributed to sediment bulking of the flood flow. This provides the opportunity to observe a range of flow conditions, and associated sedimentology, from a single flood event. The reconstructed flow conditions, coupled with lake volume estimates from the ponding above the moraine barrier suggest a minimum flow duration of 3–5 days.

1.2 References

Alley, R. B., and Bindschadler, R. A. 2001: The West Antarctic ice sheet: behavior and environment. *American Geophysical Union.* Antarctic Research Series, v. 77.

Alley, R.B., Clark, P.U., Huybrechts, P. and Joughin, I. 2005: Ice-sheet and sea-level changes. *Science 310*, 456-460.

Atkinson, N., Utting, D. J and Pawley, S. P. 2014: *Glacial Landforms of Alberta. Alberta Geological Survey,* AER/AGS, Map 604.

Atkinson, N., Pawley, S., and Utting, D. J. 2016: Flow-pattern evolution of the Laurentide and Cordilleran ice sheets across west-central Alberta, Canada: implications for ice sheet growth, retreat and dynamics during the last glacial cycle. *Journal of Quaternary Science 31*(7), 753-768.

Barber, D.C., Dyke, A., Hillaire-Marcel, C., Jennings, A.E., Andrews, J.T., Kerwin, M.W., Bilodeau, G., McNeely, R., Southon, J., Morehead, M.D., Gagnon, J.-M. 1999: Forcing of the cold event of 8,200 years ago by catastrophic drainage of Laurentide lakes. *Nature 400*, 344-348.

Carlson, A. E., and Clark, P. U. 2012: Ice sheet sources of sea level rise and freshwater discharge during the last deglaciation. *Reviews of Geophysics*, *50*(4). RG4007

Carlson, A. E., and Winsor, K. 2012: Northern Hemisphere ice-sheet responses to past climate warming. *Nature Geoscience* 5(9), 607-613.

Clark, P.U., Marshall, S.J., Clarke, G.K.C., Hostetler, S.W., Licciardi, J.M. and Teller, J.T. 2001: Freshwater forcing of abrupt climate change during the last glaciation. *Science 293*, 283-287.

Clark, P.U., Dyke, A.S., Shakun, J.D., Carlson, A.E., Clark, J., Wohlfarth, B., Mitrovica, J.X., Hostetler, S.W. and McCabe, A. 2009: The Last Glacial Maximum. *Science* 325, 710-714.

Dyke, A. S., Moore, A, and Robertson, L. 2003: Deglaciation of North America. *Geological Survey of Canada, Open File 1574*.

Golledge, N. R., Kowalewski, D. E., Naish, T. R., Levy, R. H., Fogwill, C. J., and Gasson, E. G. 2015: The multi-millennial Antarctic commitment to future sea-level rise. *Nature*, *526*(7573), 421-425.

Gregoire, L. J., Payne, A. J., and Valdes, P. J. 2012: Deglacial rapid sea level rises caused by ice-sheet saddle collapses. *Nature*, *487*(7406), 219-222.

Gregoire, L. J., Otto-Bliesner, B., Valdes, P. J., and Ivanovic, R. 2016: Abrupt Bølling warming and ice saddle collapse contributions to the Meltwater Pulse 1a rapid sea level rise. *Geophysical Research Letters*, *43*(17), 9130-9137.

Margold, M., Stokes, C.R. and Clark, C.D. 2015: Ice streams in the Laurentide Ice Sheet: identification, characteristics and comparison to modern ice sheets. *Earth Science Reviews 143*, 117-146.

Margold, M., Stokes, C. R., and Clark, C. D. 2018: Reconciling records of ice streaming and ice margin retreat to produce a palaeogeographic reconstruction of the deglaciation of the Laurentide Ice Sheet. *Quaternary Science Reviews 189*, 1-30.

Margold, M., Gosse, J. C., Hidy, A. J., Woywitka, R. J., Young, J. M., and Froese, D. 2019: Beryllium-10 dating of the Foothills Erratics Train in Alberta, Canada, indicates detachment of the Laurentide Ice Sheet from the Rocky Mountains at ~15 ka. *Quaternary Research 92*(2), 469-482.

Ó Cofaigh, C., Evans, D. J. A. and Smith, R. 2010: Large-scale reorganization and sedimentation of terrestrial ice streams during late Wisconsinan Laurentide Ice Sheet deglaciation. *Geological Society of America Bulletin 122*, 743-756.

Rignot, E., and Thomas, R. H. 2002: Mass balance of polar ice sheets. *Science 297*(5586), 1502-1506.

Rignot, E., Bamber, J. L., Van Den Broeke, M. R., Davis, C., Li, Y., Van De Berg, W. J., and Van Meijgaard, E. 2008: Recent Antarctic ice mass loss from radar interferometry and regional climate modelling. *Nature Geoscience 1*(2), 106-110.

Rignot, E., Velicogna, I., van den Broeke, M.R., Monaghan, A. and Lenaerts, J.T.M. 2011: Acceleration of the contribution of the Greenland and Antarctic ice sheets to sea level rise. *Geophysical Research Letters 38*, L05503.

Ritz, C., Edwards, T. L., Durand, G., Payne, A. J., Peyaud, V., and Hindmarsh, R. C. 2015: Potential sea-level rise from Antarctic ice-sheet instability constrained by observations. *Nature 528*(7580), 115-118.

Ross, M., Campbell, J. E., Parent, M. and Adams, R. S. 2009: Palaeo-ice streams and the subglacial landscape mosaic of the North American mid-continental prairies. *Boreas 38*, 421-439.

Stokes, C.R., Tarasov, L., Blomdin, R., Cronin, T., Fisher, T.G., Gyllencreutz, R., Hättestrand, C., Heyman, J., Hindmarsh, R.C.A., Hughes, A.L.C., Jakobsson, M., Kirchner, N., Livingstone, J.J., Margold, M., Murton, J.B., Noormets, R., Peltier, W.R., Peteet, D.M., Piper, D.J.W., Preusser, F., Renssen, H., Roberts, D.H., Roche, D.M., Saint-Ange, F., Stroeven, A.P. and Teller, J.T. 2015: On the reconstruction of palaeo-ice sheets: recent advances and future challenges. *Quaternary Science Reviews 125*, 15-49.

Tarasov, L. and Peltier, W.R. 2005: Arctic freshwater forcing of the Younger Dryas cold reversal. *Nature 435*, 662-665.

Tarasov, L., Dyke, A.S., Neal, R.M. and Peltier, W.R. 2012: A data-calibrated distribution of deglacial chronologies for the North American ice complex from glaciological modelling. *Earth and Planetary Science Letters 315*, 30-40.

CHAPTER 2: GLACIAL LANDFORMS OF NORTHWEST SASKATCHEWAN

2.1 Introduction

The Canadian Prairies contain glacial landform and sediments that document the dynamic behavior of the Laurentide Ice Sheet (LIS) during the last glacial cycle. Of particular interest are the northern parts of Alberta and Saskatchewan, where the spatial and temporal patterns of deglaciation are linked to the timing of meltwater fluxes from glacial Lake Agassiz (Fig. 2.1; Dyke et al., 2003; Fisher et al., 2009). The location of glacial Lake Agassiz in this central region of North America gives it the potential to deliver large amounts of freshwater; north to the Arctic ocean, east to Hudson Bay, east to the North Atlantic via the St. Lawrence, and south to the Gulf of Mexico. Therefore, switching of glacial Lake Agassiz outlets has been suggested to have triggered climate change during the last deglaciation (Broecker et al., 1989; Clark et al., 2001), and a number of studies have attempted to reconstruct the evolution of its drainage (e.g. Christiansen, 1979; Teller and Clayton, 1983; Fisher and Smith, 1994; Teller and Leverington, 2004; Breckenridge, 2015). However, the palaeoglaciological dynamics, on which these studies base their inferences, are still poorly understood and the chronological controls on the position of the ice sheet margin remain sparse.

Previous geomorphological investigations (first summarised in Prest et al., 1968) within the Canadian Prairies have demonstrated the rich nature of the landform-sediment record in this region. Glacially streamlined landforms have been used to identify ice-flow patterns and ice stream corridors (Moran et al., 1980; Evans et al., 2008; Ross et al., 2009; Ó Cofaigh et al., 2010; Evans et al., 2014; Margold et al., 2015a,b; Stokes et al., 2016). Equally, collections of terminal and recessional moraines have been used to reconstruct the stabilisation or slow retreat of the ice sheet margin (Christiansen, 1979; Kleman et al., 2010; Evans et al., 2014). In order to aid in further studies, the landform record for the entirety of Alberta has recently been synthesized into a province-wide glacial geomorphological map (Atkinson et al., 2014a,b). In contrast, there is an absence of comprehensive mapping to underpin Late Wisconsinan glacial and deglacial dynamics for

northwest Saskatchewan. Glacial geomorphological maps of a single landform type, such as glacial lineations, have been presented at a provincial or continental-scale only (Shaw et al., 2010; Slimmon, 2011). At a local scale, parts of and single National Topographic System (NTS) tiles have also been mapped and their Quaternary geology recorded (Campbell, 1988, 2006, 2007; Campbell et al., 2006; Hanson 2014, 2015a,b,c; Schreiner, 1984a-j; Scott, 1965; Shaw, 2010; Simpson, 1988, 1997; Slimmon, 2011).
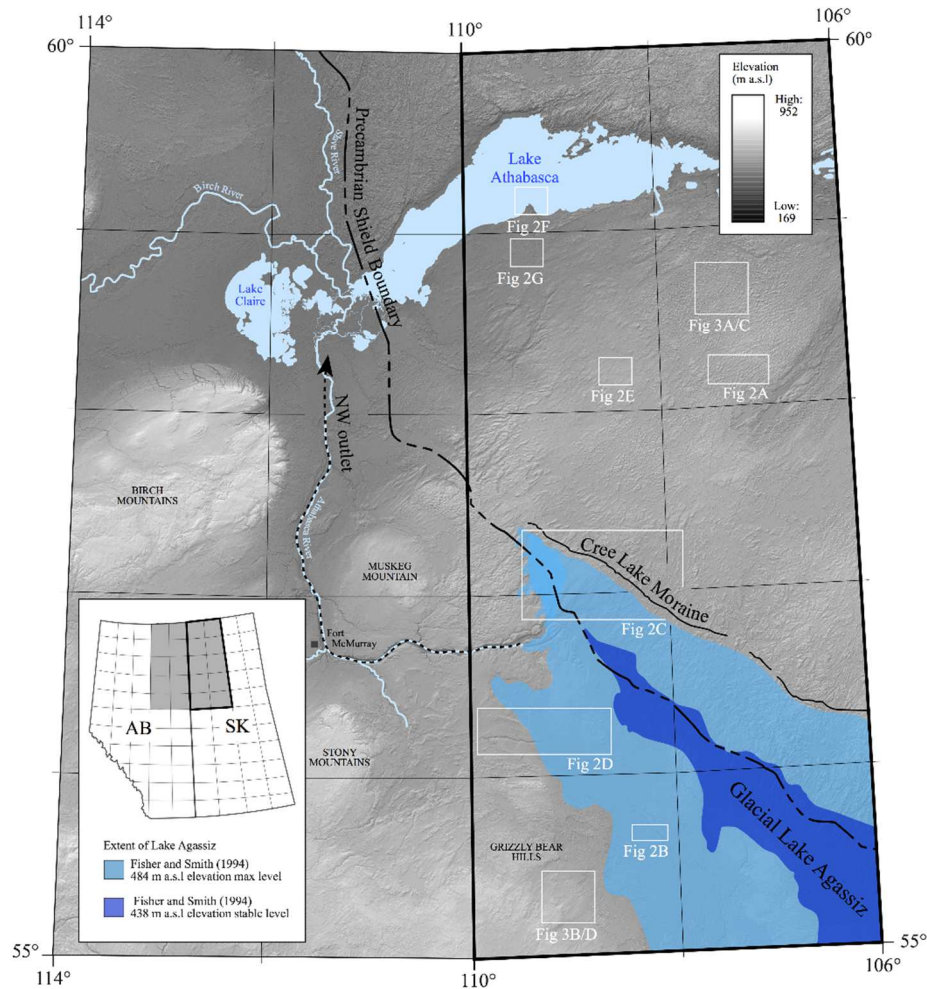
Figure 2.1: Location map showing northeast Alberta and northwest Saskatchewan. Major locations of physiographic features, including the northwest outlet of Lake Agassiz, the Precambrian Shield boundary, the Cree Lake Moraine and the extent of glacial Lake Agassiz are labelled. The bordering area within Alberta has been previously mapped by Atkinson et al. (2014). Area of mapping corresponding to this study is outlined in bold (inset). The locations of figures 2A-G and 3A-D are marked by white rectangles.

However, detailed glacial geomorphological mapping similar to that available for Alberta is absent. In an effort to aid understanding of the palaeoglaciology of northwest Saskatchewan, this study presents a detailed 150,000 km^2 glacial landform map covering the entirety of northwest Saskatchewan. The study area within this map encompasses ten 1:250,000 NTS tiles (73M-O, 74B-G, J-O; Fig. 1).

2. 2 Methods

2.2.1 Primary data

The glacial geomorphology of northwest Saskatchewan was primarily mapped from hillshade imagery derived from 1-arc second Shuttle Radar Topography Mission (SRTM) Digital Elevation Models (DEMs). These data were selected as they provide the best to-date available spatial coverage and resolution (~30m pixel size) for the study area. Data was downloaded in GeoTIFF format from GeoGratis (http://geogratis.cgdi.gc.ca) and then projected in Universal Transverse Mercator (UTM) zone 12N referenced to the North American Datum 1983.

As proposed by Smith and Clark (2005), to minimise azimuth bias, multiple illumination angles were used to aid mapping. Illumination angles orthogonal to each other were used to account for the varying orientation and scale of landforms occurring in the study area (Smith and Clark, 2005).

2.2.2 Secondary data

Additional data sources assisted the identification of landforms in the study area; surficial geology maps and structural geology data (Slimmon, 2011) helped to ensure glacial landforms were not interpreted where there was an alternative origin, either geological structure or due to anthropogenic landscape alteration. Published literature was also used to support landform identification and provide a useful component of mapping (Campbell, 1988, 2006, 2007; Campbell et al., 2006; Hanson 2014, 2015a-c; Schreiner, 1984a-j; Scott, 1965; Shaw, 2010; Simpson, 1988, 1997; Slimmon, 2011). However, as previously published maps portray varying landform types and occur at varying map scales depending on the region and purpose of the mapping, all previously mapped areas were remapped.

11

2.2.3 Landform mapping

A repeat-pass method (i.e. landform by landform and area by area type) was employed to ensure consistency in the final map. Each landform type was mapped for the entire study area ensuring multiple passes of all areas, thus allowing for details to be added or refinements made to the initial mapping with each pass. Mapping was conducted at 1:30,000 to 1:70,000. A variable scale was used depending on the landform type under investigation. Individual landforms were identified on the imagery based on their morphology, spatial arrangement and association with other features (see Table 2.1 for diagnostic characteristics). To enable detailed inspection of landforms and their associated patterns and systems, this map is designed to be printed and viewed at AO size (841 x 1189 mm). Each landform was identified and digitised as a single line or a closed polygon depending on its shape and size in relation to SRTM data resolution. Ten landform types were mapped: ice flow parallel lineations (flutings, drumlins, mega-scale glacial lineations, and crag-and-tail ridges), moraines (major and minor), ice-thrust ridges, crevasse-fill ridges, meltwater landforms (major and minor meltwater channels and eskers), palaeo-shorelines and dunes (Fig. 2.2). These landform types are now discussed below.

Table 2.1: Diagnostic criteria that underpin the identification of geomorphological features from SRTM imagery.

Landform group	Diagnostics used for landform identification	Mapping symbol
Ice flow parallel lineations	Elongate landforms which typically occur in groups with contrasting tone on either side of a linear crestline. Regular morphology, spacing and orientation often found between neighbouring landforms.	Landform crest drawn as single line
Moraines	Broadly linear ridges which exhibit variation in tone across their crestline. Ridges may be dissected by meltwater channels.	Landform outline drawn as polygon (major moraine ridge) or crestline (minor moraine ridge)
Ice-thrust ridges	Arcuate ridges with strong variation in tone along their crestline. They are often associated with a depression/basin where sediment rafts were dislocated.	Landform crest drawn as single line
Crevasse-fill ridges	Linear, curvilinear, or v-shaped ridges. They may intersect forming cross cutting patterns.	Landform crest drawn as single line
Meltwater channels	Branching networks of incised topography. The edges of these channels are defined by changes to a contrasting dark tone on either side.	Centre of incised topography drawn as single line
Eskers	Sinuous ridges. Often form complex networks with tributary eskers.	Landform crest drawn as single line
Palaeo-shorelines	Sinuous, often arcuate steps or ridges in the landscape, which mark the shorelines of former lakes. They are often found to have contrasting terrain on either side.	Landform crest drawn as single line
Dunes	Parabolic or longitudinal in shape, ridges typically occur in groups. Sharply crested and commonly asymmetric in cross profile.	Landform crest drawn as single line
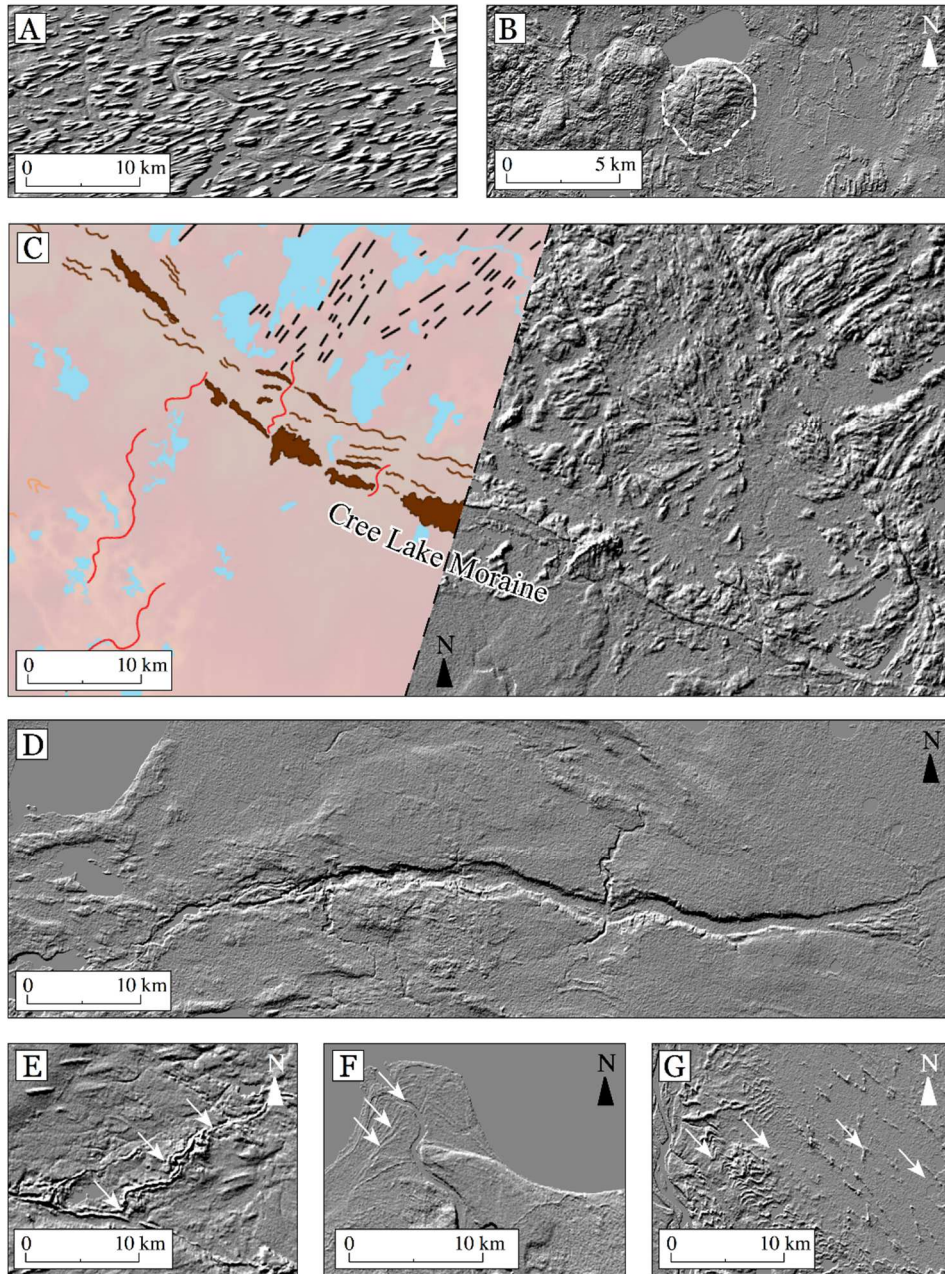
Figure 2.2: SRTM-derived hillshade imagery and geomorphological mapping of landforms. (A) SRTM imagery of drumlins north of the Cree Lake Moraine. (B) SRTM imagery of a collection of ice-thrust ridges associated with a small water filled depression (ice-thrust ridges outlined with dashed white line). (C) SRTM imagery and geomorphological mapping of the Cree Lake Moraine (major moraine ridges outlined as brown polygons, eskers indicated with red lines and lineations with black lines). (D) SRTM imagery of a major meltwater channel flowing east-west into Alberta. (E) SRTM imagery of an esker ridge and network (ridge crest indicated by white arrows). (F) SRTM imagery of palaeo-shorelines surrounding Lake Athabasca (most prominent palaeo-shorelines indicated by white arrows). (G) SRTM imagery of parabolic dunes (dune crest indicated by white arrows).

14

2.3 Results: descriptions of glacial geomorphology

2.3.1 Ice flow parallel lineations

Ice flow parallel lineations include flutings, drumlins, mega-scale glacial lineations, and crag-and-tail ridges (Fig. 2.2a). Lineations mapped here confirm and extend the previously mapped inventory; this is especially evident north of the Cree Lake Moraine where the number of lineations is considerably denser than portrayed by previous mapping. Lineations show a complex pattern across the study area and occur extensively except in areas where bedrock is exposed (e.g. in NTS 74O and 74N, north of Lake Athabasca). A clear division in the morphology of lineations is recorded within the mapped area (Fig. 2.3). In the northern part of the study area, which occupied by the Canadian Shield, lineations are of high density and comprise varied northeast-southwest orientations. These lineations are typically 100-250 m wide and 800-1500 m long, with elongation ratios between 5:1 and 8:1 (Fig. 2.3a,c). In contrast, south of the Canadian Shield boundary, glacial lineations display higher attenuation, with elongation ratios ranging between 15:1 and 86:1 (Fig. 2.3b,d). Their orientations are more complex, documenting substantial changes in ice-flow directions towards the SWLIS margin.

2.3.2 Moraines (major and minor)

Moraines occur as arcuate ridges that collectively display lobate planforms. These landforms are split into two categories based on size. Minor moraines are typically 1-10 m high, 50-100 m wide and up to 5 km long, and are mapped as single lines drawn along the ridge crest. Major moraine ridges range between 1-3 km wide, up to 60 km long and 50 m high, and exhibit obvious outlines; that enabled them to be mapped as polygons (Fig. 2.2c).

The Cree Lake Moraine approximately parallels the lithological transition to outcropping Canadian Shield (Fig. 2.1). This moraine system is broadly arcuate and extends from northwest Alberta across the majority of the mapping area. Several prominent moraines also occur northwest of the Cree Lake Moraine and are associated with a narrow topographic low north of Cree Lake. Additionally, linear moraines occur at the northwestern edge of the Grizzly Bear Hills, and mark the margin of a corridor of lineated ground. The morphology and position of these moraines in relation to lineated ground are

consistent with lateral shear moraines and are thus interpreted as marking the former margin of a zone of fast ice flow within the surrounding ice sheet (Dyke and Morris, 1988; Hodgson, 1994; Stokes and Clark, 2002).

2.3.3 Ice-thrust ridges

Ice-thrust ridges are large, parallel, and generally arcuate and sharply crested landforms. Ridges range from 10-60 m high and 150-800 m long and are visible throughout the mapped area, occurring in small concentrations. In many cases these ridges are accompanied by a depression (typically water-filled) directly behind the ridge arc, commonly known as a hill-hole pair (Fig. 2.2b). Ice-thrust ridges have previously been mapped sparsely within the study area; therefore, our mapping extends the known distribution and demonstrates that these features are considerably more widespread than previously thought.

2.3.4 Crevasse-fill ridges

Crevasse-fill ridges occur in small concentrations as linear, curvilinear, or v-shaped ridges. These ridges range from 1-5 m high and 200-1200 m long and are oriented parallel or perpendicular to ice flow. Relatively few crevasse-fill ridges have been previously mapped within the study area and we demonstrate that these features are more prevalent than prior studies suggest. We acknowledge that small crevasse-fill ridges might have been missed in our mapping because their size does not allow for their recognition at the mapping scale.

2.3.5 Meltwater channels (major and minor)

A complex and extensive system of abandoned channels occur throughout the mapped area and shows evidence that drainage has been influenced by regional ice retreat patterns (Fig. 2.2d). These channels have been primarily carved by proglacial, supraglacial, or subglacial meltwater streams and display incised meanders interspersed with straight reaches. Major channel networks (>30 km long), that are deeply incised and well-defined have been mapped as solid lines, smaller and more subdued are mapped as dashed lines. Due to the small scale of many channels, some of the mapped channel features may be perennial or

intermittent subaerial streams, but it is difficult to conclusively differentiate between these using the imagery available.

2.3.6 Eskers

Single ridge eskers and esker networks composed of large sinuous eskers, which join to multiple smaller esker ridges, are prominent throughout the mapped area (Fig. 2.2e). These range in height between 5-10 m and in length between 2-10 km. We acknowledge that small eskers might have been missed in our mapping because their size does not allow for their recognition at the mapping scale.

2.3.7 Palaeo-shorelines

Palaeo-shorelines are erosional or depositional features. These landforms are most prominent in areas to the immediate south of Lake Athabasca (Fig. 2.2f). Faint remnants of shorelines are also recorded on the northeastern edge of the Grizzly Bear Hills.

2.3.8 Dunes

Parabolic and longitudinal dunes occur throughout the study area, but most commonly on the low topography surrounding Lake Athabasca (Fig. 2.2g). While these landforms are not glacial, they are included in our mapping as they started to form shortly after deglaciation and can be considered in a broader sense as a part of the glacial modification of the landscape. We acknowledge that small or faint dunes have been missed in our mapping because their size does not allow for their recognition at the 30 m SRTM DEM mapping scale.
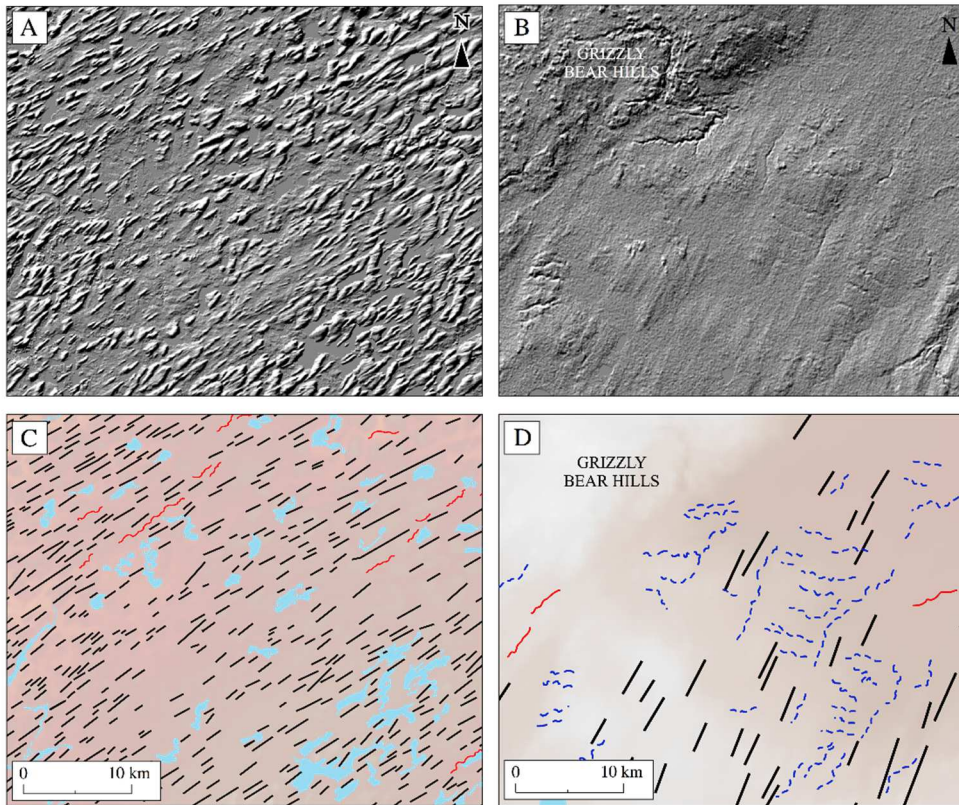
Figure 2.3: SRTM imagery displaying lineations from either side of the Shield boundary. (A) Densely spaced drumlins displaying low length to width ratios north of the Cree Lake Moraine. (B) Highly attenuated fluting orientated NE-SW east of the Grizzly Bear Hills. (C)/(D) Areas of corresponding geomorphological mapping, lineations indicated with black lines, eskers with red lines and meltwater channels with dashed blue lines. See Figure 2.1 for location of Figure 2.3 panels.

2.4 Implications and conclusions

The accompanying map provides a comprehensive representation of the glacial landform record in northwest Saskatchewan. This mapped landform assemblage documents a complex glacial history in the region, with traces of multiple ice flow directions overprinted by the landforms of the deglacial envelope. Flow patterns and dynamics revealed by our landform mapping replicated what has been reported by pre-existing literature, however, in many places adding significant additional complexities to the landform record. The existence of cross-cutting relationships between different landform packages has

18

significant implications for the spatial and temporal configuration and evolution of fast ice flow in the region, and provides the prerequisite for future reconstructions of the deglacial dynamics and chronology of northwest Saskatchewan.

2.5 References

Atkinson, N., Utting, D. J and Pawley, S. P. 2014a: *Glacial Landforms of Alberta. Alberta Geological Survey,* AER/AGS, Map 604.

Atkinson, N., Utting, D. J and Pawley, S. P. 2014b: Landform signature of the Laurentide and Cordilleran ice sheet across Alberta during the last glaciation. *Canadian Journal of Earth Sciences, 51,* 1067-1083.

Breckenridge, A. 2015: The Tintah-Campbell gap and implications for glacial Lake Agassiz drainage during the Younger Dryas cold interval. *Quaternary Science Reviews, 117,* 124-134.

Broecker, W. S., Kennet, J., Flower. R, B., Teller, J., Trumbore, S., Bonani, G. and Wolfi, W. 1989: Routing of meltwater from the Laurentide Ice Sheet during the Younger Dryas cold episode. *Nature, 341,* 318-321.

Campbell, J. E. 1988: *Surficial Geology of the Buffalo Narrows Area (73N) Saskatchewan.* Saskatchewan Research Council, Sedimentary Resources, Map 1:250,000 scale.

Campbell, J. E. 2006: *Fond-du-Lac Project: Surficial Geology of the Western Fond-du-Lac Area, South-Central Beaverlodge Domain (Part of NTS 74O/5 and 6).* 1:50,000 scale preliminary map with Summary of Investigations 2006, Volume 2, Saskatchewan Geological Survey, Saskatchewan Industry and Resources, Miscellaneous Report 2006-4.2.

Campbell, J. E. 2007: *Quaternary Investigations in the Fond-du-Lac Area (part of NTS 74O/6 and /7), Southeast Beaverlodge Domain (Fond-du-Lac Project).* 1:50,000 scale preliminary map with Summary of Investigations 2007, Volume 2, Saskatchewan Geological Survey, Saskatchewan Industry and Resources, Miscellaneous Report 2007-4.2.

Campbell, J. E., Ashton. K. E, and Knox, B. 2006: *Fond-du-Lac Project: Ice Flow Indicators, Western Fond-du-Lac Area, South Central Beaverlodge Domain (Part of NTS 74O/5 and 6).* 1:50,000 scale preliminary map with Summary of Investigations 2006, Volume 2, Saskatchewan Geological Survey, Saskatchewan Industry and Resources, Miscellaneous Report 2006-4.2.

Christiansen, E. A. 1979: The Wisconsinan deglaciation, of southern Saskatchewan and adjacent areas. *Canadian Journal of Earth Sciences, 16*, 913-938.

Clark, P. U., Marshall, S. J., Clarke, G. K. C., Hostetler, S.W., Licciardi, J.M. and Teller, J.T. 2001: Freshwater forcing of abrupt climate change during the last glaciation. *Science, 293,* 283-287.

Dyke, A. S. and Morris, T. F. 1988: Drumlin fields, dispersal trains, and ice streams in Arctic Canada. *Canadian Geographer, 32,* 86-90.

Dyke, A. S., Moore, A. and Robertson, L. 2003: *Deglaciation of North America.* Geological Survey of Canada, Open File 1574.

Evans, D. J. A., Clark, C. D. and Rea, B. R. 2008: Landform and sediment imprints of fast glacier flow in the southwest Laurentide Ice Sheet. *Journal of Quaternary Science, 23,* 249-272.

Evans, D. J. A., Young, N. J. P. and Ó Cofaigh, C. 2014: Glacial geomorphology of terrestrial-terminating fast flow lobes/ice stream margins in the southwest Laurentide Ice Sheet. *Geomorphology, 204,* 86-113.

Fisher, T. G. and Smith, D. G. 1994: Glacial Lake Agassiz: its northwest maximum extent and outlet in Saskatchewan (Emerson phase). *Quaternary Science Reviews, 13,* 845-858.

Hanson, M. A. 2014: *Ice-flow indicator map, Pine Channel and Fond du Lac River area (parts of NTS 74O01, 02, 07 and 08).* 1:50,000 scale preliminary map with Summary of Investigations 2014, Volume 2, Saskatchewan Geological Survey, Saskatchewan Ministry of the Economy, Miscellaneous Report 2014-4.2.

Hanson, M. A. 2015a: *Ice-flow indicator map, Pine Channel and Fond du Lac River areas (parts of NTS 74O01, 02, 07, and 08, and 74P05, and 06).* 1:50,000 scale preliminary map with Summary of Investigations 2015, Volume 2, Saskatchewan Geological Survey, Saskatchewan Ministry of the Economy, Miscellaneous Report 2015-4.2.

Hanson, M. A. 2015b: *Preliminary ice-flow indicator mapping, Fond du Lac River area, southern Tantato Domain and northern Athabasca Basin, Saskatchewan.* 1:50,000 scale preliminary map with Summary of Investigations 2015, Volume 2, Saskatchewan Geological Survey, Saskatchewan Ministry of the Economy, Miscellaneous Report 2015-4.2.

Hanson, M. A. 2015c: *Surficial Geology of the West Fond du Lac River area (parts of NTS 74O01, 02, 07 and 08).* 1:50,000 scale preliminary map with Summary of Investigations 2015, Volume 2, Saskatchewan Geological Survey, Saskatchewan Ministry of the Economy, Miscellaneous Report 2015-4.3.

Hodgson, D. A. 1994: Episodic ice streams and ice shelves during retreat of the northwestern most sector of the Late Weichselian Laurentide Ice Sheet over the central Canadian Arctic Archipelago. *Boreas, 23,* 14-28.

Kleman, J., Jansson, K., De Angelis, H., Stroeven, A. P., Hatterstrand, C., Alm G. and Glasser, N.F. 2010: North American ice sheet build-up during the last glacial cycle, 115-21 kyr. *Quaternary Science Reviews, 29,* 2036-2051.

Margold, M., Stokes, C. R. and Clark, C. D. 2015a: Ice streams in the Laurentide Ice Sheet: identification, characteristics and comparison to modern ice sheets. *Earth Science Reviews, 143,* 117-146.

Margold, M., Stokes, C. R. and Kleman, J. 2015b: Ice streams in the Laurentide Ice Sheet: a new mapping inventory. *Journal of Maps, 11,* 380-395.

Moran, S. R., Clayton, L., Hooke, R. L., Fenton, M. M. and Andriashek, L. D. 1980: Glacier-bed landforms of the prairie region of North America. *Journal of Glaciology, 25,* 457-476.

Ó Cofaigh, C., Evans, D. J. A. and Smith, R. 2010: Large-scale reorganization and sedimentation of terrestrial ice streams during late Wisconsinan Laurentide Ice Sheet deglaciation. *Geological Society of America, 122,* 743-756.

Prest, V. K., Grant, D. R. and Rampton, V. N. 1968: *Glacial map of Canada.* Geological Survey of Canada, Map 1253A.

Ross, M., Campbell, J. E., Parent, M. and Adams, R. S. 2009: Palaeo-ice streams and the subglacial landscape mosaic of the North American mid-continental prairies. *Boreas, 38,* 421-439.

Schreiner, B. I. 1984a: *Quaternary geology of the Precambrian Shield, Saskatchewan.* Saskatchewan Energy and Mines, Report 221.

Schreiner, B. I. 1984b: *Quaternary geology of the Ile-a-la-Crosse area (NTS 73O).* Saskatchewan Energy and Mines, Open File Rep. 84-5.

Schreiner, B. I. 1984c: *Quaternary geology of the Mudjatik area (NTS 74B).* Saskatchewan Energy and Mines, Open File Rep. 84-8.

Schreiner, B. I. 1984d*: Quaternary geology of the La Loche area (NTS 74C).* Saskatchewan Energy and Mines, Open File Rep. 84-9.

Schreiner, B. I. 1984e: *Quaternary geology of the Cree Lake area (NTS 74G).* Saskatchewan Energy and Mines, Open File Rep. 84-12.

Schreiner, B. I. 1984f: *Quaternary geology of the Lloyd Lake area (NTS 74F).* Saskatchewan Energy and Mines, Open File Rep. 84-13.

Schreiner, B. I. 1984g: *Quaternary geology of the Livingstone Lake area (NTS 74J).* Saskatchewan Energy and Mines, Open File Rep. 84-16.

Schreiner, B. I. 1984h: *Quaternary geology of the William River area (NTS 74K).* Saskatchewan Energy and Mines, Open File Rep. 84-17.

Schreiner, B. I. 1984i: *Quaternary geology of the Fond-du-Lac area (NTS 74O).* Saskatchewan Energy and Mines, Open File Rep. 84-20.

Schreiner, B. I. 1984j: *Quaternary geology of the Tazin Lake area (NTS 74N).* Saskatchewan Energy and Mines, Open File Rep. 84-21.

Scott, B. P. 1965: *Geology of the Upper Clearwater Area. Saskatchewan Energy and Mines.* Open File Report 85-2.

Shaw, J., Sharpe, D., and Harris, J. 2010: A flowline map of glaciated Canada based on remote sensing data. *Canadian Journal of Earth Sciences, 47*, 89-101.

Simpson, M. A. 1988: *Surficial geology of the Ile-a-la-Crosse Area (73O) Saskatchewan.* Saskatchewan Research Council, Sedimentary Resources, Map 1:250,000 scale.

Simpson, M. A. 1997: *Surficial geology map of Saskatchewan. Saskatchewan Energy and Mines/ Saskatchewan Research Council.* Map 1:1000,000 scale.

Slimmon, W. L. 2011: *Geological Atlas of Saskatchewan; Saskatchewan.* Ministry of Energy and Resources, Miscellaneous Report, 2011-7 CD_ROM, version 14, URL: http://www.infomaps.gov.sk.ca/website/SIR_Geological_Atlas/SK.

Smith, M. J. and Clark, C. D. 2005: Methods for the visualization of digital elevation models for landform mapping. *Earth Surface Processes and Landforms, 30*, 885-900.

Stokes, C. R. and Clark, C. D. 2002: Ice Stream Shear Margin Moraines'. *Earth Surface Processes and Landforms, 27,* 547-558.

Stokes, C. R., Margold, M., Clark. C. D. and Tarasov, L. 2016: Ice stream activity scaled to ice sheet volume during Laurentide Ice Sheet deglaciation. *Nature, 530,* 322-326.

Teller, J. T. and Clayton, L. (eds). 1983: Glacial Lake Agassiz. *Geological Association of Canada, Special Paper 26,* 117-131.

Teller, J. T. and Leverington, D. W. 2004: Glacial Lake Agassiz: a 5000 yr history of change and its relationship to the d18O record of Greenland. *Geological Society of America Bulletin, 116,* 729-742.

CHAPTER 3: RAPID RETREAT OF THE SOUTHWESTERN LAURENTIDE ICE SHEET DRIVEN BY BØLLING-ALLERØD WARMING

3.1 Introduction

Deglaciation of the Laurentide Ice Sheet (LIS) dominated Late Pleistocene (~15 to 11.6 ka) sea level rise (Carlson and Clark, 2012; Clark and Tarasov, 2014); its retreat serves as a valuable example for understanding the dynamics of continental-scale ice sheet change. The LIS response to Northern Hemisphere warming during the Bølling-Allerød (BA) interstadial (14.6-12.9 ka) is of particular interest as it allows for an assessment of ice sheet sensitivity to abrupt millennial-scale climate change. Despite this, the mass loss and meltwater equivalent contribution of the LIS during this period remains uncertain.

Numerical modelling (Gregoire et al., 2012; Gregoire et al., 2016) and recent field evidence (Margold et al., 2019) indicate that rapid drawdown of the convergence zone (recently termed a "saddle" see Gregoire et al. (2012)) connecting the CIS and southwestern LIS, was driven by initial BA warming (~14.6 ka). The Cree Lake Moraine, a large moraine system >1000 kms northeast of the convergence zone at the boundary of the Canadian Shield, has been hypothesized (Dyke et al., 2003) as the location of southwestern LIS stabilization, subsequent to warming at the onset of the Younger Dryas (YD) (12.9- 11.7 ka: Broecker et al., 1989; Clark et al., 2001). An absence of chronological control on this moraine system and, large discrepancies between alternative dating methods (e.g. Dyke et al., 2003; Wolfe et al., 2004; Fisher et al., 2009; Munyikwa et al., 2001; 2017; Froese et al., 2019; Dalton et al., 2020) across this formally glaciated region, mean the deglacial response of the southwestern LIS proceeding initial detachment requires further examination.

The most cited reconstruction of the LIS is that of Dyke et al. (2003) recently updated by Dalton et al. (2020). Such radiocarbon-based chronologies are limited by, the largely unquantified, biases related to the delay between the timing of ice retreat and the colonization of a region by plants and animals (see Froese et al., 2019). Consequently, there is an inherent need for chronometers that can complement minimum-limiting radiocarbon
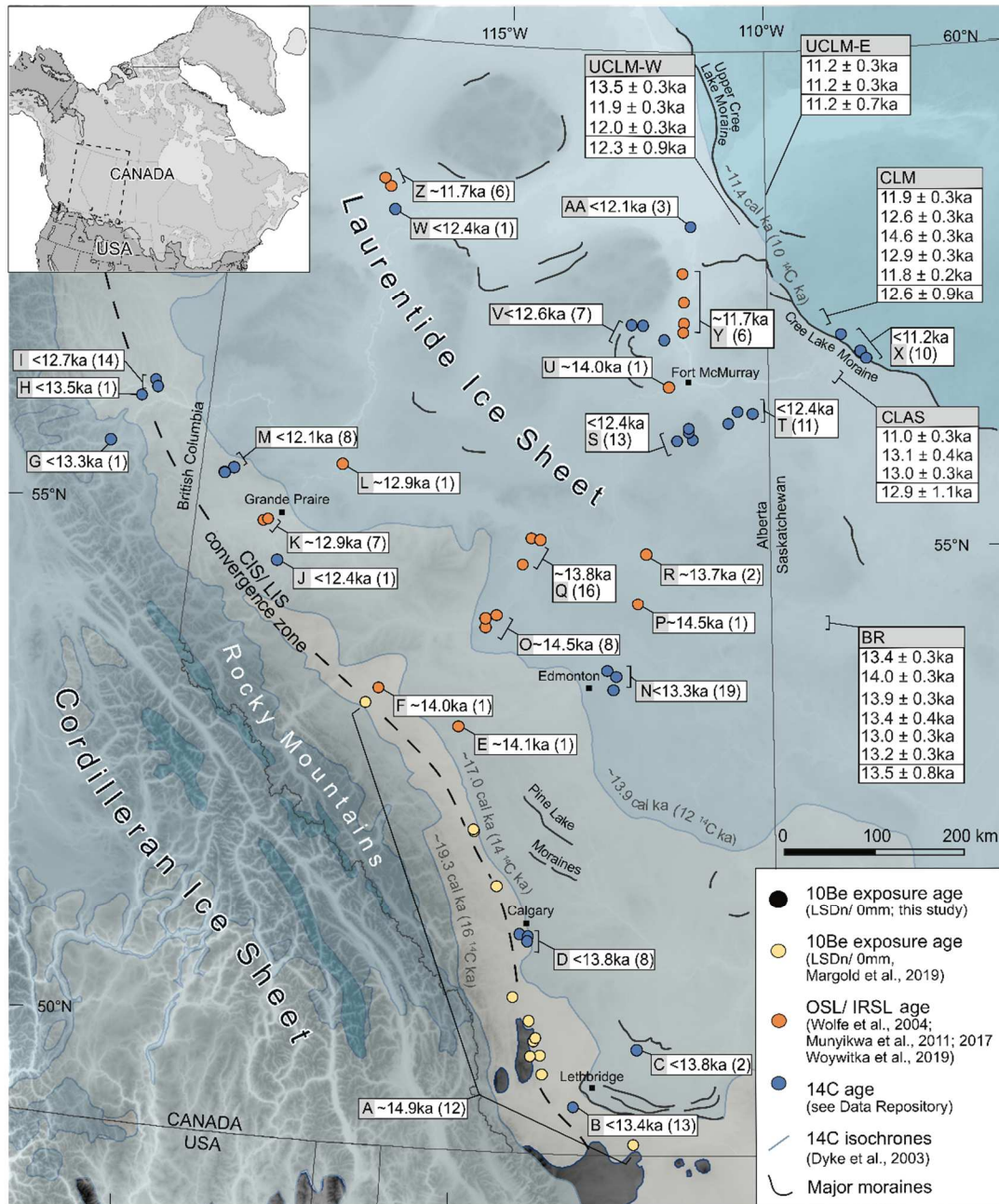
Figure 3.1. Southwestern sector of the Laurentide Ice Sheet and locations of [10]Be surface exposure sample sites from the PL-Pine Lake, BR-Beaver River, CLAS-Clearwater Lower Athabasca Spillway, CLM- Cree Lake Moraine, UCLM-W-Upper Cree Lake Moraine-West and UCLM-E-Upper Cree Lake Moraine-East. Individual sample ages and average ages for each site are shown. Regional ice sheet configuration and deglacial isochrones from ca. 19,000-11,400 cal yr B.P. are shown in shades of grey (after Dyke et al., 2003). Pre-existing selected luminescence, [10]Be surface exposure ages radiocarbon chronological labels (A-Z, AA) showing dates or groups of dates (closely >40km located sites). Outliers have been removed following original authors or as explained in Table S3, and average ages are indicated along with number of samples (n) for each site (all data are summarised in Table S3).

age-based chronologies. Within the SWLIS, luminescence dating, and a small number of cosmogenic nuclide dates have been used to complement radiocarbon chronologies. Here, we present a database of [10]Be surface exposure ages from glacial erratics spanning the western Interior Plains (Fig 3.1). We combine these data with geomorphic mapping and pre-existing [10]Be surface exposure, luminescence, and minimum-limiting radiocarbon chronologies, exclusive of dates on bulk sediments, terrestrial shells or mixed assemblages, to determine the timing and deglacial retreat rate of the southwestern LIS. Our newly compiled dataset presents a consistent record of retreat between chronological methods. These data indicate, concurrent with BA warming, that the southwestern LIS retreated >1200 km from its former convergence with the CIS reaching its YD position in ≤ 2500 yrs.

3.2 Methods

Surface samples from 26 boulders were collected for cosmogenic surface exposure dating using [10]Be at five locations along a ~1200 km transect across the western Interior Plains. These included: four samples from the crest of the Pine Lake Moraine (PLM), six from gravel bars within the Beaver River Spillway (BR), five from erosional residuals situated at the head of the Clearwater Athabasca Spillway (CLAS), five from the crest of the Cree Lake Moraine (CLM) and six from the western and eastern parts of the upper-Cree Lake Moraine (UCLM-W and UCLM-E) (Fig 3.2). The sampled erratics consisted of Precambrian rocks from the Athabasca Group sandstone and granites from the Canadian Shield (Fig 3.3). All samples were processed in CRISDal Lab, Dalhousie University, and the [10]Be concentrations were measured at the Centre for Accelerator Mass Spectrometry, Lawrence Livermore National Laboratory, UC, Berkeley.

Ages are reported using the time-dependent CRONUS LSDn production-rate scaling of Lifton et al. (2014), and the 'primary' production rate of Borchers et al. (2016) (for a description of the sample processing procedures and alternative age calculations see Appendix B). We report exposure ages with no correction for snow shielding and with a zero-erosion rate (see Appendix B). In contrast, glacial isostatic adjustment (GIA) affects

25

the elevation and thus the measured nuclide concentration of our samples. In this region, the majority of surface rebound occurred subsequent to ice retreat meaning our samples were at a lower than modern elevation for the majority of their exposure history. In this regard, we apply a GIA correction to all 26 samples using Lambeck et al's. (2017) ice sheet reconstruction. (see Appendix B).

We perform a χ^2 test (p= 0.05) to confirm that ages from each sample site are normally distributed and thus represent a single depositional event. In order to systemically identify outliers, we use Chauvenet's criterion of exclusion. We then report weighted mean ages for each site, with age uncertainties reported using a weighted standard deviation combined in quadrature with production rate uncertainty.

Following Froese et al. (2019), we combine our new [10]Be surface exposure ages with a filtered database of pre-existing luminescence, [10]Be surface exposure ages, and recalibrated minimum limiting radiocarbon chronologies. This database of 'high-quality dates' is exclusive of anomalous ages, dates on bulk sediments, terrestrial shells or mixed assemblages, to provide an updated chronology for the retreat of the SWLIS (see Appendix B; Table SB3).

3.3 Results

Our new [10]Be exposure dates are internally consistent, with mean ages recording stepwise north-eastward ice retreat. Samples from PLM yield ages ~6-8 ka years younger than all other sites. We interpret erratics at this site to have been exhumed post-glacially and they are excluded from further discussion. Our most southerly reliable ages from BR, yield a mean deglacial age of 13.5 ±0.8 ka (n=6). Samples from the CLAS record ice-free conditions at 12.9 ± 1.1 ka (n=4). Samples from the CLM record moraine deposition at 12.6 ± 0.9 ka (n=5). We excluded one outlier (CLM-S-02; 16.9 ± 0.3 ka) from this site which we assume results from inherited [10]Be caused by limited erosion (see Appendix B; Table SB2). Ages from UCLM-W indicate this site was ice free by 12.3 ± 0.9 ka (n=3). Our most northeasterly site UCLM-E, yields two concordant dates, returning an exposure

age of 11.2 ± 0.7 ka (n=2), excluding one older outlier (UCLM-E-05; 15.9 ± 0.3 ka), interpreted as resulting from inherited [10]Be caused by limited erosion (see Appendix B; Table SB2).
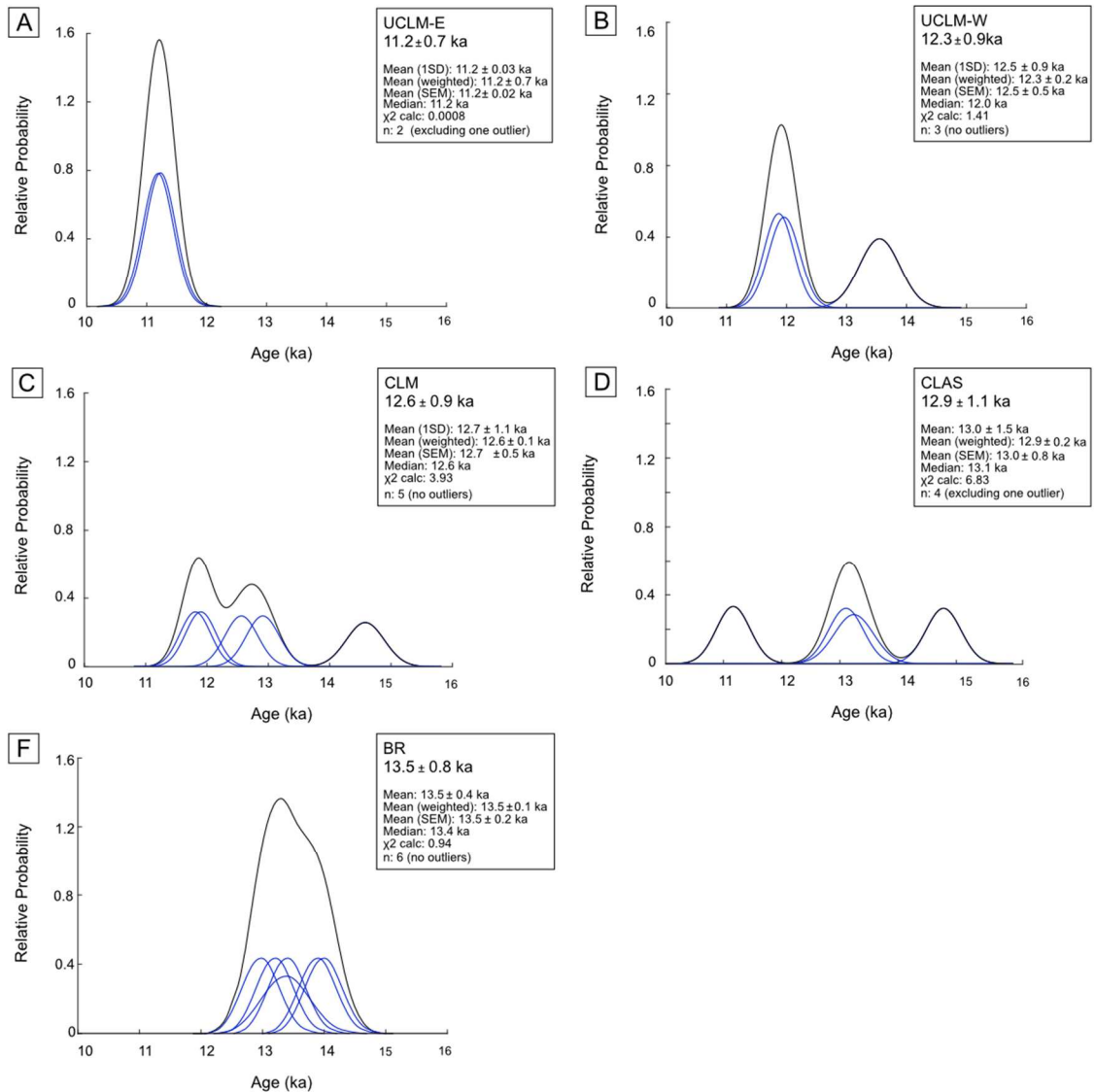
Figure 3.2. Probability density functions (i.e. ' camel plots') for all [10]Be surface exposure samples sites. Blue lines represent age and reported 1 SD uncertainty, black lines are summed probabilities. Vertical black line represents the mean and grey boxes 1 SD excluding outliers of each sample site. Average ages, in bold, with propagated uncertainly calculated using the default calibration set of Borchers et al. (2016) and the time dependent 'LSDn' production scaling scheme of Lifton et al. (2014), with no correction for snow shielding and a zero erosion rate.

Figure 3.3. Photographs of boulders sampled for [10]Be surface exposure ages. The sampled erratics consist of Precambrian rocks from the Athabasca Group sandstone and granites from the Canadian Shield.

Collation of the [10]Be exposure, luminescence, and minimum-limiting radiocarbon dates from the SWLIS present a consistent record of ice sheet retreat. Individual dates are summarised in table SB3. These data indicate LIS-CIS detachment beginning at ~14.9 ka and rapid retreat of the LIS to the CLM and UCLM complex where the LIS stabilizes between ~12.6-11.2 ka.By combining our dataset with 16 existing [10]Be exposure ages

(Margold et al., 2019) collected along the former LIS and Cordilleran Ice Sheet (CIS) convergence zone (the Foothills Erratic Train) we calculate margin retreat rates. We demonstrate the southwestern margin of the LIS experienced initial rapid retreat of 500 m a^{-1} from initial CIS-LIS separation (~14.9 ka) until ~13.5 ka. Subsequently, retreat rates slowed to ≤ 350 m a^{-1} until ~11.2 ka.

3.4 Discussion

The chronology presented here indicates that the deglaciation of the southwestern LIS began at ~14.9 ka and retreated 1200 km to its YD position in ≤ 2500 yrs. The timing of deglaciation presented from new cosmogenic dates, combined with a database of previously collected chronologies, present an internally consistent dataset. These data suggest the SWLIS experienced significant mass loss concurrent with BA warming.

3.4.1 Marginal retreat chronology and implications

Initial detachment of the southern LIS and CIS is reported at ~14.9 ka from [10]Be exposure ages from the Foothills Erratic Train (Margold et al., 2019) (Site A). Luminescence ages from the same region (Sites E-F; Table S3) suggest initial margin retreat ranged from 15.9 to 12.3 ka and tightly clustered minimum limiting radiocarbon dated-bones from the SWLIS periphery imply deglaciation before ~13.8 ka BP (Site B-D; Table SB3). Minimum limiting radiocarbon ages and luminescence ages suggest slightly later detachment, with deglaciation of the region commencing at 13.5ka (Site G-M; Table S3). Based on this chronology, we suggest LIS-CIS detachment began at ~14.9 ka, with substantial retreat and the formation of a deglacial "ice-free corridor[1]" between Beringia and continental North America only by ~13.5 ka.

---

[1] Following Heintzman (2016) the use of the term "ice-free corridor" is retained to refer to the deglacial biogeographic connection between Beringia and continental North America.
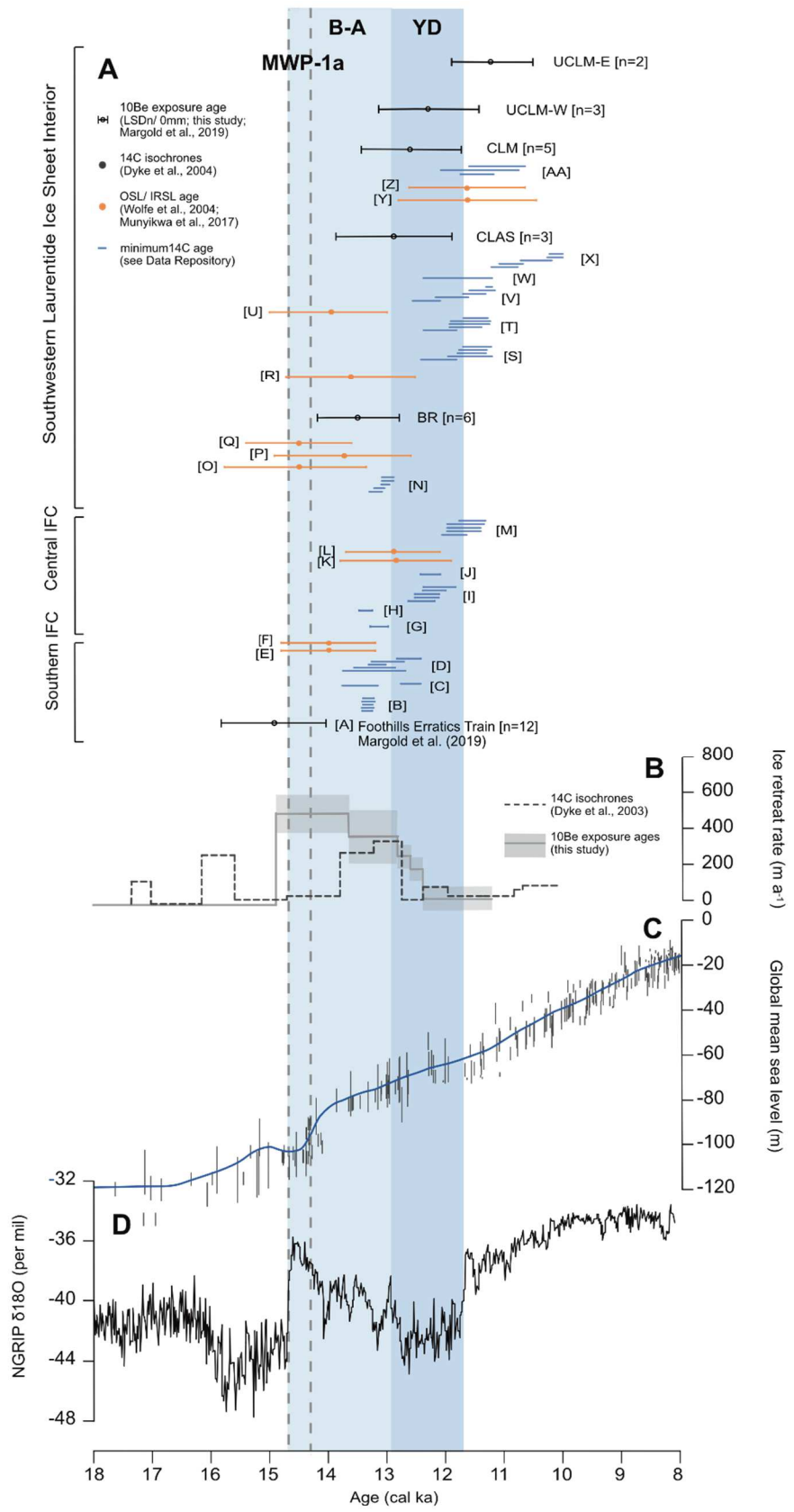
Figure 3.4. Complied chronologies, retreat rates and meltwater equivalent relating to the deglaciation of the southwestern Laurentide Ice Sheet (LIS). Key climate proxies are shown for comparison. (A) [10]Be surface exposure, luminescence and radiocarbon chronologies display a consistent record of rapid deglaciation between 14.9 and 12.6 ka BP. [10]Be surface exposure ages are reported with one standard deviation uncertainty combined with production rate uncertainty. Grouped (>40 km region) mean luminescence ages are presented at one standard deviation uncertainty. Radiocarbon dates are recalibrated using IntCal13 and presented at two standard deviation uncertainty (see Table S3 for summary of ages). (B) Bold grey line shows mean deglaciation rate (using mean LSDn/ 0mm ages). A minimum and maximum range for deglaciation is shown by the shaded grey region. Dashed grey line indicates the average rate of deglaciation across southwestern Laurentide Ice Sheet from Dyke et al. (2003) deglaciation. (C) Global mean sea level (Lambeck et al., 2014). (D) $\delta^{18}O$ record from the North Greenland Ice Core Project (Rasmussen et al., 2006).

Following initial ice sheet separation, rapid deglaciation of the SWLIS interior is indicated. Our cosmogenic dates imply the southwestern edge of the LIS retreated in ~1500 yrs to the BR region by ~13.5 ka. Tightly clustered radiocarbon dates between these regions record deglaciation by 13.3 ka, including dates on bison and horse from east of Edmonton (Site N; Table S3) and luminescence records, though variable, concur with this chronology (Sites O-Q; Table S3). Farther north, the cosmogenic ages indicate deglaciation of the CLAS region at ~12.9 ka. These ages agree with luminescence ages to the northwest, near Fort McMurray (Sites Y and Z; Table S3). Minimum limiting radiocarbon ages are also consistent with deglaciation prior to ~12.6 ka. The timing of ice-free conditions in this sector provides a minimum estimate on the timing of proglacial meltwater drainage across the Churchill/Athabasca drainage divide. Geological interpretations in northern Alberta (Smith and Fisher, 1993) and OSL evidence from the mouth of the Mackenzie River delta (Murton et al., 2010) propose that this spillway constituted the north-western outlet of glacial Lake Agassiz. Our chronology supports this conclusion and implies the CLAS provided a viable link for the north-western drainage of glacial Lake Agassiz during the YD.

Cosmogenic ages from the CLM and UCLM-W suggest formation by ~12.6 ka and ~12.3 ka. Conversely, radiocarbon ages in the same region suggest significantly later ice retreat (~10.7 ka). However, when considered in the context of older more southernly cosmogenic, luminescence and radiocarbon dates we suggest these samples reflect the minimum-limiting nature of deglacial ^{14}C dates. Therefore we, regard the CLM and UCLM-W as the

YD position of the southwestern sector of the LIS. This moraine system extends > 600 km across northeast Alberta and Saskatchewan and represents a significant stabilisation of the LIS during this cold reversal. This also indicates that fast ice flow (Ross et al., 2009; Margold et al., 2015) that fed ice streams from onset zones in the Athabasca and Churchill valleys ceased shortly before the YD, during the late BA. The UCLM-E records deposition more than 1100 yrs later at ~11.2 ka. We cannot determine whether recession and re-advance preceded the formation of the OCM outer moraines or whether these moraines simply represent a >1000 yr stillstand during recession. Nevertheless, this system of moraines signifies considerable reduction in LIS mass loss during the YD following rapid deglaciation of the SWLIS during BA time.

3.4.2 Ice sheet response to climate forcing

Our chronology demonstrates a climatically driven pattern of retreat for the southwestern LIS (Fig. 3.2). Peak retreat rates (~500 m yr^{-1}) follow initial ice sheet detachment coinciding with early BA warming. The rapid succession of ice stream orientations across the western Interior Plains (Ross et al., 2009; Ó Cofaigh et al., 2010; Margold et al., 2015; 2018; Atkinson et al., 2016; Norris et al., 2017) provide geomorphic and sedimentological evidence of a rapidly evolving deglacial system. These dynamics indicate large scale reorganization of the western LIS took place numerous times during deglaciation, switching over millennial to centennial timescales. Rapid deglaciation and ice sheet dynamic changes, while governed by abrupt warming, may have been enhanced by the reverse topographic gradient of the western Interior Plains.

During the YD, low retreat rates or stabilisation of the ice sheet coincides with a rise in topography at the transition to the Canadian Shield. Compared to pre-existing continental ice sheet reconstructions (Dyke et al., 2003) our results demonstrate, initial deglaciation and formation of the deglacial ice-free corridor region occurred several thousand years later than previously than recent reconstructions (Pederson et al., 2016; Potter et al., 2018). The constraint of the YD position results in retreat rates over the Interior Plains that are 60% higher. Our chronology records a climatically controlled ice margin response to BA climate forcing. Recent reconstruction of the CIS (Menounos et al., 2017) suggests similar rapid

ice sheet retreat and thinning signifying the Northern Hemisphere ice sheet complex underwent coherent deglaciation during the BA.

3.5 Conclusions

The deglacial response of the southwestern LIS has so far not been clearly constrained. Our new reconstruction of [10]Be exposure ages in addition to pre-existing high-quality cosmogenic, luminescence and minimum-limiting radiocarbon dates, present an internally consistent and robust retreat record. These data demonstrate a rapid climatically driven deglaciation of the ice sheet contemporaneous with initial BA warming. [10]Be exposure ages establish, for the first time, the hypothesized YD ice margin position in the region. Direct dating from CIS-LIS convergence to this marginal position demonstrates the LIS retreated >1200 km from its former convergence with the CIS in ≤ 2500 years.

3.6 References

Atkinson, N., Pawley, S. and Utting, D. J. 2016: Flow-pattern evolution of the Laurentide and Cordilleran ice sheets across west-central Alberta, Canada: implications for ice sheet growth, retreat and dynamics during the last glacial cycle. *Journal of Quaternary Science*, *31*(7), 753-768.

Borchers, B., Marrero, S., Balco, G., Caffee, M., Goehring, B., Lifton, N., Nishiizumi, K., Phillips, F., Schaefer, J. and Stone, J. 2016: Geological calibration of spallation production rates in the CRONUS-Earth project. *Quaternary Geochronology 31,* 188–198.

Carlson, A. E. and Clark, P. U. 2012: Ice sheet sources of sea level rise and freshwater discharge during the last deglaciation. *Reviews of Geophysics*, *50*(4).

Clark, P. U., and Tarasov, L. 2014: Closing the sea level budget at the Last Glacial Maximum. *Proceedings of the National Academy of Sciences*, *111*(45), 15861-15862.

Dalton A.S., Margold M., Stokes C.R.; Tarasov L., Dyke A. S., Adams R. S., Allard S., Arends H. E., Atkinson N., Attig J. W., Barnett P. J., Barnett R. L.., Batterson M., Bernatchez P., Borns H. W., Breckenridge A., Briner J. P., Brouard E., Campbell J. E., Carlson A. E., Clague J. J., Curry B. B., Daigneault R., Dubé-Loubert H., Easterbrook D. J., Franzi D. A., Friedrich H. G., Funder S., Gauthier M. S., Gowan A. S., Harris K. L., Hétu B., Hooyer T. S., Jennings C.E., Johnson M. D., Kehew A. E., Kelley S. E., Kerr D., King E. L., Kjeldsen K. K., Knaeble A. R., Lajeunesse P., Lakeman T. R., Lamothe M., Larson P., Lavoie M., Loope H. M., Lowell T. V., Lusardi B. A., Manz L., McMartin I.,. Nixon C. F, Occhietti S., Parkhill M. A., Piper D. J.W., Pronk A. G., Richard P. J.H., Ridge

J. C., Ross M., Roy M., Seaman A., Shaw J., Stea R. R., Teller J. T., Thompson W. B., Thorleifson L., Utting D. J., Veillette J. J., Ward B. C., Weddle T. K. and Wright H. E. 2020: An updated radiocarbon-based ice margin chronology for the last deglaciation of the North American Ice Sheet Complex. *Quaternary Science Reviews.* 234 (106223).

Dyke, A.S., Moore, A. and Robertson, L. 2003: *Deglaciation of North America.* Geological Survey of Canada, Ottawa.

Froese, D. G., Young, J. M., Norris, S, L. and Margold, M. 2019: Availability and viability of the ice-free corridor and pacific coast routes for the peopling of the Americas. SAA Archaeological Record. 19, 27-33.

Gregoire, L. J., Payne, A. J. and Valdes, P. J. 2012: Deglacial rapid sea level rises caused by ice-sheet saddle collapses. *Nature*, *487*(7406), 219-222.

Gregoire, L. J., Otto-Bliesner, B., Valdes, P. J. and Ivanovic, R. 2016: Abrupt Bølling warming and ice saddle collapse contributions to the Meltwater Pulse 1a rapid sea level rise. *Geophysical Research Letters*, *43*(17), 9130-9137.

Heintzman, P.D., Froese, D., Ives, J.W., Soares, A.E., Zazula, G.D., Letts, B., Andrews, T.D., Driver, J.C., Hall, E., Hare, P.G. and Jass, C.N. 2016: Bison phylogeography constrains dispersal and viability of the Ice Free Corridor in western Canada. *Proceedings of the National Academy of Sciences*, *113*(29), 8057-8063.

Lambeck, K., Purcell, A. and Zhao, S. 2017: The North American late Wisconsin ice sheet and mantle viscosity from glacial rebound analyses. *Quaternary Science Reviews,* 158, 172–210.

Lifton, N., Sato, T. and Dunai, T. J. 2014: Scaling in situ cosmogenic nuclide production rates using analytical approximations to atmospheric cosmic-ray fluxes. *Earth and Planetary Science Letters*, *386*, 149-160.

Margold, M., Stokes, C.R. and Clark, C.D. 2015: Ice streams in the Laurentide Ice Sheet: identification, characteristics and comparison to modern ice sheets. *Earth Science Reviews 143*, 117-146.

Margold, M., Stokes, C. R. and Clark, C. D. 2018: Reconciling records of ice streaming and ice margin retreat to produce a palaeogeographic reconstruction of the deglaciation of the Laurentide Ice Sheet. *Quaternary Science Reviews, 189*, 1-30.

Margold, M., Gosse, J. C., Hidy, A. J., Woywitka, R. J., Young, J. M. and Froese, D. 2019: Beryllium-10 dating of the Foothills Erratics Train in Alberta, Canada, indicates detachment of the Laurentide Ice Sheet from the Rocky Mountains at~ 15 ka. *Quaternary Research, 92*(2), 469-482.

Menounos, B., Goehring, B. M., Osborn, G., Margold, M., Ward, B., Bond, J. and Caffee, M. W. 2017: Cordilleran Ice Sheet mass loss preceded climate reversals near the Pleistocene Termination. *Science*, *358*(6364), 781-784.

Murton, J. B., Bateman, M. D., Dallimore, S. R., Teller, J. T. and Yang, Z. 2010: Identification of Younger Dryas outburst flood path from Lake Agassiz to the Arctic Ocean. *Nature*, *464*(7289), 740-743.

Norris. S. L., Margold, M. and Froese, D. G. 2017: Glacial landforms of northwest Saskatchewan. *Journal of Maps*. 13:2, 600-607.

Ó Cofaigh, C., Evans, D. J. A. and Smith, R. 2010: Large-scale reorganization and sedimentation of terrestrial ice streams during late Wisconsinan Laurentide Ice Sheet deglaciation. *Geological Society of America*, 122, 743-756.

Pedersen, M.W., Ruter, A., Schweger, C., Friebe, H., Staff, R.A., Kjeldsen, K.K., Mendoza, M.L., Beaudoin, A.B., Zutter, C., Larsen, N.K. and Potter, B.A. 2016: Postglacial viability and colonization in North America's ice-free corridor. *Nature*, *537*(7618), 45-49.

Potter, B.A., Baichtal, J.F., Beaudoin, A.B., Fehren-Schmitz, L., Haynes, C.V., Holliday, V.T., Holmes, C.E., Ives, J.W., Kelly, R.L., Llamas, B. and Malhi, R.S. 2018: Current evidence allows multiple models for the peopling of the Americas. *Science Advances*, *4*(8), eaat5473.

Rasmussen, S. O., Andersen, K. K., Svensson, A. M., Steffensen, J. P., Vinther, B. M., Clausen, H. B. and Bigler, M. 2006: A new Greenland ice core chronology for the last glacial termination. *Journal of Geophysical Research: Atmospheres*, *111*(D6).

Ross, M., Campbell, J.E., Parent, M. and Adams, R.S. 2009: Palaeo-ice streams and the subglacial landscape mosaic of the North American mid-continental prairies. *Boreas* 38, 421–439.

Smith, D. G. and Fisher, T. G. 1993: Glacial Lake Agassiz: The northwestern outlet and paleoflood. *Geology*, *21*(1), 9-12.

CHAPTER 4: RAPID DYNAMIC RESPONSE OF THE SOUTHWESTERN LAURENTIDE ICE SHEET TO BØLLING-ALLERØD WARMING

4.1 Introduction

The contribution of mass loss from modern ice sheets to global sea-level rise has accelerated over recent decades, largely resulting from enhanced ice-flow rates and increased ice sheet thinning (Alley et al., 2005; Rignot et al., 2008, 2011). Ice sheet instability is of particular concern given the potential meltwater equivalent contribution of ice sheets in Greenland and Antarctica (Golledge et al., 2015; Ritz et al., 2015). However, limited observations spanning more than a few decades, mean the response of modern ice sheets to future climatic change over longer timescales remains uncertain. Reconstructing palaeo-ice sheet behaviour in response to past climatic fluctuations is therefore critical to assessing future changes to contemporary ice sheets (Alley and Bindschadler, 2001; Rignot and Thomas, 2002; Clark et al., 2009; Carlson and Clark, 2012). Due to its complexity and often well-preserved imprint, the Late Wisconsinan, Laurentide Ice Sheet (LIS) is recognised as a valuable example that can be used to assess a continental-sized ice sheets' response to rapid climate change (Stokes et al., 2015; Margold et al., 2015, 2018). In particular, geomorphic and sedimentary investigations of parts of the southwestern LIS (SWLIS), have documented major ice flow reorganisations (Ross et al., 2009; Ó Cofaigh et al., 2010; Atkinson et al., 2016). However, until recently discrepancies between chronometers have led to uncertainties surrounding the timing of these dynamics. A new deglacial chronology (Norris et al., in prep; chapter 3), indicates the SWLIS underwent rapid deglaciation in response to abrupt Bølling-Allerød (BA) warming. These data indicate deglaciation of the 800,000 km^2 region occurred in ≤ 2500 yrs.

Here, we reconstruct the ice flow dynamics associated with this period of rapid climate change. Our reconstruction reveals a complex ice flow network, reflective of at least three ice sheet scale reorganisations in ≤ 2500 yrs. These rapid, decadal to centennial changes in ice-flow geometry demonstrate not only how ice streams can influence an ice sheet's broader response to external climate forcing, but also how ice sheets, through changes to

ice flow regime are sensitive to rapid climate change. While the terrestrially margin of the SWLIS differed greatly in comparison to modern Antarctic and Greenland environments, the dynamic ice sheet response we reconstruct reveals, rapid ice sheet scale reorganisations are not limited to marine terminating environments.

4.2. Study Area

4.2.1 Physiographic setting and surficial geology

The SWLIS was fed by ice flowing from the Keewatin Ice Divide and converged with the Cordilleran Ice Sheet (CIS) to the west, extending into the northern mid-western United States (Fig. 4.1). This sector of the ice sheet covered two broad physiographic regions, the Interior Plains in the south and the Canadian Shield to the north comprised of crystalline Precambrian rock. Bordering the eastern foothills of the Rocky Mountains, the western parts of the SWLIS subsumed several uplands. These topographic highs are bedrock remnants composed of Cretaceous shales and sandstones, which in places are draped by thin late Tertiary and Quaternary deposits (Andriashek and Barendregt, 2017). Large preglacial valley systems separate uplands and are composed of thick Quaternary deposits, comprising stacked sequences of diamict, glaciofluvial sands and gravels and glaciolacustrine silts and clays, overlying bedrock and up to 60 m locally (cf. Andriashek and Atkinson, 2007).
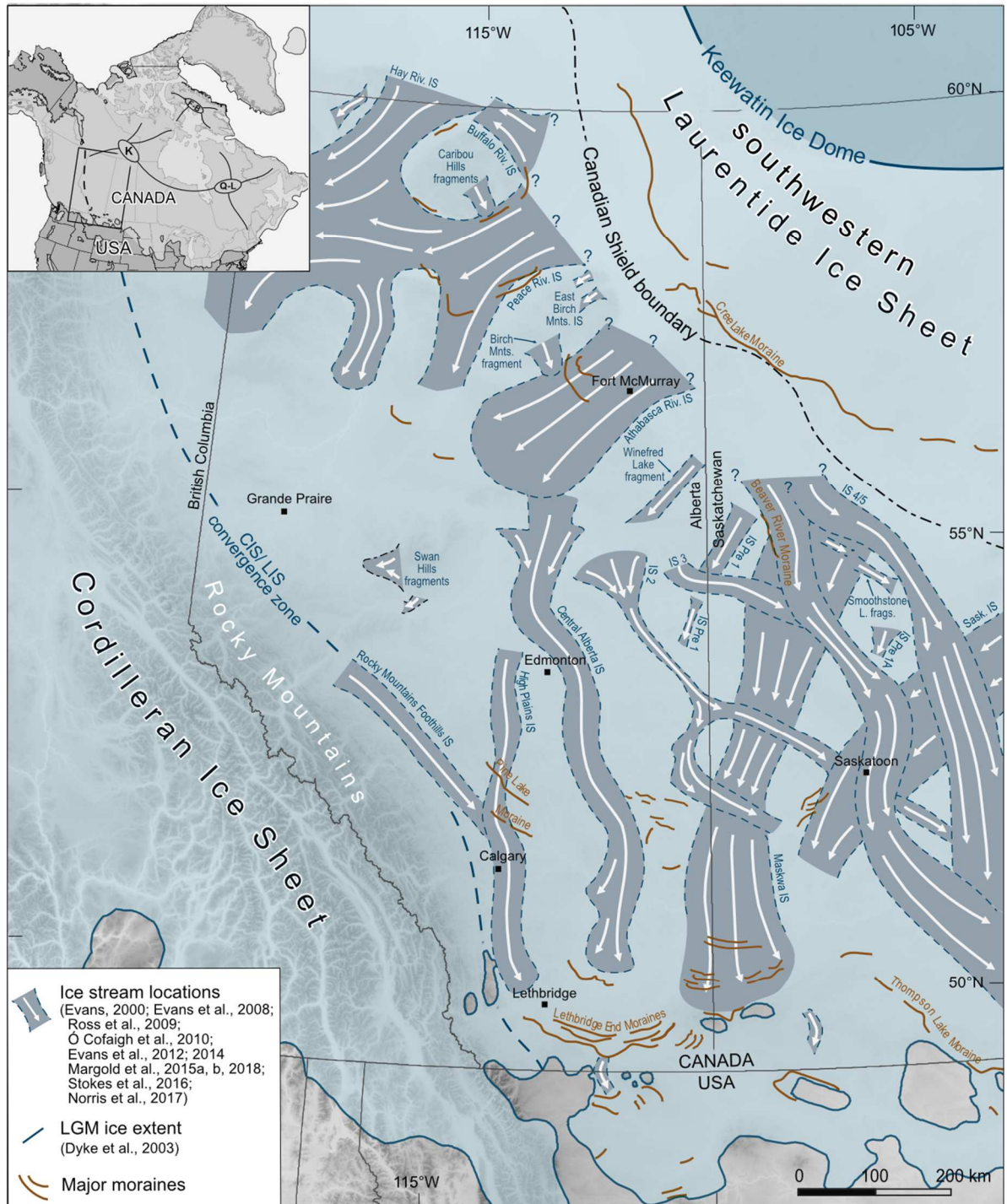
Figure 4.1: Regional ice flow configuration of the southwestern sector of the Laurentide Ice Sheet. Previously identified ice stream locations summarised from; Evans, 2000; Evans et al., 2008; Ross et al., 2009; Ó Cofaigh et al., 2010; Evans et al., 2012, 2014; Margold et al., 2015a, b, 2018; Stokes et al., 2016.

4.2.2 Regional glacial history

The geomorphic imprints of ice streams within the SWLIS have been well documented, with glacial bedforms being used to reconstruct ice flow evolution and highlighting complex ice flow activity at a regional scale (Evans, 2000; Evans et al., 2008; Ross et al., 2009; Ó Cofaigh et al., 2010; Evans et al., 2012, 2014; Margold et al., 2015; Norris et al., 2017). Towards the margin of the SWLIS, cross-cutting landforms document several ice stream reorganisations. Ice stream trajectories in these regions have orientations varying from WSW to SE, most probably indicative of an advancing ice sheet, a SW to S flow associated with Last Glacial Maximum (LGM) extent and ice flow changing from S to SE and then back to S and finally SW during ice retreat (Evans, 2000; Evans et al., 2008; Ross et al., 2009; Ó Cofaigh et al., 2010; Evans et al., 2012, 2014, 2020; Norris et al., 2017). While these changes in ice stream configuration are prominent in the landform record, the cause of such switches and how they may relate to climate warming or internal flow dynamics during deglaciation is largely undetermined. Furthermore, the ice flow dynamics within the interior SWLIS is poorly understood. Continental-scale reconstructions (Margold et al., 2015a, b; 2018) indicate this region also exhibited complex ice flow activity during the Late Wisconsinan; however, these dynamic changes have remained understudied.

Moraines and other ice-marginal landforms relating to ice sheet recession have been the focus of several studies of the SWLIS (Christiansen, 1979; Dyke and Prest, 1987; Dyke et al., 2003; Evans et al., 2008, 2012, 2014 2020; Kleman et al., 2010; Fisher et al., 2009). The most prominent moraine complex, demarcating advanced stages of regional recession, the Cree Lake Moraine, situated at the boundary of the Canadian Shield, has been of particular interest due to its suggested Younger Dryas age (YD 12.9- 11.7 ka) (Dyke et al., 2003). An absence of chronological control on this moraine system and, large discrepancies between dating methods more widely (e.g. Fisher et al., 2009; Munyikwa et al., 2011; 2017; Wolfe et al., 2004; Dyke et al., 2003; Froese et al., 2019) have hindered attempts to reconstruct the deglacial response of the SWLIS. Norris et al. (in prep; chapter 3) address these discrepancies by combining [10]Be surface exposure ages, with pre-existing luminescence and the most viable minimum-limiting radiocarbon dates (i.e. exclusive of

dates on bulk sediments, terrestrial shells or mixed assemblages) to determine the timing of deglaciation. This compilation proposes a consistent record of retreat between chronological methods and suggests that the SWLIS retreated from its convergence with the CIS to its Younger Dryas position (the Cree Lake Moraine) in ≤ 2500 yrs (Norris et al., in prep), across a distance of more than 1200 km.

4.3 Methods

4.3.1 Geomorphological mapping

In order to construct a comprehensive inventory of ice streams, the glacial geomorphology within the former SWLIS's cover was mapped. Geomorphic mapping from LiDAR imagery (5-15 m resolution) (Atkinson et al., 2014) at a 1:100,000 scale, was utilised for Alberta. Supplementary mapping of the Saskatchewan part of the study area was completed at a 1:100,000 scale as a precursor to this study (Norris et al., 2017; chapter 2). Due to a lack of accessible LiDAR data within Saskatchewan, mapping was completed from 1-arc second SRTM (~30 m resolution) and ALOS (~30 m resolution) imagery. Collation of these maps (redrawn using a consistent legend in Fig. SC1) forms the basis for reconstructing the configuration and dynamics of evolving ice flow patterns within the SWLIS interior portions.

4.3.2 Glacial flowset mapping

The ice stream inventory is compiled from ~30,000 mapped landforms within the interior SWLIS (see Appendix C; Fig. SC1), using a process of landform generalisation that facilitated palaeo-ice dynamics to be interpreted and reconstructed (Fig. 4.2). A 'flowset approach' (see Kleman and Borgström, 1996; Kleman et al., 1997; Greenwood and Clark, 2009a) was utilised, which formalises traditional morphometric mapping techniques (Dyke et al., 1992) using a pre-existing understanding of landform genesis to reconstruct ice sheet properties from the mapped characteristics and distribution of glacial geomorphology, specifically the subglacial lineation record. Following the procedures adopted by Atkinson et al. (2016) in the palaeoglaciological reconstruction of part of the SWLIS marginal

regions, the traditional 'flowset approach' was used in combination with the 'landsystem approach' (see Evans, 2003, 2013, 2017). The latter enables sediment-landform associations to be integrated into assemblages that relate to particular genetic processes, thereby facilitating a more holistic appreciation of process-form regimes in the final assessment of ice sheet behaviour.

Ice flow patterns were grouped into spatially coherent flowsets based on their morphometry, proximity and parallel concordance, (following the principle that lineations in the same flowset should have near identical orientations) (Clark, 1999), and similar sediment-landform association (c.f. Evans, 2003; Evans et al., 2008, 2014, 2020). Subglacial bedforms were used to inform the geometry of the flowsets, and associated landforms such as eskers, moraines, crevasse squeeze ridges and lateral meltwater channels. These collective landform assemblages were used to elaborate on glaciodynamics, and the pattern and style of ice retreat. Each flowset was then divided into one (or more) of four categories: (i) deglacial, (ii) ice stream, (iii) event, (iv) unknown (Table 1). Flowsets were then classified according to relative age based on overprinting and crosscutting relationships (Kleman et al., 2002, 2010; Greenwood and Clark, 2009a,b; Hughes et al., 2014) and thereby inform a spatial and temporal reconstruction of ice stream dynamics.
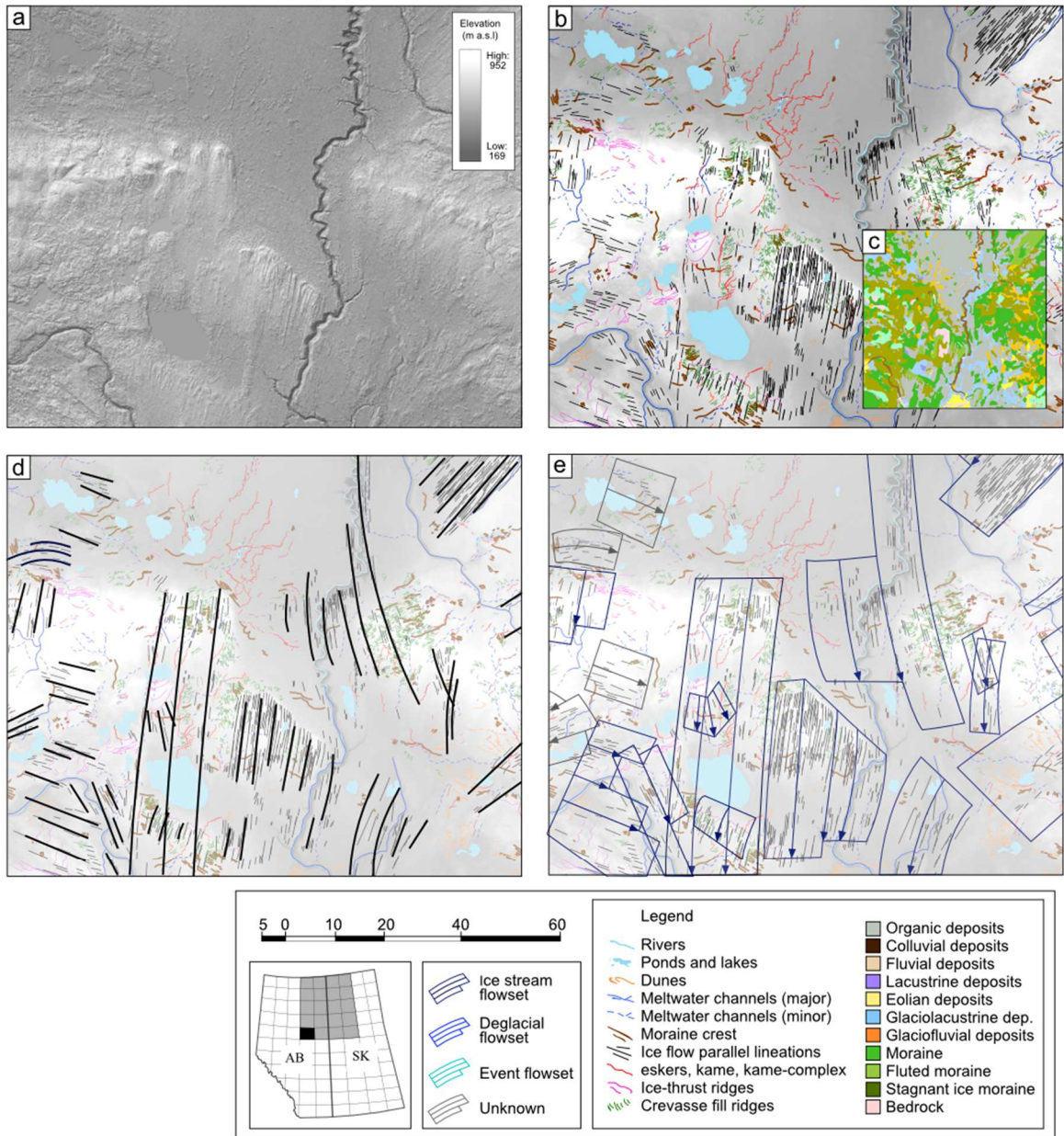
Figure 4.2: Classification of glacial geomorphology into flowsets. (a) Shuttle Radar Topography Mission (SRTM) imagery displaying the onset of the Central Alberta Ice Stream. (b) Area of corresponding geomorphological mapping and, (c) surficial geological units (d). Simplification of geomorphic mapping and surficial geological units into 'flowlines' (e) Classification of flowlines into individual flowsets as either 'ice stream', 'deglacial', 'event' or 'unknown. See Figure 1 for location of Figure 3 panel.

4.3.3 Deglacial dynamics

In order to place our reconstruction into chronological context, we embed our reconstruction, as well as previously identified ice streams from the SWLIS marginal regions, into the deglacial chronology of Norris et al. (in prep). Using this combination of comprehensive geomorphic reconstruction and ages from moraines ridges (Norris et al., in prep), isochrones reflecting ice-marginal geometry across the study area are presented. We use the configuration of continental-scale ice margins from Dyke et al. (2003) to extrapolate where ice margins are uncertain.

4. Geomorphologic imprint of the SWLIS interior region

Based on the cross-cutting nature of the flowsets, it is clear that ice flow dynamics within the SWLIS interior region were complex and underwent several major sector reorganisations (Fig. 4.3). We briefly describe these dynamics, before considering the SWLIS as a whole.

Phase 1- Initial ice flow was NE to SW and is composed of four flowsets (Fig. 4.3: flowsets 5, 6, 9 and 11) delineated diamicton-cored by drumlinoid ridges and flutings. These occur within two unconstrained ice stream tracts that extend for >70 km across the Stony Mountains (see Fig. 4.4 for place names). The widespread distribution of well-developed streamlined subglacial bedforms on high ground, with no significant localised deflection, indicates that the ice sheet was sufficiently thick to flow across the Grizzly Bear Hills. Lineations in flowsets 5 and 6 can be traced to lineations comprising palaeo-ice stream flow path 'pre 1' of Ó Cofaigh et al. (2010).

Phase 2- The initial NE to SW flow path is cross-cut by N to S aligned flows (Fig. 4.4a). During this phase, flowsets 17, 18, 20-26, 64 and 66 (Fig 4.3) mark the onset of ice streaming within the Athabasca River Valley. Its association with previously mapped flowsets (Prest et al., 1968; Evans et al., 2008; Atkinson et al., 2014) indicates that this is the onset zone of the Central Alberta Ice Stream and High Plains Ice Stream (hereafter CAIS and HPIS), although it does not exhibit a clear zone of convergent flow (i.e. Prest et

al., 1968; Evans et al., 2008). While it is plausible that the region of convergence was not preserved (cf. De Angelis and Kleman, 2008) we think it more likely that multiple topographically constrained tributaries rather than a large region of convergence was the initiator of fast ice flow. This is consistent with the subtle changes in ice stream orientation recorded within the onset zone and the existence of multiple topographically confined flowsets.

The onset zone of the Maskwa Ice Stream (Maskwa IS), is also recorded within the study area. This is evidenced by flowset 2 which marks the distal parts of the convergent flow. This flowset extends to join southwest trending MSGLs previously identified as the ice streams trunk zone (Evans et al., 2008; Ross et al., 2009; Ó Cofaigh et al., 2010). An onset zone in this location or potentially extending to the Canadian Shield boundary is further confirmed by regional airborne gamma-ray spectrometry surveys (GSC 2008; Ross et al., 2009).

<u>Phase 3</u>**-** The landform record during this phase depicts a major change in ice stream orientation (NW-SE). Widespread streamlined subglacial bedforms, composed of drumlins and flutings, occur over an ~85 km wide, topographically constrained tract. Bedforms appear subdued by a surface cover of diamict, and at the northwestern section of flowset 36 become progressively muted by glaciolacustrine sediment, and hence ice flow direction is difficult to identify based solely on bedform morphology. Glaciotectonic bedrock rafts also occur along flowset 36. These landform associations collectively delineate an ice flow trajectory that extends NW to SE across the study area.
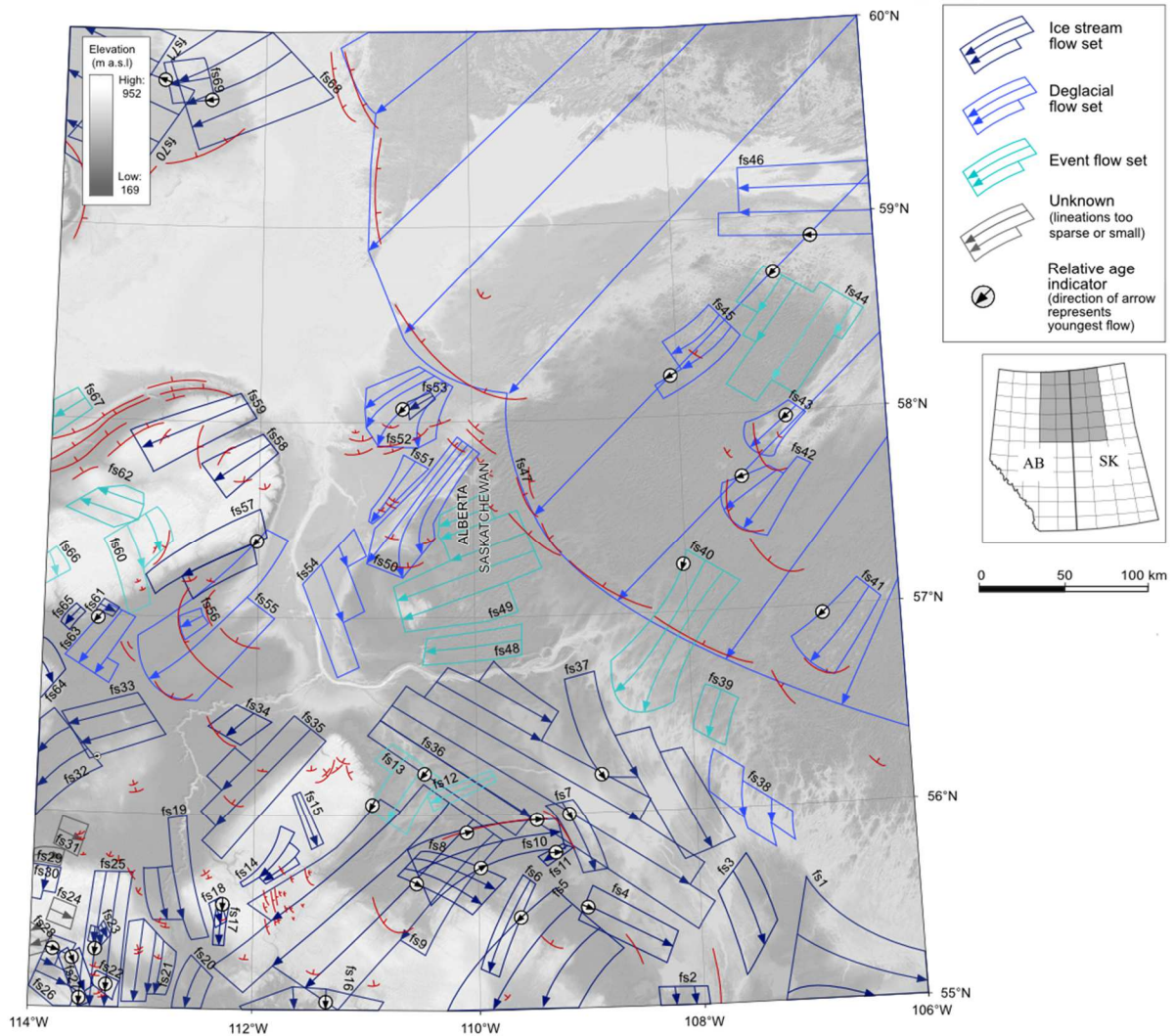
Figure 4.3: Flowset map of the Interior portions of the southwestern Laurentide Ice Sheet. Flowset configuration reflects a highly dynamic system of fast flow caused by multiple reconfigurations in ice sheet drainage.

Phase 4- Subsequent to the proposed NW to SE ice streaming, major ice streams became active in the Peace, Athabasca and Churchill river valleys. Fragmented evidence for ice flow is also found on the Birch Mountains plateau (flowsets 58, 59), indicating fast ice flow was unconstrained by topography. Within the Churchill River Valley, three examples of ice stream orientation (SWW to SE, NW to SE and NW to S figure 4.4d) are visible. The superimposition of these landforms suggests they formed as a single but evolving ice drainage system migrating from SW to SE. This is also seen in the migration and cross-

46

cutting of lateral shear moraines (see Stokes and Clark, 2002, Fig. 4.4d). Collectively these landforms depict a time transgressive shift from an unconstrained to topographically constrained ice stream system.

Phase 5- This phase marks the initial deglaciation of the study area. A subtle change in ice stream orientation within the Athabasca Valley is also recorded between this phase and phase 4. This change is presumably the result of thinning and progressive retreat of the ice margin. Within the Peace, Athabasca and Buffalo River valleys, ice flow was orientated in a westerly direction, recording the separation of this margin into a series of topographically confined lobes. Comparatively, within the Churchill River Valley, ice flow was directed in an easterly direction around the Grizzly Bear Hills. North of the Caribou Mountains, a switch from SW ice streaming (feeding into the previously identified Hay River and Peace River Ice Streams of Margold et al. (2015b) to NW ice streaming (feeding into the previously identified Buffalo River Ice Stream of Margold et al. (2015b) is also visible. Examination of the finer directional details of the area show that lineations display a gradational transition rather than a simple overprinting; thus, producing a time transgressive landform assemblage with the two stages of ice stream presented north of the Caribou Mountains in phases 4 and 5 (figure 4.4d & e) being the two end members.

Unlike the majority of flowsets that represent increased topographic control, flowsets on the Birch Mountains represents a further deglacial complexity (flowsets 60, 62). A clear suite of lineations, ice-marginal channels, eskers and moraines, which overprint older flow from the east, indicate that local flow from the Birch Mountains occurred during deglaciation. These landforms crosscut recessional moraines within the Athabasca Valley suggesting the lowland regions were ice free prior to their formation.

Phase 6- By the time of initiation of this phase, the SWLIS had retreated onto the Canadian Shield to form the > 600 km Cree Lake Moraine. At this point the ice margin is no longer confined to valleys and narrow outlet lobes but is instead characterised by an extensive arcuate margin fed by less prominent ice streams.

48
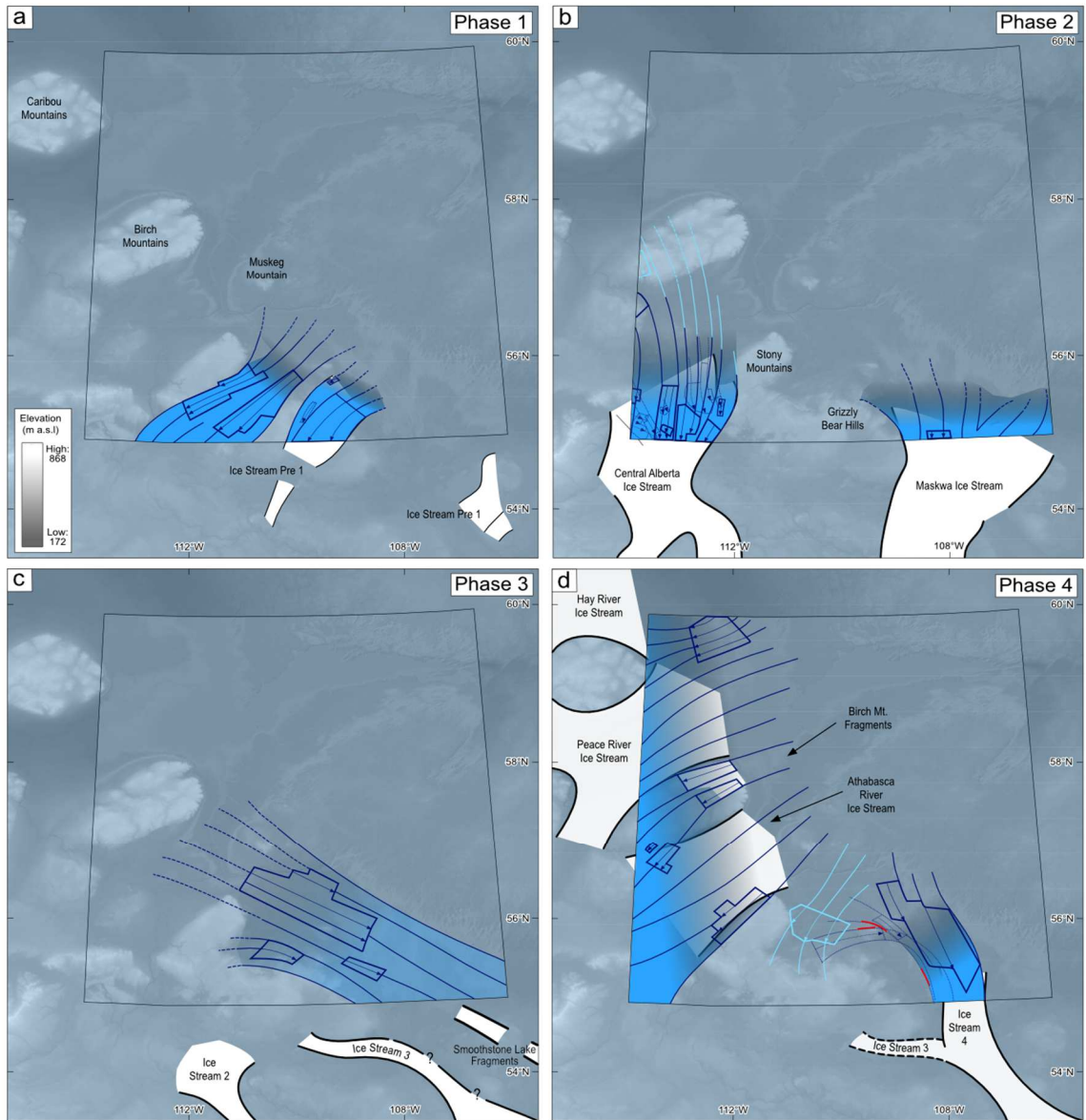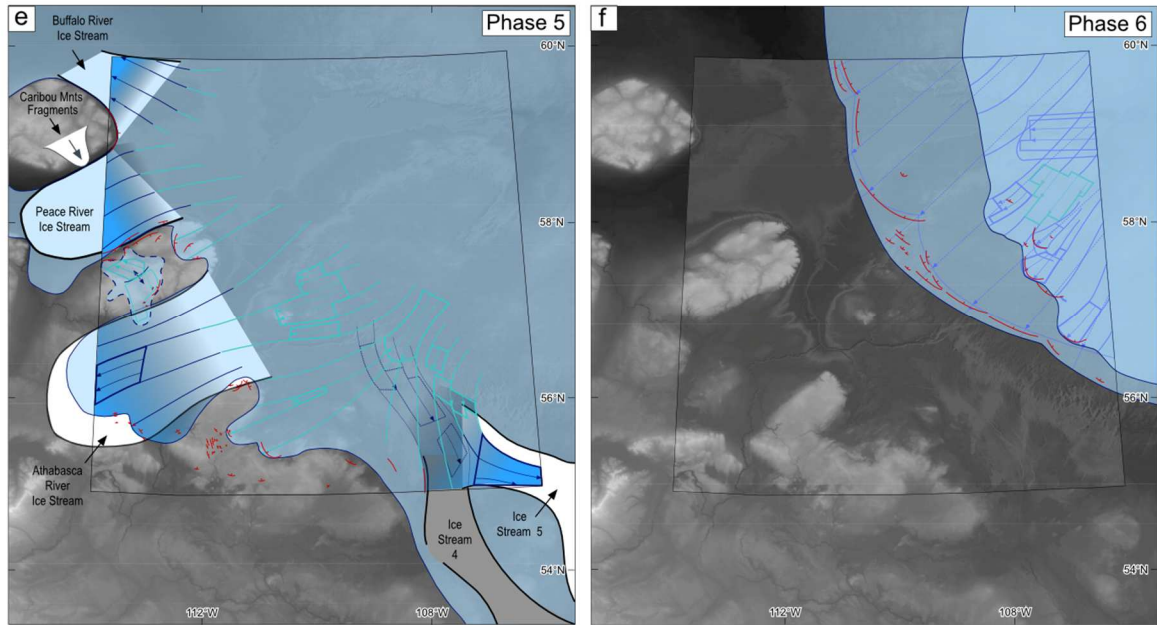
Figure 4.4: Ice sheet reconstruction of the interior partas of the SWLIS. (a) Lineations record ice flow from northeast to southwest over the Stony Mountains and Grizzly Bear Hills. This flow is delineated by faint drumlinoid ridges and flutings. (b) Topographically constrained north to south flow within the Athabasca and Churchill valleys. Flowsets comprise mega-scale glacial lineations, drumlins, meltwater channels and well-defined lateral margins. (c) Flowsets depict a shift to southeasterly ice streaming in the Churchill Valley. Flowsets are composed of mega-scale glacial lineations and flutings. (d) Ice streaming is active in the Peace, Athabasca and Churchill valleys. Northeast to southwest flow is also recorded on the Birch Mountains. Within the Churchill River Valley a progressive evolution from, SWW to SE, NW to SE and NW to S is recorded by flutings, drumlins and cross cut lateral shear margin moraines. (e) Flowsets record progressive thinning and retreat of the SWLIS within the Peace, Athabasca and Churchill valleys. Local ice flow is also recorded on the Birch and Caribou Mountains. (f) Broad unconstrained flowsets comprising almost entirely bedrock drumlins terminate at the Cree Lake Moraine.

4.5 Discussion

4.5.1 Dynamic evolution of the SWLIS

Using the geomorphic and flowset mapping in combination with existing palaeoglaciological models for the SWLIS marginal regions (Evans, 2000; Evans et al., 2008; Ross et al., 2009; Ó Cofaigh et al., 2010; Evans et al., 2012, 2014; Margold et al., 2015a, b), we reconstruct its ice stream evolution and subsequent deglaciation. To place this reconstruction into chronological context, we embed flowset and ice-marginal geomorphologic mapping into the deglacial chronology of Norris et al. (in prep). Using

assigned ages for moraines, we draw isochrones showing the geometry of the ice margin during its recession (figure 4.5).

Pre LGM ice flow pattern- Fragmentary evidence of fast ice flow draining to the southwest, relating to the period prior to CIS and LIS convergence is visible throughout the region. While this record is only preserved on upland areas, ice flow orientation consistently documents an ice source from a more easterly location than that displayed by LGM ice streams (see below). Little evidence is available relating to the pre-LGM ice sheet evolution within the region; nevertheless, a southwesterly ice flow orientation is compatible with previous continental reconstructions (Dyke et al., 2002; Batchelor et al., 2019) of pre-LGM buildup following MIS 3 minimum ice extents. Further south, overridden glaciotectonic composite ridges record the advance and proglacial thrusting of bedrock and pre-LGM deposits and importantly outline the lobate margins of the HPIS, CAIS and Maskwa IS as they advanced southwards (Evans et al., 2008, 2012, 2014). This configuration indicates that ice stream flow during ice sheet marginal advance into southern Alberta and Saskatchewan was directed by LIS/CIS convergence.

LGM ice flow pattern- During the LGM, the Maskwa IS extended from the onset zone within the interior SWLIS (upper Churchill Valley; Fig 4.5) and terminated on the north slopes of the Cypress Hills (Ross et al., 2009; Ó Cofaigh et al., 2010; Margold et al., 2015a, b; 2019). Based on the evidence presented by Ó Cofaigh et al. (2010), it is also likely that this system fed ice to smaller lobes south of the Cypress Hills, towards the LGM margin in Montana where its margin was contiguous with those of the CAIS and HPIS.

Following build-up of the western part of the Keewatin Ice Dome, and/or the migration of the dome to the west, and the build-up of the CIS-LIS convergence zone due to ice input of the CIS over the Rocky Mountains, flow of the CAIS and HPIS and Rocky Mountain IS commenced synchronously with the Maskwa IS (Evans et al., 2008. 2020; Ross et al., 2009; Ó Cofaigh et al., 2010; Margold et al., 2015a, b; 2019). Although the absolute age of these four ice streams is not constrained, the existing sub-till radiocarbon chronology within the SWLIS (Young et al., 1994; Ives et al., 2013) suggests that these ice streams were in operation for >5000 years. Unlike many parts of the LIS, LGM ice streams within the SWLIS were topographically unconstrained. This is likely a result of the large ice

thicknesses coupled with low topographic relief of the Interior Plains. The large topographically unconstrained convergent onset zone of the Maskwa IS in a region of substantial ice thickness attests to this. Comparatively, the tributary style onset zones CAIS/HPIS onset zone positioned between the Birch Mountains and Stony Mountains and in a region peripheral to maximum ice thicknesses demonstrates the effect a small change in internal controls can have on ice streams' dynamics.

Weakening and collapse of the LIS and CIS convergence zone 'ice saddle'- While the early part of the Late Glacial (18-15 ka) saw minimal reduction in the SWLIS western extent, the rate of ice margin retreat rapidly increased around 15 ka (Margold et al., 2019; in review). The CIS-LIS convergence zone began to thin, and their southern margins separated by ~14.9 ka BP (Margold et al., 2019; Norris et al., in prep). Additional ^{10}Be exposure ages from the northwest LIS indicate the northern portions of the convergence zone there underwent rapid surface lowering (4-6 m per year) by ~14.4 ka BP (Margold et al., 2019; in review). These results in addition to numerical model simulations (Gregoire et al., 2016) suggest that down wasting and separation of the CIS and LIS occurred rapidly; triggered by abrupt BA warming and coincident with MWP-1A (Margold et al., in review).

Concurrent with the separation of the LIS and CIS, a rapid ice flow reorganisation across the majority of the SWLIS is apparent in the palaeo-ice stream record. Abrupt changes in ice stream flow directions had already been in operation immediately prior to the separation, the clearest evidence for this is presented by Ó Cofaigh et al. (2010) who document the short-lived IS2 which replaced the north to south flow of the Maskwa IS. We suggest that the change from the topographically unconstrained system of the Maskwa IS to the topographically constrained southeastward flow reflects rapid thinning of the ice surface which inhibited flow across topographic highs. The sharp cross-cutting relationship between these ice streams provides further evidence for a rapid switch. Rapid ice sheet thinning is also supported within the interior SWLIS where a south-westerly flow sharply cross-cuts the onset zone of the Maskwa IS. A series of shear moraines mark this thinning and increased topographic control following this reorganisation (Fig. 4.5).

Following surface lowering of the LIS-CIS, rapid down-wasting and retreat characterised the initial deglaciation of the Interior Plains. Based on the onset location of south-eastward

flowing networks, we suggest these ice streams could only have been in operation during the period of rapid surface lowering of the LIS-CIS convergence zone and would have ceased shortly after initial LIS-CIS separation. Subsequently, the onset zones of these ice streams would have had insufficient input from the west to be sustained. The timing of initial LIS retreat across the Interior Plains suggests that following initial detachment with the CIS very rapid retreat rates continued to characterise SWLIS deglaciation in response to BA warming (Norris et al., in prep). We suggest that southeasterly-oriented ice flow networks, therefore, were only in operation for ~500 yrs before westerly ice flow towards the retreating ice margin replaced it.

Such a rapid reorganisation in ice flow configuration, resulting from initial BA warming, documents a major dynamic response to external forcing, which was then modulated by regional topographic control. The response of the SWLIS, flowing southwest from the Keewatin Ice Divide, is in stark contrast to its north-eastern sectors of the LIS which remain relatively stable during this period of abrupt climate change. While ice draining north-easterly from the Keewatin Ice Divide underwent periodic deglacial oscillations, between 14.6-12.9 ka, limited ice stream and/or deglacial changes occurred (see De Angelis and Kleman, 2005; England et al., 2006; Margold et al., 2018). Consequently, we suggest the stability of the north-eastern portions of the ice divide during the BA further highlights the likelihood of a direct climatic response of the SWLIS, with minimal influence from the opposing regions of the ice divide. Thus, the SWLIS represents a system in which there was little-to-no lag time in the ice sheet dynamic response to BA warming.

Deglaciation of the Interior Plains- Ice margin retreat chronology presented by Norris et al. (in prep) reveals deglaciation of the SWLIS began at ~14.9 ka and retreated >1200 km to its YD position in ≤ 2500 yrs, driven by rapid BA warming. The initial stages of retreat to the Beaver River lowland (600 km northeast of the former CIS-LIS convergence zone) records the highest rate of retreat (0.5 km yr^{-1}). Following this, retreat rates remain high (0.4-0.3 km yr^{-1}) until the southwestern margin reaches the Canadian Shield during the YD. Within the northwest part of the margin (Athabasca, Peace valleys) arcuate moraines record that ice retreated as a series of discrete lobes between upland regions. Farther east within the Churchill valley, the ice margin is markedly different maintaining a broader front. This

is likely the result of the less relief within the east, presumably meaning the ice margin did not retreat around local uplands; instead, it retreated as single broad front synchronous across much of eastern Alberta and western Saskatchewan.

Within the eastern part of the study area, subsequent to regional retreat, we identify evidence of a local dispersal centre confined to the Birch Mountains. In this location moraines and meltwater channels that descend into the Athabasca Valley, together with the spatial distribution of flowsets, are consistent with the development of a remnant local dispersal centre. Similar evidence has also been documented on the Swan Hills and Caribou Hills recording further local dispersal centres. Based on the morpho-stratigraphic signature of landforms on these uplands we suggest that these dispersal centres were active after their surrounding valleys were ice-free. Though no chronology is available to constrain the timing of these dispersal centres formation, based on their relative location compared to regional deglacial isochrones we suggest a centre on the Swan Hills could not have flowed into an ice-free valley until after ~13.5 ka BP while those on the locations and the Caribou Hills and Birch Mountains until after ~12.7 ka. Hence there is a possibility that these upland dispersal centres may have been invigorated as a localised response to Younger Dryas cooling.

Younger Dryas ice flow pattern- Minimal retreat, or stagnation of, the SWLIS at the Cree Lake Moraine during the Younger Dryas is proposed by Norris et al. (in prep). Resulting from this, ice streaming within the Interior Plains shut down as the ice sheet retreated onto the Canadian Shield. At this time, the change in the character of its bed (from weak, fast-ice-flow-conducive Quaternary till cover to more highly resistant bedrock), coupled with the shift in climate, brought about a different pattern of the ice drainage network with the final ice margin retreat of the SW LIS associated with much smaller deglacial ice streams and/or lobes. We suggest this marked contrast in ice sheet dynamics, during and following YD, contrast to other sectors of the LIS which see similar patterns of ice retreat spanning this time period. This contrast within the SWLIS is therefore likely a consequence of both external climate forcing coupled with regional topography and geology.
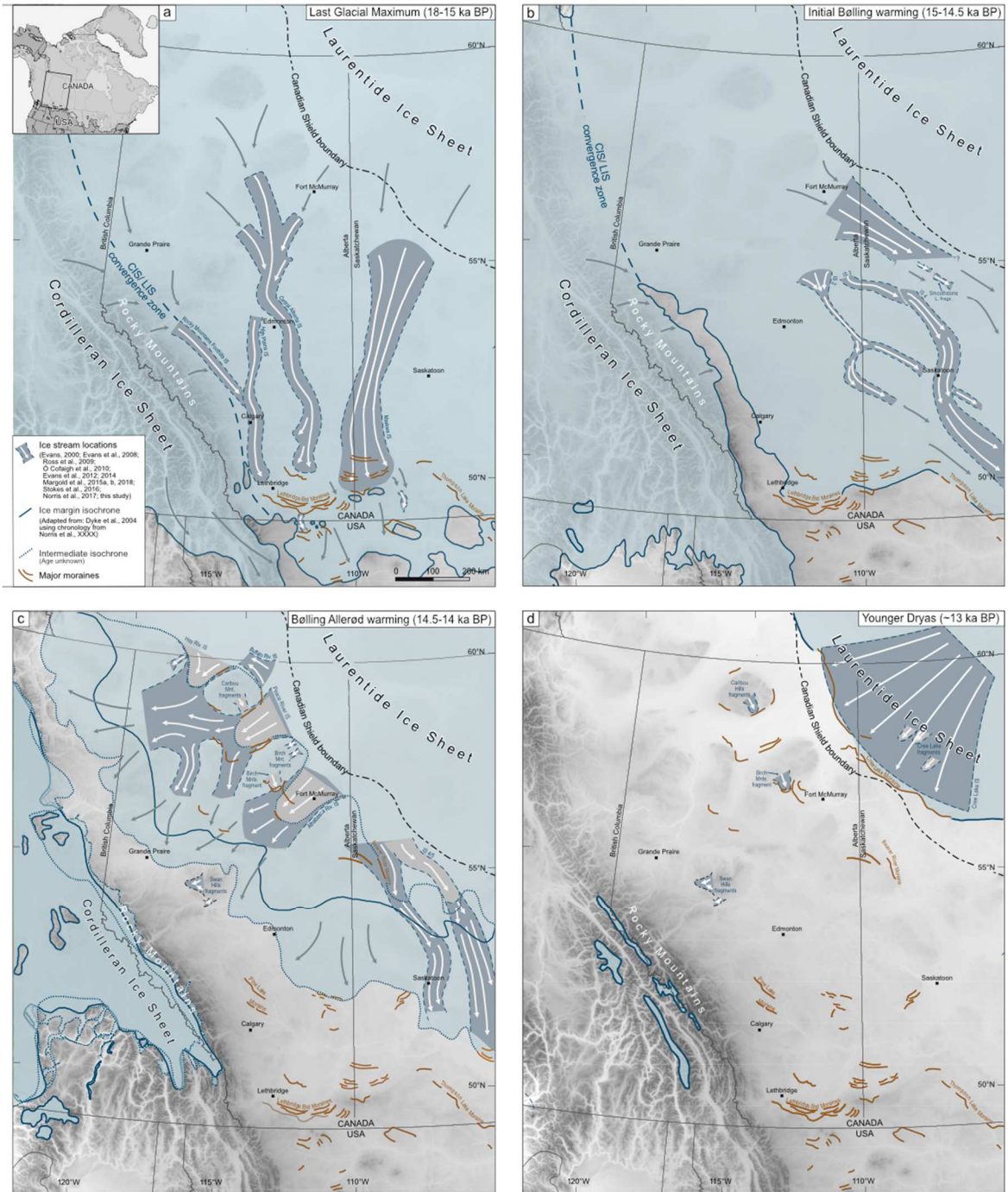
Figure 4.5: Deglacial ice flow dynamics of the southwestern Laurentide Ice Sheet (SWLIS). This reconstruction presents a comprehensive synthesis, collating pre-existing ice stream mapping from the peripheral region of the SWLIS (Evans, 2000; Evans et al., 2008; Ross et al., 2009; Ó Cofaigh et al., 2010; Evans et al., 2012, 2014; Margold et al., 2015a, b, 2018; Stokes et al., 2016) with ice streams presented in this study. Timing of using the ice flow reorganisations are constrained using the deglacial chronology of Norris et al. (in prep).

4.5.2 The geomorphic imprint of abrupt climate change

The regional deglacial imprint of the SWLIS documents the early active recession and warm polythermal snout lowering, followed by ice stream flow switching and ultimately by the collapse of a terrestrial ice sheet margin driven by abrupt climate change. The spatial variability in landforms diagnostic of these changing ice dynamics is best documented by the changes in the deglacial assemblages from south to north along the axes of the HPIS, CAIS and Maskwa IS. At the southern limits of these ice streams, extensive zones of inset push moraines dominate the landscape, most prominently the Lethbridge Moraine and the recessional moraines that onlap the Cypress Hills. Such landforms represent active recession, which appears to have characterised the margin of the HPIS until it had retreated as far north as the Bow River; in contrast, outside of the HPIS ice stream track, the active recession imprint within and north of the Lethbridge Moraine is interspersed with arcuate zones of aligned hummocks and ponds and ice-walled lake plains (controlled moraine) diagnostic of warm polythermal ice-marginal conditions (Evans et al., 2014).

North of the Oldman/Bow River, the landforms of the CAIS change to those of an ice stream trunk, as do those of the Maskwa IS to the east, both indicative of a N-S aligned ice stream shut down prior to the switch in fast flow corridors to a NW-SE alignment. These significant changes in ice stream flow directions, together with the widening and narrowing of ice stream tracks, resulted in the development of large swaths of inter-ice stream hummocky terrain containing the products of ice stagnation large glaciotectonic landforms and localised and/or fragmented arcuate moraine and fluting assemblages (e.g. Evans 2000; Evans et al. 2008, 2014, 2016, 2020; Ó Cofaigh et al. 2010). Further north again, within their onset zones (Athabasca and Churchill valleys) inset push moraines, eskers and meltwater channels once again dominate the landscape documenting representing active recession.

The juxtaposition of these varied geomorphic imprints (regions of ice stream switching and regions of stagnation terrain) directly corresponds with regions that have been crosscut by ice streams flowing southeast (see Fig 4.5). Thus, it appears this varied geomorphic imprint occurs as areas between ice streams become disconnected and stagnate. Based on this correspondence we suggest the rapidity of ice sheet retreat and the dynamic change

associated with this, act as a key control on the deglacial landform imprint. It thus seems likely that the juxtaposition of active retreat with stagnation terrain may be a valuable identifier of regions that underwent very rapid terrestrial deglaciation.

4.5.3 Implications for modern ice sheet and ice stream evolution

This study highlights the behaviour of highly dynamic ice streams networks in the SWLIS from the LGM to deglaciation. Our new compilation builds on existing research that demonstrates the SWLIS was characterised by a complex series of flow events. Such marked spatial and temporal shifts in flow trajectory imply that ice streaming may have been transitory in many cases. Our new data coupled with regional deglacial chronology provide insight into the timing of major reorganisations. These data indicate that three major flow shifts occurred over a short time frame of ~2500 yrs in direct response to CIS-LIS separation, driven by BA warming. We propose, due to the sharp cross-cutting nature of ice stream flowpaths and limited time period over which ice stream operated, that such changes occurred rapidly on decadal to centennial timescales.

While down wasting and retreat of the SWLIS was a result of rapid BA warming, its deglacial dynamics are also clearly modulated by local topographic controls. Furthermore, changes in regional geology during the Younger Dryas as the ice sheet retreated across the Canadian Shield highlight the role geological change can have on ice flow characteristics and margin configuration. Collectively these dynamic changes demonstrate the importance of considering not only external climate forcing but also internal factors (i.e. geology changes, regional topography, substrate controls) when assessing ice sheet evolution over time.

The changes recorded within the SWLIS provide an opportunity to access ice stream dynamics of a portion of a large continental-scale ice sheet during a period of rapid climatic change. The behaviour of the SWLIS, though operating on a much larger scale, show similarity to deglacial changes within the interior portions of the last British Irish Ice Sheet (Davies et al., 2019; Greenwood and Clark, 2009), and Late Weichselian Svalbard-Barents Sea Ice Sheet (Landvik et al., 2014). These examples collectively demonstrate that palaeo-

ice streams were extremely sensitive to external climate forcing and large-scale ice stream flow reconfigurations were commonplace. Based on the reconstruction we provide here and these analogs examples, we propose understanding ice streams dynamics is fundamental to access and predict the response of modern-day ice sheets in the future.

4.6 Conclusions

The timing of deglacial dynamics and ice flow behaviour of the SWLIS has so far been poorly constrained. Here, we build upon new ice margin chronological constraints (Norris et al., in prep) and existing ice stream mapping to document rapid palaeo-ice flow dynamics during the BA. Our reconstruction reveals a complex pattern of ice stream behaviour characterised by substantial flow switches and reconfiguration. Initial westward flow, most probably indicative of an evolving ice stream network during LGM advance, is confined to upland regions. An LGM system comprising the southward flow of Maskwa, CAIS and HPIS and signifies flow, unconstrained by topography. Following this our reconstruction shows a major glaciodynamic shift characterised by topographically controlled south-eastward flow constrained by palaeo-valley systems. This is subsequently replaced by a second switch in flow orientation to the southwest corresponding with an increase in the influence of topography on streaming flow during ice retreat. Using new chronological control on ice margin retreat (Norris et al., in prep) we suggest the SWLIS underwent reorganisation at least three times in $\leq$ 2500 yrs. These extremely rapid, decadal to centennial, changes in ice stream orientations demonstrate not only how ice streams can influence an ice sheet's broader response to external climate forcing, but also how ice sheets, through changes to ice flow regime changes are highly sensitive to rapid climate change.

4.7 References

Alley, R. B. and Bindschadler, R. A. 2001: The West Antarctic ice sheet: behavior and environment. *American Geophysical Union.*

Alley, R.B., Clark, P.U., Huybrechts, P. and Joughin, I. 2005: Ice-sheet and sea-level changes. *Science 310*, 456-460.

Andriashek, L. D. and Atkinson, N. 2007: *Buried channels and glacial-drift aquifers in the Fort McMurray region, northeast Alberta*. Alberta Energy and Utilities Board.

Andriashek, L. D. and Barendregt, R. W. 2017: Evidence for Early Pleistocene glaciation from borecore stratigraphy in north-central Alberta, Canada. *Canadian Journal of Earth Sciences*, *54*(4), 445-460.

Atkinson, N., Utting, D. J. and Pawley, S. P. 2014: *Glacial Landforms of Alberta. Alberta Geological Survey,* AER/AGS, Map 604.

Atkinson, N., Pawley, S. and Utting, D. J. 2016: Flow-pattern evolution of the Laurentide and Cordilleran ice sheets across west-central Alberta, Canada: implications for ice sheet growth, retreat and dynamics during the last glacial cycle. *Journal of Quaternary Science*, *31*(7), 753-768.

Batchelor, C. L., Margold, M., Krapp, M., Murton, D. K., Dalton, A. S., Gibbard, P. L., and Manica, A. 2019: The configuration of Northern Hemisphere ice sheets through the Quaternary. *Nature communications*, *10*(1), 1-10.

Carlson, A. E. and Clark, P. U. 2012: Ice sheet sources of sea level rise and freshwater discharge during the last deglaciation. *Reviews of Geophysics*, *50*(4).

Christiansen, E. A. 1979: The Wisconsinan deglaciation, of southern Saskatchewan and adjacent areas. *Canadian Journal of Earth Sciences, 16*, 913-938.

Clark, P.U., Dyke, A.S., Shakun, J.D., Carlson, A.E., Clark, J., Wohlfarth, B., Mitrovica, J.X., Hostetler, S.W. and McCabe, A. 2009: The Last Glacial Maximum. *Science* 325, 710-714.

Clark, P. U., Alley, R. B. and Pollard, D. 1999: Northern Hemisphere ice-sheet influences on global climate change. *Science*, *286*(5442), 1104-1111.

Davies, B. J., Livingstone, S. J., Roberts, D. H., Evans, D. J. A., Gheorghiu, D. M. and Ó Cofaigh, C. 2019: Dynamic ice stream retreat in the central sector of the last British-Irish Ice Sheet. *Quaternary Science Reviews*, *225*, 105989.

De Angelis, H., Kleman, J. 2005: Palaeo-ice streams in the northern Keewatin sector of the Laurentide ice sheet. *Annals of Glaciology. 42,* 135-144.

De Angelis, H. and Kleman, J. 2008: Palaeo-ice-stream onsets: examples from the north-eastern Laurentide Ice Sheet. *Earth Surface Processes and Landforms: The Journal of the British Geomorphological Research Group*, *33*(4), 560-572.

Dyke, A.S. and Prest, V.K. 1987: Late Wisconsinan and Holocene retreat of the Laurentide Ice Sheet. Geological Survey of Canada. Map 1702A.

Dyke, A. S., Andrews, J. T., Clark, P. U., England, J. H., Miller, G. H., Shaw, J. and Veillette, J. J. 2002: The Laurentide and Innuitian ice sheets during the last glacial maximum. *Quaternary Science Reviews*, *21*(1-3), 9-31.

Dyke, A. S., Moore, A. and Robertson, L. 2003: Deglaciation of North America. *Geological Survey of Canada, Open File 1574*.

England, J., Atkinson, N., Bednarski, J., Dyke, A.S., Hodgson, D.A. and Ó Cofaigh, C. 2006: The Innuitian Ice Sheet: configuration, dynamics and chronology. *Quaternary Science Reviews,* 25, 689-703.

Evans, D. J. A., Clark, C. D. and Rea, B. R. 2008: Landform and sediment imprints of fast glacier flow in the southwest Laurentide Ice Sheet. Journal of Quaternary. *Science*, 23, 249-272.

Evans, D. J. A., Young, N. J. P. and Ó Cofaigh, C. 2014: Glacial geomorphology of terrestrial-terminating fast flow lobes/ice stream margins in the southwest Laurentide Ice Sheet. *Geomorphology, 204,* 86-113

Evans, D.J.A. 2000: Quaternary geology and geomorphology of the Dinosaur Provincial Park area and surrounding plains, Alberta, Canada: the identification of former glacial lobes, drainage diversions and meltwater flood tracks. *Quaternary Science Reviews, 19* (10), 931–958.

Evans, D.J.A., Hiemstra, J. F., Boston, C. M., Leighton, I., Ó Cofaigh, C. and Rea, B. R. 2012: Till stratigraphy and sedimentology at the margins of terrestrially terminating ice streams: case study of the western Canadian prairies and high plains. *Quaternary Science Reviews*, *46*, 80-125.

Evans, D.J.A., Young, N. J. and Ó Cofaigh, C. 2014: Glacial geomorphology of terrestrial-terminating fast flow lobes/ice stream margins in the southwest Laurentide Ice Sheet. *Geomorphology*, *204*, 86-113.

Evans, D.J.A. 2005: The glacier-marginal landsystems of Iceland. *Iceland: Modern processes and past environments*, 93-126.

Fisher, T. G., Waterson, N., Lowell, T.V. and Hajdas, I. 2009: Deglaciation ages and meltwater routing in the Fort McMurray region, northeastern Alberta and northwestern Saskatchewan, Canada. *Quaternary Science Reviews, 28,* 1608-1624.

Froese, D.G., Young, J. M., Norris, S, L. and Margold, M. 2019: Availability and viability of the ice-free corridor and pacific coast routes for the peopling of the Americas. SAA Archaeological Record. 19, 27-33.

Golledge, N. R., Kowalewski, D. E., Naish, T. R., Levy, R. H., Fogwill, C. J. and Gasson, E. G. 2015: The multi-millennial Antarctic commitment to future sea-level rise. *Nature*, *526*(7573), 421-425.

Greenwood, S. L. and Clark, C. D. 2009: Reconstructing the last Irish Ice Sheet 2: a geomorphologically-driven model of ice sheet growth, retreat and dynamics. *Quaternary Science Reviews*, *28*(27-28), 3101-3123.

GSC Geological Survey of Canada 2008: Geoscience Data Reposi- tory. Available at: http://gdr.nrcan.gc.ca/index_e.php. Natural Resources Canada, Ottawa

Ives, J. W., Froese, D., Supernant, K. Yanicki, G. 2013: Vectors, vestiges and Valhallas: Rethinking the corridor. *Paleoamerican odyssey*, 149-169.

Hughes, A. L., Clark, C. D. and Jordan, C. J. 2014: Flow-pattern evolution of the last British Ice Sheet. *Quaternary Science Reviews*, *89*, 148-168.

Kleman, J. and Borgström, I. 1996: Reconstruction of palaeo-ice sheets: the use of geomorphological data. *Earth surface processes and landforms*, *21*(10), 893-909.

Kleman, J., Hättestrand, C., Borgström, I. and Stroeven, A. 1997: Fennoscandian palaeoglaciology reconstructed using a glacial geological inversion model. *Journal of glaciology*, *43*(144), 283-299.

Kleman, J., Jansson, K., De Angelis, H., Stroeven, A. P., Hatterstrand, C., Alm G. and Glasser, N.F. 2010: North American ice sheet build-up during the last glacial cycle, 115-21 kyr. *Quaternary Science Reviews, 29,* 2036-2051.

Landvik, J. Y., Alexanderson, H., Henriksen, M. and Ingólfsson, Ó. 2014: Landscape imprints of changing glacial regimes during ice-sheet build-up and decay: a conceptual model from Svalbard. *Quaternary Science Reviews*, *92*, 258-268.

Margold, M., Stokes, C.R. and Clark, C.D. 2015a: Ice streams in the Laurentide Ice Sheet: Identification, characteristics and comparison to modern ice sheets. Earth Sci. Rev. 143, 117e146.

Margold, M., Stokes, C.R., Clark, C.D. and Kleman, J., 2015b: Ice streams in the Laurentide Ice Sheet: a new mapping inventory. J. Maps 11, 380e395.Margold, M., Stokes, C. R., and Clark, C. D. 2018: Reconciling records of ice streaming and ice margin retreat to produce a palaeogeographic reconstruction of the deglaciation of the Laurentide Ice Sheet. *Quaternary Science Reviews 189*, 1-30.

Margold, M., Gosse, J. C., Hidy, A. J., Woywitka, R. J., Young, J. M. and Froese, D. 2019: Beryllium-10 dating of the Foothills Erratics Train in Alberta, Canada, indicates detachment of the Laurentide Ice Sheet from the Rocky Mountains at~ 15 ka. *Quaternary Research 92*(2), 469-482.

Munyikwa, K., Feathers, J.K., Rittenour, T.M. and Shrimpton, H.K. 2011: Constraining the late Wisconsinan retreat of the Laurentide ice sheet fromwestern Canada using luminescence ages from post- glacial aeolian dunes. Quaternary Geochronology 6, 407–422.

Munyikwa, K., Rittenour, T. M. and Feathers, J. K. 2017: Temporal constraints for the Late Wisconsinan deglaciation of western Canada using eolian dune luminescence chronologies from Alberta. *Palaeogeography, palaeoclimatology, palaeoecology*, *470*, 147-165.

Norris. S. L., Margold, M. and Froese, D. G. 2017: Glacial landforms of northwest Saskatchewan. *Journal of Maps*. 13:2, 600-607.

Ó Cofaigh, C., Evans, D. J. A. and Smith, R. 2010: Large-scale reorganization and sedimentation of terrestrial ice streams during late Wisconsinan Laurentide Ice Sheet deglaciation. *Geological Society of America 122*, 743-756.

Prest, V. K. 1968: *Nomenclature of moraines and ice-flow features as applied to the glacial map of Canada* (p. 32). Department of Energy, Mines and Resources.

Rignot, E., and Thomas, R. H. 2002: Mass balance of polar ice sheets. *Science*, *297*(5586), 1502 1506.

Rignot, E., Bamber, J. L., van den Broeke, M. R., Davis, C., Li, Y., Van De Berg, W. J., and Van Meijgaard, E. 2008: Recent Antarctic ice mass loss from radar interferometry and regional climate modelling. *Nature Geoscience 1*(2), 106-110.

Rignot, E., Velicogna, I., van den Broeke, M.R., Monaghan, A. and Lenaerts, J.T.M. 2011: Acceleration of the contribution of the Greenland and Antarctic ice sheets to sea level rise. *Geophysical Research Letters 38*, L05503.

Ritz, C., Edwards, T. L., Durand, G., Payne, A. J., Peyaud, V. and Hindmarsh, R. C. 2015: Potential sea-level rise from Antarctic ice-sheet instability constrained by observations. *Nature 528*(7580), 115-118.

Ross, M., Campbell, J. E., Parent, M. and Adams, R. S. 2009: Palaeo-ice streams and the subglacial landscape mosaic of the North American mid-continental prairies. *Boreas 38*, 421-439.

Stokes, C. R., and Clark, C. D. 2002: Are long subglacial bedforms indicative of fast ice flow?. *Boreas*, *31*(3), 239-249.

Stokes, C.R., Tarasov, L., Blomdin, R., Cronin, T., Fisher, T.G., Gyllencreutz, R., Hättestrand, C., Heyman, J., Hindmarsh, R.C.A., Hughes, A.L.C., Jakobsson, M., Kirchner, N., Livingstone, J.J., Margold, M., Murton, J.B., Noormets, R., Peltier, W.R., Peteet, D.M., Piper, D.J.W., Preusser, F., Renssen, H., Roberts, D.H., Roche, D.M., Saint-Ange, F., Stroeven, A.P. and Teller, J.T. 2015: On the reconstruction of

palaeo-ice sheets: recent advances and future challenges. *Quaternary Science Reviews 125*, 15-49.

Wolfe, S., Huntley, D. and Ollerhead, J. 2004: Relict late Wisconsinan dune fields of the northern Great Plains, Canada. Géographie physique et Quaternaire 58, 323–336.

Young, R. R., Burns, J. A., Smith, D. G., Arnold, L. D. and Rains, R. B. 1994: A single, late Wisconsin, Laurentide glaciation, Edmonton area and southwestern Alberta. *Geology*, *22*(8), 683-686.

CHAPTER 5: GEOMORPHIC, SEDIMENTARY AND HYDRAULIC RECONSTRUCTION OF A GLACIAL LAKE OUTBURST FLOOD IN NORTHERN ALBERTA, CANADA

5.1 Introduction

Glacial lake outburst floods played a significant role in landscape evolution of the Interior Plains during deglaciation of the Laurentide Ice Sheet (LIS) (Kehew, 1982; Kehew and Lord, 1986, 1987; Lord and Kehew, 1987; Fisher and Smith, 1994; Kehew and Teller, 1994; Fisher et al., 2009; Fisher and Lowell, 2017). Meltwater from the LIS, impounded by the region's reverse topographic slope, formed large interconnected systems of proglacial lakes draining across topographic thresholds and carving spillways. This resulted in the failure of unstable dams and outburst floods. The outburst floods frequently fed other topographically lower proglacial lakes, which in response also drained, producing a 'domino' like sequence of lake-drainage floods (Kehew and Clayton, 1983). Flow during these catastrophic events was of high magnitude, short-lived and very erosive, carving spillways (Kehew and Lord, 1986). Reconstructions of these events infer that the freshwater output from large glacial lakes associated with the LIS had the potential to cause abrupt changes in global climate via the disruption of ocean circulation patterns (Broecker et al., 1989; Clark et al., 2001; Fisher et al., 2002; Teller et al., 2002). Despite the existence of many spillways and the inferred broader impact of outburst floods, extensive sedimentary deposits are relatively rare, limiting palaeohydraulic reconstruction of flood deposits within the Interior Plains.

Here, we examine the geomorphology, sedimentology and palaeohydraulics of a catastrophic flood caused by the sudden drainage of an ice-dammed lake, glacial Lake Algar in north-central Alberta (Fig. 5.1). We assess the nature and dynamics of the flood by analysis of the identified spillway and other well preserved erosional and depositional features. We reconstruct the hydraulics of the outburst flood using a GIS-based model and a Digital Elevation Model (DEM) derived from Shuttle Radar Topography Mission (SRTM) data. Peak discharge is then inferred within a HEC-RAS model constrained by field evidence of the high water stage. We then assess the significance of this event in the

context of both wider flood dynamics on the northern Plains, and the deglacial history of the region.

5.2 Regional setting

The modern-day Beaver River cuts through the Sand River, Cold Lake and Meadow Lake regions of Alberta and Saskatchewan, extending from its source (Beaver Lake, Alberta) ~240 km into northwest Saskatchewan. The river occupies a wide (0.2-0.9 km), deep (40 m), steep-walled channel (herein referred to as the Beaver River Channel) (Fig. 5.1). A comparison of the modern-day river to the deeply incised channel suggests a considerably higher magnitude discharge was needed to explain its size and morphology (Dury, 1976). The formation of the western portion of the channel has been attributed to the drainage of a large proglacial lake, glacial Lake Algar (Utting et al., 2015) (Fig. 1). The lake first drained to the east, forming the western portion of the Beaver River channel, after which the lake drainage became deflected southwards, through an ice walled channel and into the Kehiwin Channel (Fig. 1).

While a clear formation mechanism for the western portion of the Beaver River Channel exists, to date only a brief mention of the eastern Beaver River Channel, as a meltwater channel feeding glacial Lake Meadow, between 13.9 and 13.3 ka BP (12-11.5 ^{14}C ka BP; Dyke et al., 2003) has been made (Christiansen, 1979; Schreiner, 1983; Andriashek and Fenton, 1989). Furthermore, no explanation has been proposed to adequately explain the size and morphology of the eastern portion of the channel. This portion of the Beaver River Channel is partially incised in predominantly thick sand and clay-rich glacial deposits (see Andriashek and Fenton, 1989). In some areas, it has also incised through a thin veneer of sand and gravel which overlie the glacial deposits (Fig. 5.1). Approximately 50 km west of the Alberta/Saskatchewan border (Fig. 5.1), the channel dissects a ~10 km wide area of streamlined and morainic terrain. This zone is dominated by hummocky mounds, lakes and flutings associated with an area of localised fast ice flow, at its highest rising 10-12 m above the valley floor on either side (herein termed moraine barrier; see Fig. 5.1). Surrounding the channel the moraine barrier appears heavily eroded to a distance of ~2.5 km on both sides. Built into the eastern portion of the Beaver River Channel, 12 gravel and sand deposits are visible. These deposits are large pendant bars that occur mostly at the

inside of channel bends and constitute primary bedforms (Lord and Kehew, 1987), mostly unmodified post-deposition.

Across the Canadian Prairies, morphologically and structurally similar deposits and landforms to those in the Beaver River region have been attributed to large subglacial meltwater events (e.g. Sjogren and Rains, 1995; Munro-Stasiuk, 1999; Beaney, 2002). However, in contrast to these events, the Beaver River Channel links two proglacial lakes, Algar and Meadow. Both lakes are demarcated by shorelines (Christiansen, 1979; Schreiner, 1983; Fisher and Smith, 1994; Utting et al., 2015) and in the case of glacial Lake Meadow a delta occurs where the Beaver River Channel enters the lake. The geographic context for flood sediments and geomorphology clearly documents a former ice margin. Multiple ice-marginal positions have been mapped (Utting et al., 2015) which deflect waters from glacial Lake Algar first to the south and then progressively retreating north of the Beaver River Channel. For these reasons, we consider it appropriate to interpret the channel morphology and sedimentology in the context of proglacial and marginal meltwater discharge.
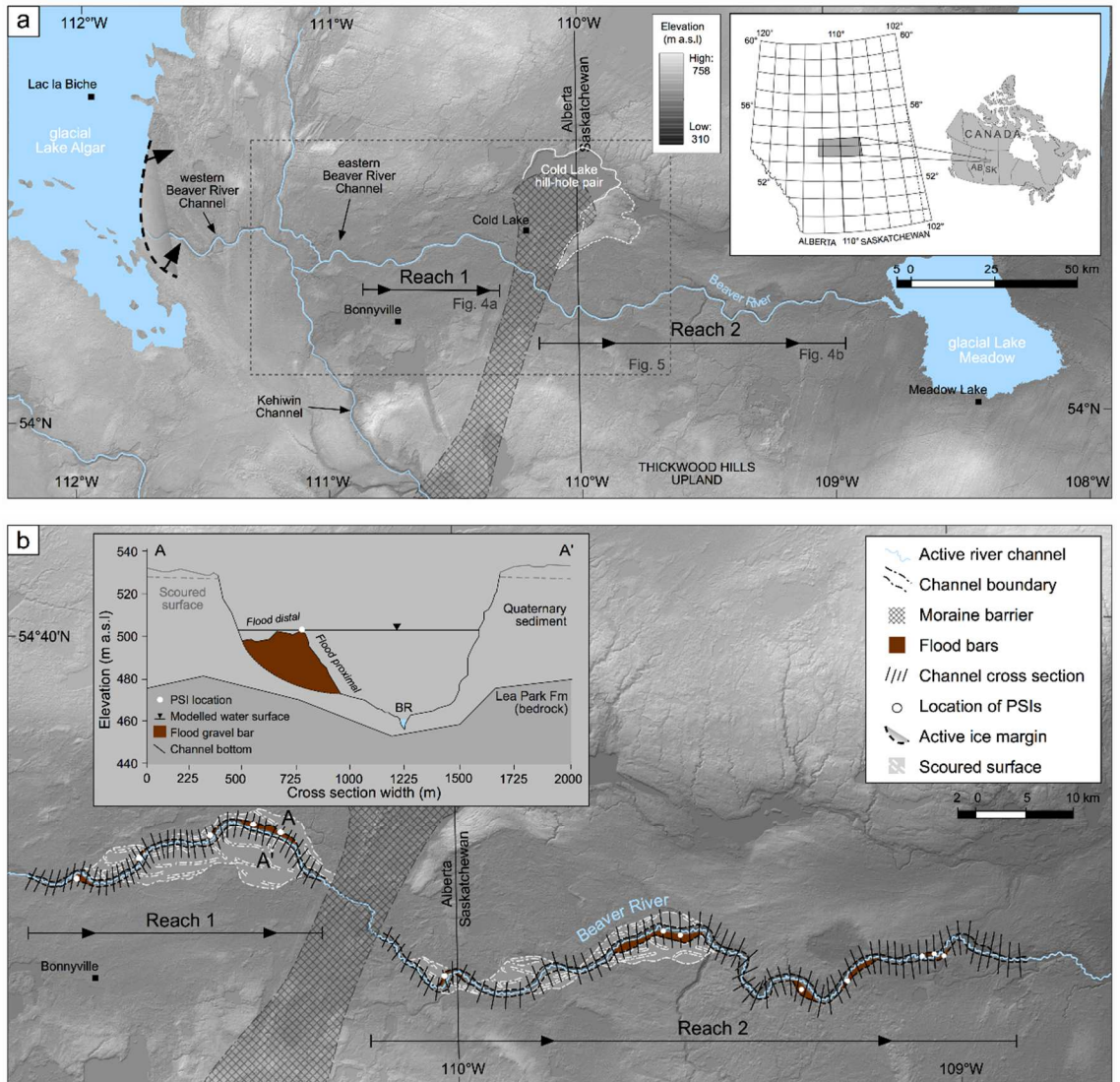
Figure 5.1: A. Map of the study area showing the locations of modelled reaches in the Beaver River Channel. Flow direction is shown by the reach arrows. The maximum extent of glacial Lake Algar is shown west of the Beaver River Channel and glacial Lake Meadow to the east (from Utting et al., 2015). The locations of Figs. 5.4A, 5.4B and 5.5 are marked. B. Step-backwater reach cross sections. The locations of PSIs are indicated with white circles. Cross-sectional profile for A-A' is displayed as an inset diagram, showing the modelled water surface and deposited PSI.

5.3 Methods

5.3.1 Glacial-lake outburst indicators

Channel morphology, erosional landforms, outburst flood deposits and the locations of palaeostage indicators (PSIs) were identified from a combination of field mapping, aerial photography, SRTM (1-arc, 30 m) and, where available, LiDAR (10 m) imagery. We use the crest of pendant bars as PSIs within the channel (Table 5.1). The location and elevation (m a.s.l.) of the PSIs were recorded using a hand-held GPS and loaded into ArcMap in order to utilise them in hydraulic modelling (see Table 5.1 for PSI summary). We consider these features to have formed rapidly during steady flow conditions that followed the initial flood wave subsequent to flood initiation. These PSIs thus provide a conservative estimate of peak discharge.

Table 5.1: Locations and elevations of PSIs along the Beaver River Channel.

PSI type	Latitude[1] (decimal deg.)	Longitude[1] (decimal deg.)	Elevation[1] (m a.s.l.)	Downstream distance in modelled reach[2] (km)
Pendant bar crest	54.3845	-110.7546	519	5.1
Pendant bar crest	54.4075	-110.6313	520	15.3
Pendant bar crest	54.4385	-110.4840	531	28.6
Pendant bar crest	54.4473	-110.4149	524	31.4
Pendant bar crest	54.4402	-110.3784	525	34.5
Pendant bar crest	54.2556	-110.0304	512	15.0
Pendant bar crest	54.3070	-109.5558	490	48.6
Pendant bar crest	54.3064	-109.5330	502	60.5
Pendant bar crest	54.2433	-109.2956	510	85.2
Pendant bar crest	54.2553	-109.2167	506	90.3
Pendant bar crest	54.2790	-109.0460	486	100.5
Pendant bar crest	54.2766	-109.0452	485	102.5
Pendant bar crest	54.2724	-109.0421	485	105.3

[1] Location and elevation of PSIs recorded in-field using a hand-held GPS
[2] Downstream distance within HEC-RAS modelled reaches (Fig. 5.4)

Where exposed, the internal structure of deposits was examined. The sedimentology of 16 exposures in 12 gravel pits was recorded, with vertical profile logging or section sketches. Sediment particle (b-axis) measurements were taken at 6 gravel pits within the flood reaches (extensive aggregate excavation limited the measurement of *in situ* samples at all 12 bars). Because all particles (particularly boulder-sized clasts) were not in their original depositional position, clast orientation was not measured, only the b-axis and roundness were recorded.

67

5.3.2 Step-backwater modelling

5.3.2.1 Pre-processing. – A one-dimensional, step-backwater method in conjunction with PSIs was employed in HEC-RAS (Horrit and Bates, 2002) to model palaeoflood flow-behaviour. Topographical data for use in the hydraulic model were extracted from SRTM imagery. Incomplete spatial coverage meant LiDAR imagery was not utilised for the hydraulic modelling. Using HEC-GeoRAS 3.1 as an extension within ArcGIS 10.3, a total of 176 cross-sections were extracted from the DEM (spaced 750 m apart) along two sections of the channel.

5.3.2.2 Model development. – Using the established flow geometry and determined cross sections, a steady state flow simulation in a 'mixed flow regime' mode produced a hydraulic reconstruction of the outburst flood for each of the two reaches. A water-surface elevation associated with peak discharge was then calculated by running the hydraulic model until the modelled water surface at respective cross-sections best matched the PSIs.

Flow energy losses are accounted for in HEC-RAS using coefficients for flow expansion and contraction and using a roughness coefficient (Manning's *n*). In accordance with previous outburst flood reconstructions (Herget, 2005; Carling et al., 2010; Margold et al., 2018), to account for the uncertainty associated with assigning Manning's *n* values in a palaeoenvironment, a range of *n* values were used from 0.025 to 0.075. Pre-defined expansion and contraction coefficients 0.1 and 0.3 respectively were retained due to the uniform channel width in both reaches (Hydrologic Engineering Center, 2001).

Table 5.2: Predicted hydraulic variables from sediment particle b-axis calculations.

| Reach location | | | | Hydraulic parameter | | | | | | |
| | | | | Costa (1983) | | | O'Connor (1993) | | | Ferguson (1994) |
Lat. Long. (dd)[1]	Reach downstream distance (m)[2]	d_{max} (d, m)[3]	d_{50} (d, m)[4]	Threshold velocity (V_c, m s^{-1}) $V_c = 0.18d^{0.49}$	Peak discharge (Q, m^3 s^{-1}) Q = AV — Cross sectional area (A, m^2)	Q	Threshold velocity (V_c, m s^{-1}) $V_c = 0.29d^{0.6}$	Peak discharge (Q, m^3 s^{-1}) Q = AV — Cross sectional area (A, m^2)	Q	Peak discharge (Q, m^3 s^{-1})
Reach 1										
54.4075- 110.6313	15.3	0.15	0.07	2.1	8745	18 000	1.5	8745	13 000	22 000
54.4061 - 110.6301	28.6	0.28	0.04	2.8	9639	27 000	2.1	9639	21 000	24 000
54.4477 - 110.4346	31.4	0.31	0.05	3.0	7994	24 000	2.3	7994	18 000	18 000
Reach 2										
54.2698 - 110.0260	15.7	1.66	0.40	6.8	9309	63 000	6.2	9309	58 000	270 000
54.3080 - 109.5453	61.2	1.40	0.37	6.2	14 615	92 000	5.6	14 615	82 000	260 000
54.2604 - 109.2072	90.6	1.52	0.29	6.5	11 906	77 000	5.9	11 906	70 000	150 000
54.2792 - 109.0458	102.5	1.30	0.25	5.8	10 007	60 000	5.3	10 007	54 000	140 000

[1] Location and elevations recorded in-field using a hand-held GPS
[2] Downstream distance within HEC-RAS modelled reaches (Fig. 5.4)
[3] Refers to the mean of the b-axis measured from the five largest clasts found *in situ* as each site
[4] Refers to the median grain size of the 100 measured clasts

5.3.3 Local hydraulic variables derived from particle diameter

To provide a comparable, independently derived calculation of key hydraulic variables (velocity and peak discharge) used in step-backwater modelling, variables were also derived from the intermediate (b-axis) diameter of the five largest sediment particles at each bar (d_{max}) (Costa, 1983; Williams, 1983; O'Connor, 1993; Komar, 1987; Ferguson, 1994). Only the five largest *in situ* sediment particles were measured to avoid underestimating hydraulic variables, as smaller sediment particles on the bar surface may have been deposited during lower discharges subsequent to peak discharge (O'Connor, 1993).

Empirical relationships for determining hydraulic variables in this way have been derived by multiple authors. Only those datasets that incorporate a range of particle diameters concordant with those observed in the Beaver River Channel are applied (Costa, 1983; O'Connor, 1993; Komar, 1987; Ferguson, 1994) (Table 5.2).

Following Costa (1983), velocity can be estimated by:

$$V_c = 0.18d_{max}^{0.49} \hspace{3cm} (1)$$

where V_c = threshold velocity, and d_{max} is mean of the b-axis of the five largest sediment particles in mm

An alternative regression-derived function is provided by O'Connor (1993):

$$V_c = 0.29d_{max}^{0.6} \hspace{3cm} (2)$$

where V_c = threshold velocity, and d_{max} is mean of the b-axis of the five largest sediment particles in mm

Using the relationships derived by Costa (1983) and O'Connor (1993) discharge along the Beaver River Channel was estimated using the continuity equation:

$$Q = A \ V \hspace{3cm} (3)$$

where Q = discharge (m³/s), A = channel cross sectional area (m²) and V = mean flow velocity (m/s).

The final method for determining discharge (critical unit discharge (p_c)) is provided by Komar (1987) as reworked by Ferguson (1994). This method is based on the principle that on a bed of mixed clast sizes, flow competence is a function of clast-size relative to the median diameter of the deposit as a whole:

$$q_c = a \, d_{50}^{1.5} \, (d_{max}/d_{50})^{(1-x)(c+1.5)}/S^{(c+1)} \tag{4}$$

$$\text{where } a = m(8g)^{0.5}((p_s/p-1) \, \tau_c*_{50})^{c+1.5} \tag{5}$$

where d_{50} is the median grain size of a sample of 100 clasts at each site (see Table 5.2), S is the local channel gradient (m m⁻¹), *ps* is the density of clasts (2650 kg m⁻³), *p* is the density of water at 4 degrees Celsius (1000 kg m³), g is gravitational acceleration, x is the hiding factor (x = 0.9; Parker, 1990), m and c are constants related to a specified flow resistance relationship (c = 0.37, m = 1.14; Thompson and Campbell, 1979), and τ_c*_{50} is the critical dimensionless shear stress (0.045).

5.4 Results

5.4.1 Channel morphology and outburst deposits

Scoured surfaces and inner channel.- Based on in-field observations and LiDAR/SRTM imagery reviewed in ArcMap, the Beaver River Channel comprises two major sections: a deep inner channel and a scoured outer surface. The deep (40 m) inner channel is wide (0.2-0.9 km) and flat-bottomed. The channel has steep walls, and isolated coarse gravel deposits (pendant bars) form intermittent terraces along its length. Outburst sediments are not visible along the bottom of the inner channel. The scoured surface is discontinuous and occurs typically at pendant bars. These surfaces are often capped by a littering of boulders with a b-axis of 0.7-2 m.

The largest area of scoured surface occurs immediately west of the ~10 km wide moraine barrier (Fig. 5.1). Here a ~4 km wide area of isolated scoured surfaces is dissected by shallow (1-3 m deep) anastomosing channels. Borehole logs from the scoured surface

71

(AGS-SRT-11 [54.3624°N, 110.6307°W], AGS-SRT-6, [54.4131°N, 110.4366°W], AGS-SRT-30 [54.3404°N, 110.4051°W]) comprise ~4 m of sorted sands and gravel overlying >50 m of sandy or clay-rich diamict.

5.4.2 Pendant Bars

Based on mapping from LiDAR/SRTM imagery, 12 pendant bars are visible within the Beaver River Channel (Fig. 5.1). Pendant bars, mostly unmodified by erosion, have been deposited mostly at the inside of channel bends. Bars form terraces, with a gentle reverse distal slope leading to a steep proximal face (Fig. 5.1). Average bar dimensions are 2 km long, 0.5 km wide, and 20 m thick.

The sedimentological characteristics of pendant bars can be characterised as two distinct groups (summarised in Fig. 5.3). Pendant bars in the first 40 km (Reach 1; Fig. 5.1) of the eastern Beaver River Channel, upflow of the moraine barrier, consist of 4-7 m of large-scale, cross-bedded downstream-directed gravels interspersed with granular and coarse sand beds. In the proximal portions of these bars this unit is overlain by horizontally-bedded coarser gravels (Figs 5.2A, 5.3A). The petrology of gravels is varied, with an abundance of metamorphic and igneous rocks within the largest fraction. Rip-up clasts are also interspersed within the gravels. These clasts are recorded (though infrequently) at all gravel bars, and range in diameter from 7-30 cm. Rip-up clasts contain clay-rich diamict, occasional pebbles and exhibit a thin armour of coarse gravels.

Large-scale crude cross-bedding in the proximal parts of bars exhibits medium to thick (30-60 cm) beds of poorly sorted, silt to cobbles (>20 cm in diameter) with a dip of 10-20° (Figs 5.2A, 5.3A). At these locations, cross-beds grade into 2-2.5 m of horizontally bedded (30-100 cm) coarser gravels (maximum clast size of 20-30 cm). Maximum clast size within the horizontally bedded gravel unit decreases downstream between bars within the 40 km reach. Away from proximal zones, cross-beds are thinner (>50 cm thick) and become finer away from the main channel, comprising clasts with a maximum diameter >15 cm (Figs 5.2B, 5.3B). At some locations, a 20-30 cm unit of thin (<10 cm) cross-bedded sands overlie the gravels, though this unit is not present at all bars (Fig. 5.3B).

A 1-1.5 m unit of thinly laminated sand, silt and clay caps gravels in the most distal part of one pendant bar (Figs 5.2C, 5.3B). This unit typically consists of rhythmically bedded sand/silt and clay-silt couplets. Individual couplets are 2-15 cm thick with the clayey-silt layer constituting 10 cm of the couplet. Thicker couplets contain climbing ripples as well as soft sediment deformation structures (flames and ball-and-pillow structures) (Figs 5.2D, 3B). Notably, in two places, this unit is overlain by a thin >50 cm diamict. However, based on its sporadic occurrence and the considerable aggregate excavation at this site it seems highly likely the diamict is the result of ongoing land reclamation on this pendant bar. If the diamict at the section interpreted as moved into place during aggregate excavation is in fact *in situ* till, the sediments composing this pendant bar would be an erosional remnant, that was deposited in a pre-last glacial channel, overridden by the glacier ice and subsequently incised by the present channel.

Within the remaining 120 km of the eastern Beaver River Channel (Reach 2; Fig. 5.1) pendant bars differ sedimentologically (Fig 5.3). The proximal zones of individual bars comprise massive, inversely graded, matrix-supported cobble and boulder gravel (up to 1-2.3 m in diameter) (Figs 5.2E, 5.3C). Coarser clasts are weakly imbricated, but the gravel is otherwise structureless. The gravel is sedimentologically identical to that described above and rip-up clasts are also present, though in much higher frequencies and often larger in diameter (10-50 cm). The composition of the bars is nearly identical in appearance from one bar to another, however within a single bar gravel fines markedly away from the main channel, i.e. from proximal to distal (Figs 5.3C, 5.3D).

In the distal portions of these bars, finer-grained gravel (30 to 120 mm) containing cross-stratification and lenses of horizontally stratified sands and fine gravel are present (Fig. 5.3D). In some places, a thin 5-10 cm unit of planar cross-bedded sand overlies the gravel. However, at the majority of bars this unit is not present and the surface of bars, especially at their proximal portions, is covered with a littering of boulders (Fig. 5.2F).

5.4.3 Hydraulic analysis

Step-backwater modelling was performed for Reach 1 (40 km) and Reach 2 (120 km) of the eastern Beaver River Channel (see Fig. 5.1 for reach locations). These sections of the channel were selected for their high PSI density and minimal flow irregularities. Step-backwater calculations for these reaches provide discharge estimates that closely coincide with PSI evidence at modelled minimum discharges of 14 000-21 000 m^3 s^{-1} (Reach 1) and 23 000- 40 000 m^3 sec^{-1} (Reach 2) based on a Manning's n range of 0.025-0.075 (minimum peak discharge rounded to the nearest 500 m^3 s^{-1} at which pendant bars are submerged) (Fig. 5.4). Within Reach 1 the fit was good (±4 m) within all sections of the reach. Within Reach 2 the fit was good (±5 m) within the upper 75 km of the modelled reach, whereas within the lower 45 km this discharge produced a water surface 3-4 m below the PSI evidence. Nevertheless, the best-fit water surface was achieved with a 23 000- 40 000 m^3 s^{-1} peak discharge.

In addition to step-backwater modelling within HEC-RAS, we applied three empirical equations to independently calculate key hydraulic variables from sediment particle b-axis data. Within Reach 1, empirical equations yield hydraulic variables (velocity and peak discharge) in the same order of magnitude to those obtained from HEC-RAS modelling (Table 5.2). In contrast, within Reach 2 hydraulic variables show large discrepancies. These values show on average a fivefold increase compared to those derived from HEC-RAS.
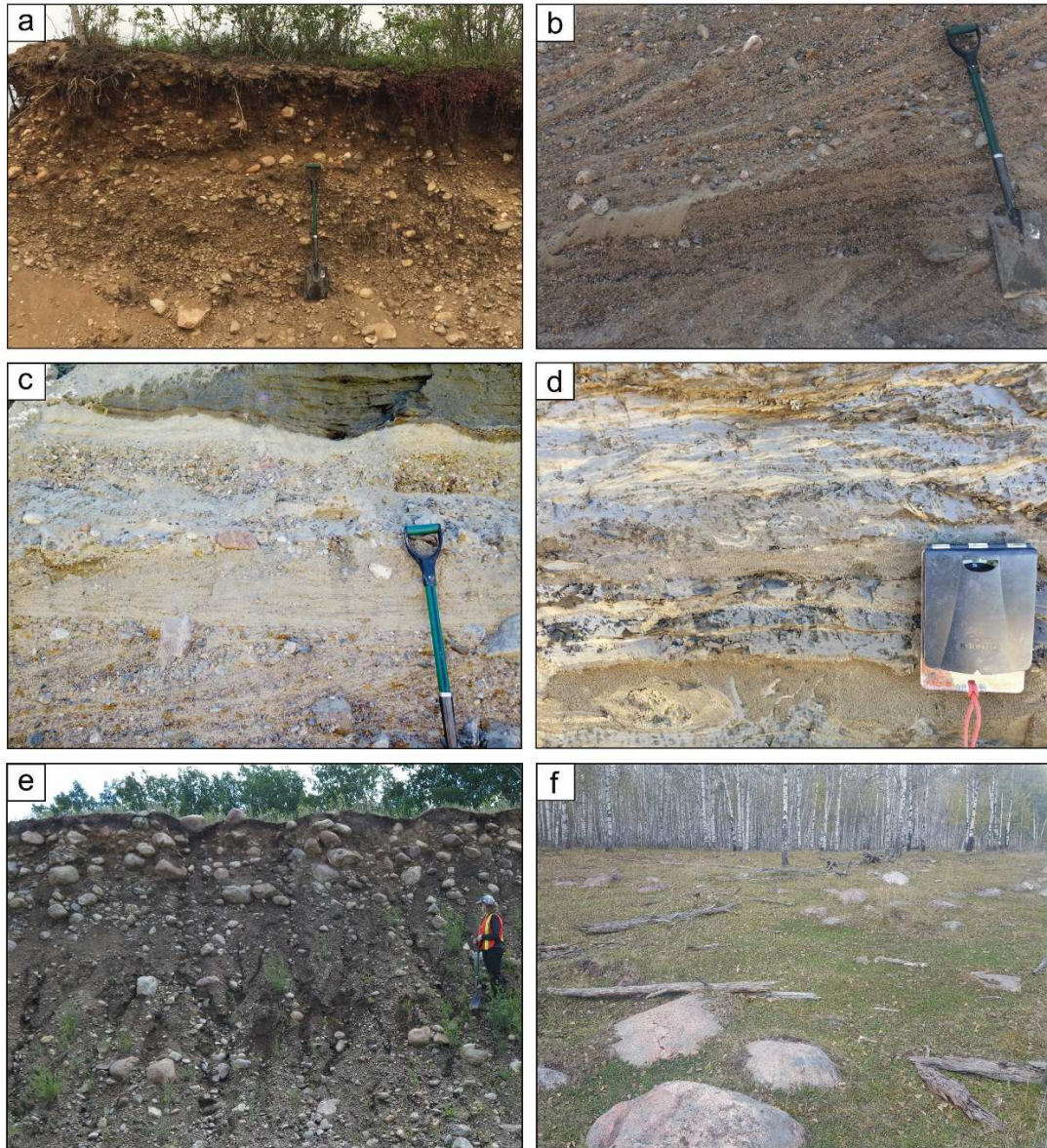
Figure 5.2: Flood deposits observed at pendant bars along the Beaver River Channel. A. Exposure from a gravel pit on the proximal parts of a pendant bar (54.4073°N, 110.6313°W) located upstream of the moraine barrier. Clast supported gravels with downstream-directed cross-bedding overlain by coarser horizontal bedded gravel. Direction of flow is from left to right. B. Thinner cross-bedded gravel and sand on the distal part of a pendant bar (54.4421°N, 110.3785°W), upstream of the moraine barrier. C. Cross bedded gravel interspersed with granules and coarse sand beds unconformably overlain by ripple cross-laminated sand, silt and clay (54.4422°N, 110.3780°W). D. Ripple cross laminated sand, silt and clay with soft-sediment deformation structures (flames and ball-and-pillow structures) (54.4402°N, 110.3713°W). E. Massive, matrix supported, inversely graded boulder gravel (54.2541°N, 109.2164°W). Coarser clasts are weakly imbricated indicating flow from right to left. F. Boulders littering the surface of a pendant bar 30 km downstream of the moraine barrier (54.2781°N, 109.0456°W). For scale, horizontal log is 1.4 m long.

5.5 Interpretation

5.5.1 Channel morphology

Based on comparisons of previously reported spillways known to be linked with catastrophic lake drainage (e.g. Malde, 1968; Baker, 1973; Kehew and Lord, 1986; Lord and Kehew, 1987; Maizels, 1991; Kehew, 1993; O'Connor, 1993; Cutler et al., 2002; Fisher and Taylor, 2002; Kozlowski et al., 2005), we interpret the (eastern) Beaver River Channel as a spillway (herein referred to as the Beaver River Spillway) formed by catastrophic flood drainage. Evidence for this interpretation includes: (i) a steep-walled, trench-like channel morphology; (ii) the occurrence of large (pendant) bars; and (iii) regions of erosional/scoured sub-upland/terrace.

We interpret the scoured surfaces as characteristic of initial down-cutting by floodwater where a deep valley did not pre-exist. The scoured surfaces bear resemblance to the 'Outer Scour Zone' described by Kehew and Lord (1986). In their model, the Outer Scour Zone represents the initial stages of erosion, when no channel of sufficient size was available to convey the flood, and water covered a broad area (covered by anastomosing channels). Boulders exposed on the scoured surface were likely exhumed by erosion during channel incision, which promoted washing of finer surface sediment downstream, leaving coarser clasts exposed at the surface (Kehew and Lord, 1986). As flow continued, erosional enlargement concentrated within a smaller cross-section began to erode the inner channel. Geomorphic and stratigraphic relations along the eastern Beaver River Spillway conform to this model. Here, the scoured surfaces are expansive and contain small channels making this initial flood zone inefficient because of its large wetted perimeter, leading to the progressive development of the trench-like main spillway channel (Kehew and Lord, 1986). In addition to the large wetted perimeter, the boundary-resistance to flow progressively increased within the scoured surface, with the development of the observed boulder lag, quickening the formation of a deep, narrow inner channel (Kehew and Lord, 1986; Maizels, 1997).
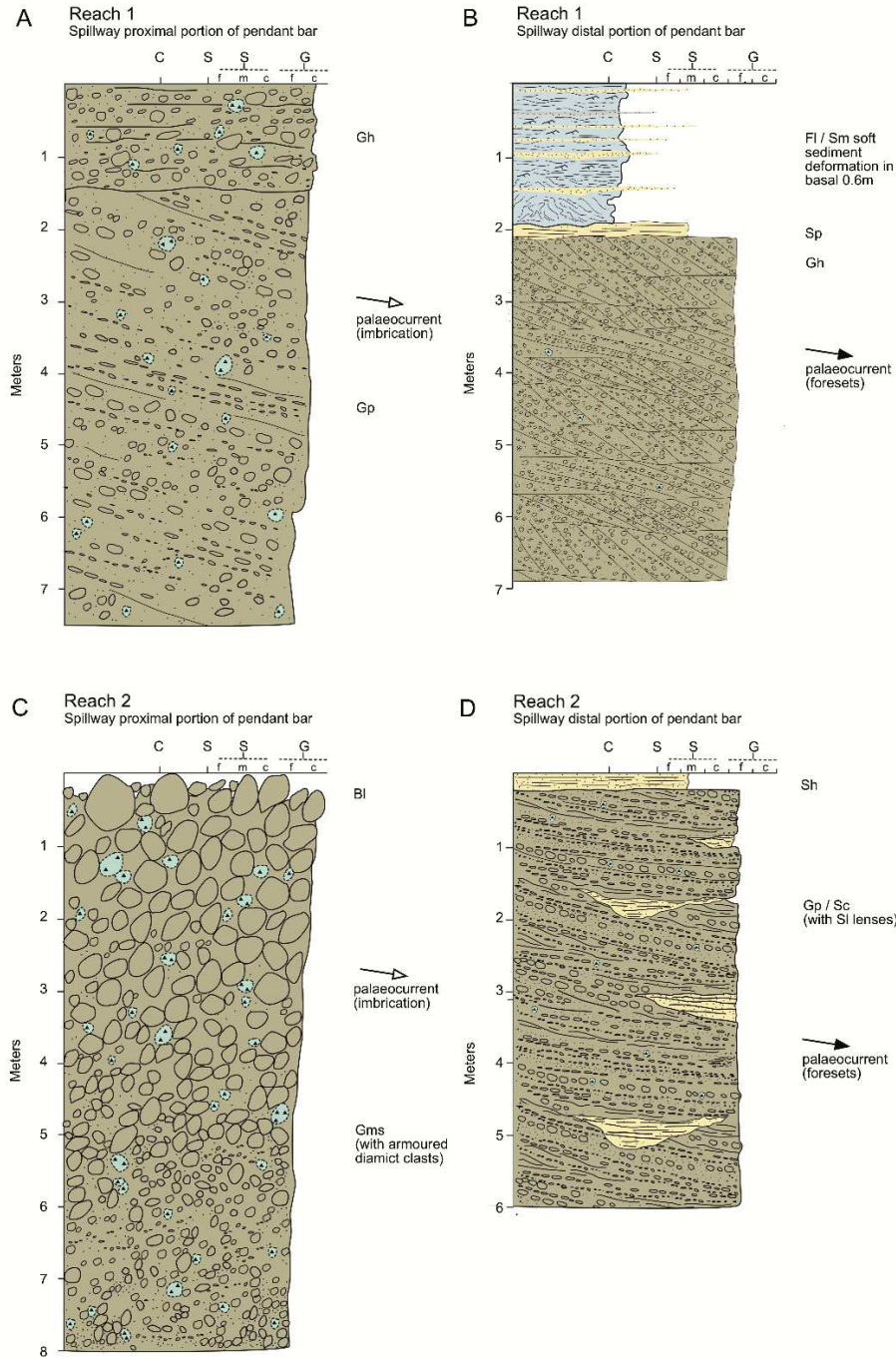
Figure 5.3: Summary stratigraphic logs for Reach 1: spillway proximal A. and distal B. portions of pendant bars and; Reach 2: spillway proximal C. and distal D. parts of pendant bars. Fl/Sm = fine laminations of silt and clay with small ripples and minor fine sand/ massive sands; Sp = medium to coarse planar crossed bedded sands; Gh = horizontally-bedded medium to coarse grained gravel; Gp = planar crossed-bedded gravel; Sh = horizontally bedded sand; Gp/Sc = planar cross-bedded gravel/ planar cross-bedded sand; Sl = horizontally laminated sand (lenses); Bl = boulder lag; Gms = matrix-supported, massive gravel.

5.5.2 Outburst deposits and depositional processes

Pendant bars recorded in Reach 1 of the eastern Beaver River Channel, upflow of the moraine barrier resemble in form, though are smaller in size than those produced by Pleistocene Lake Bonneville catastrophic floods (Malde, 1968) and Lake Missoula (Baker, 1973; O'Connor, 1994). Their internal structure is also similarly composed of downstream-oriented foresets overlain by horizontally-bedded coarser gravel (Fig. 5.3A). The formation mechanism of Baker (1973) and O'Connor (1993) in which bars grow as material transported as bedload across the surface of a bar is deposited on the downstream side, is invoked to explain these deposits. This sequence therefore reflects deposition by a single (fluid flow) flood not considerably deeper than the bar surface. Smaller-scale cross-bedding and sediment-fining in the flood's distal part of pendant bars are consistent with such a model and indicate regions of lower velocity farther from the main channel (Carling, 2013).
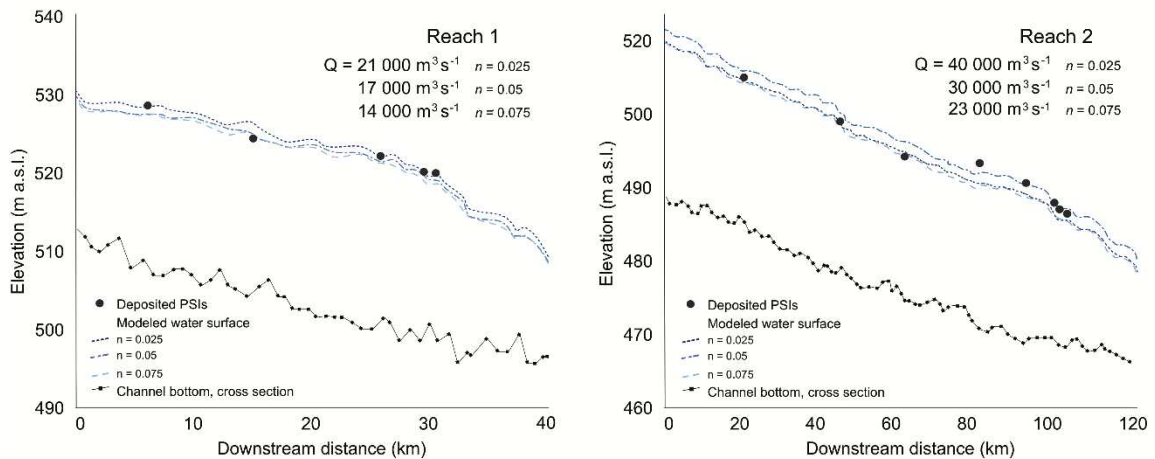
Figure 5.4: HEC-RAS water-surface profiles and comparison with PSIs at modelled, maximum discharges of 14 000-21 000 m^3 s^{-1} and 23 000-40 000 m^3 s^{-1} for Reach 1 and 2, respectively.

Thinly laminated sand, silt and clay cap gravel in the most distal part of one pendant bar (Figs 5.2C, 5.3B). Similar deposits have been interpreted as slackwater deposits (Bretz et al., 1956; Waitt, 1980, 1985; O'Connor et al., 2001). In our study, however, due to the

localised nature of these deposits we simply interpret them to have formed in an area of flow stagnation or quiescence in the distal portion of a bar adjacent to the high energy floodway.

The remaining pendant bars, downflow of the moraine barrier, exhibit differing internal structure lacking cross-stratification and considerably larger boulder clasts (Figs. 5.2C, 5.2D). Such deposits are more akin to those described by Lord and Kehew (1987) and Kehew and Lord (1987) in the Souris Spillway, and by Kozlowski et al. (2005) in the Central Kalamazoo River Valley, consistent with a type F5 vertical sedimentary profile (Maizels, 1997). Massive, matrix-supported, inversely graded gravels capped by a boulder layer in these studies have been inferred or documented to be the product of an intermediary flow between debris and fluid flow that has been 'hyperconcentrated' (40-70% sediment concentration by weight; Costa, 1984; Lord and Kehew, 1987). In such flows, boundary shear stress can travel through the flood flow as a dispersive pressure, forcing coarser grains to move to the edges of the channel where shear is lower, thus producing inversely graded sequences with larger boulder-sized clasts left as an armoured surface (Fig. 5.2E) (e.g. Pierson, 1981; Smith, 1986; Maizels, 1997; Carling, 2013).

Armoured rip-up clasts comprised of till occur frequently in pendant bars downflow of the moraine barrier. It is possible that rip-up clasts have been dislodged/eroded from frozen ground and were transported into place by the proposed hyperconcentrated flow. The higher frequency of such clasts in these pendant bars, compared to those upstream of the moraine barrier, attests to such an interpretation as rip-up clast moving by saltation or rolling, that would be more easily broken down (Fisher 1993). However, while the presence of such clasts has been previously described as diagnostic of subglacial excavation (Russell et al., 2006), based on the clear proglacial setting of this flood (see above we suggest that such features cannot be used as indicative of a subglacial setting.

In the distal parts of bars, upflow from the moraine barrier, finer grained gravels containing indistinct cross-stratification and lenses of stratified sand and fine-gravel are present (Fig. 5.2D). The presence of such deposits are characteristic of fluid flow and therefore indicate a lateral transition within the flow. Todd (1989) reports similar lateral transition in a flood flow associated with sediment bulking, where the basal portion of a flow moves as a

79

hyperconcentrated flow while the upper and distal parts exhibit fluid flow characteristics. This interpretation is favoured in the Beaver River Spillway due to the sedimentary variation within a single pendant bar.

5.5.3 Comparison of modelling results to channel deposits

Comparison of local hydraulic variables (velocity and peak discharge), derived from the step-backwater modelling and from b-axis of the 10 largest sediment particles within Reach 1, show good agreement (Table 5.1). In contrast, within Reach 2 values derived from b-axis measurements are considerably (40-240% peak discharge) higher. Previous studies acknowledge (Lord and Kehew, 1987; O'Connor, 1993) that the relationship between particle diameter and indices of flow may be overestimated. Data sets from which this relationship is derived may include samples not related to peak discharge but rather samples deposited during lower discharge after peak discharge (see O'Connor 1993 for review). However, it is doubtful this would create changes large enough to explain the discrepancy observed here. Alternatively, these overestimates are more likely the result of high sediment concentrations (Lord and Kehew, 1987) within Reach 2. As indicated above, and based on the sedimentary observation (Fig. 3C, 3D) these flows would have been hyperconcentrated. Such concentrations may have lowered the shear stress needed to transport boulders (0.89-1.66 m) by altering the viscosity of the flow (Lord and Kehew, 1987). Thus palaeohydraulic calculations made assuming a Newtonian fluid result in unrealistically large values.

5.6 Discussion

5.6.1 Palaeohydraulic reconstruction

The step-backwater modelling of the Beaver River flood allows hydraulic variables in the flood path to be compared and associated with field evidence. From this modelling, we estimate peak discharge achieved along the eastern Beaver River Spillway was 14 000-21 000 m^3 s^{-1} upstream of the moraine barrier and, 23 000-40 000 m^3 s^{-1} distal to it. There is a good agreement, (> ±4, 6 m Reach 1 and 2, respectively) between flood geomorphology (PSIs) and hydraulic variables derived in HEC-RAS in both reaches (Fig. 5.4).

Hydraulic variables derived from the b-axis of the five largest boulders, recorded at multiple pendant bars provide independent verification of HEC-RAS results. Within Reach 1 hydraulic variables derived from the two methods are consistent. In contrast, overestimated values were produced in Reach 2 when hydraulic variables were derived from *in situ* boulders. Based on the lack of association between boulder diameter, indices of flow and supporting sedimentological evidence, it is hypothesized that within this 120 km part of the spillway, the sediment concentration (and also the volume), and therefore its peak discharge, increased. By comparison in Reach 1, the 40 km more proximal to the flood source, transported large boulders are lacking and the sedimentological evidence is consistent with 'normal' fluid flows. Such a relationship contrasts to proposed models of glacial lake outburst floods where gradual reduction in suspended sediment concentration in hyperconcentrated flows as the outburst flood propagates downstream can lead to the development of Newtonian flow dynamics (Maizel, 1993, 1997). These characteristics signify a more complex system operated in the Beaver River channel.

Based on the assumption of a hyperconcentrated flow, the limitations of using a 1-D steady state HEC-RAS model warrants discussion. This modelling approach assumes that a sediment-enriched flow can be modelled as a Newtonian fluid in which the mass and density remain unchanged. This approach is unlikely to be valid when applied to a high-concentration debris flow; however, the method may provide a reasonable estimate for the hydraulic dynamics of a dilute hyperconcentrated flow when properly calibrated. Due to the low gradient of the slope we would expect a fluid flow enriched with sediment to travel at a lower velocity than a traditional fluid flow, thus the peak discharge derived in this study for Reach 2 may be overestimated and should be treated as a maximum estimate.

To account for this overestimation of velocity and provide a more accurate peak discharge range, a small number of studies have suggested that HEC-RAS input-parameters be altered in order to account for the higher viscosities and densities of hyperconcentrated flows (Travis et al., 2012). The principle of this approach alters the normal parameters (expansion and contraction coefficients and Manning's *n*) to experimentally determined 'bulked' parameters that account for the bulked-flow effects (Travis et al., 2012). This

provides a more realistic reconstruction of flow conditions consistent with sedimentological evidence of hyperconcentration.

Following Travis et al., (2012) expansion/contraction coefficients and Manning's *n* can be recalculated allowing a peak discharge to be modelled in HEC-RAS. Using this modification, the original Manning's n value-range becomes 0.07-0.21 and expansion and contraction coefficients for bulked flow become $1.7x10^{-5}$ and $5.2x10^{-5}$. Using these new values, a peak discharge range of 18 000-26 000 m^3 s^{-1} is estimated. However, this range likely provides an upper estimate of peak discharge as it assumes the whole water column has a single 'bulked' viscosity.

5.6.2 Formation of the Beaver River Spillway

The following series of events (summarised in Fig. 5.5) are proposed to explain the geomorphic, sedimentary, and hydraulic evidence observed in the Cold Lake/Meadow Lake region. During northeast ice retreat, across regional reverse topography, multiple proglacial were impounded (Utting et al., 2015). The largest of these lakes was glacial Lake Algar, which drained into the westerly part of the Beaver River Spillway. Due to an ice margin blocking drainage to the eastern part of the Beaver River Spillway, meltwater was deflected south, travelling through an ice walled channel into the Kehiwin Channel (Fig. 5.5A) (Utting et al., 2015).

 Based on the juxtaposition of this ice walled channel and a series of subaerial channels which have been eroded into progressively lower topography, we propose that as the ice margin retreated from its initial position (Fig. 5.5A), and/or discharge from glacial Lake Algar increased, the southern deflection of floodwaters no longer occurred or was significantly reduced. Instead the flood progressively travelled in a more easterly direction to form the remaining eastern Beaver River Spillway. As water began to flow east towards the Alberta/Saskatchewan border, the ice margin would have been positioned north of the Beaver River Spillway. Evidence for this has previously been recognised by Andriashek and Fenton (1989) in terms of who identify a ~12 km wide belt of glacially compressed and thrusted landforms (Fig. 5.5B) extending from Barbara Lake eastward to Cold Lake. Prior to ice retreat to this position, a ~10 km wide, localised area of streamlined, and

morainic topography developed (the moraine barrier). This moraine barrier has previously been attributed to a readvance extending ~80 km southwest from Cold Lake (Andriashek and Fenton, 1989). However, due to the very small width and significant length of the terrain zone, we suggest this topography was instead formed by local fast ice flow, which may have been initiated by the large amount of glaciotectonised material available immediately to the north (i.e. the Cold Lake hillhole pair) (Fig. 5.1). As flood flow travelled eastward it was impounded by this moraine barrier. As a result, flood water would have been temporarily impounded west of the moraine barrier. A thin veneer of sands and gravel, possibly of glaciolacustrine origin my support this (Andriashek and Fenton, 1989). Based on the elevation of morainic deposits surrounding the spillway, the impounded water spanned an area of 554 km^2 at 540 m a.s.l. reaching ~5.5 km^3. A larger volume could not have been sustained above this elevation as water would have drained to the south via the Kehiwin Channel. Only once the water level was such that it could overtop the moraine barrier, would flood flow have started cutting across the region. The initial breach would have then deepened and widened to erode a ~2.5 km swath of eroded streamlined terrain/moraine on both sides of the Beaver River Spillway.

As the flood progressed through the landscape, it would initially have been largely unconfined, its area equivalent to the scoured surfaces, travelling first as sheet flow and evolving to a progressively more channelized system. As flow continued, erosional enlargement concentrated within a smaller cross-section and hence would have begun to erode the inner spillway. Prior to the moraine barrier, flow would have had Newtonian characteristics. This type of flow was evidenced by well-preserved sedimentary evidence, downstream orientated foresets overlain by horizontally bedded coarser gravel, and the consistency between hydraulic variables derived empirically from particle diameter and from HEC-RAS. As this flood travelled through the easily erodible moraine barrier, it would have drastically increased its abundance of sediment by weight. This produced matrix-supported, inversely graded gravel capped by a boulder layer indicative of a hyperconcentrated flow. Additionally, this sediment-rich flow also produces erroneously high peak discharges when modelled as a Newtonian fluid.

In contrast to many spillways within the Interior Plains where deposits are absent, the eastern Beaver River Spillway displays an excellent sedimentary record. The path of the Beaver River Spillway cuts through thick sand and clay rich glacial deposits, commonly >50 m thick (Fig. 5.1). We suggest that a large amount of easily erodible till in the pathway of this flood allowed formation of such deposits. This is particularly significant as it indicates a relationship between the abundance of coarse-grained, easily erodible material and the formation of depositional landforms. In regions of the Interior Plains where spillways do not coincide with thick packages of easily erodible material, this may explain the lack of depositional landforms.

Using our reconstruction of lake volume and peak discharge we can estimate the floods duration. Based on the range of peak discharges, 14 000- 26 000 m^3 s^{-1}, the 5.5 km^3 lake would have drained in 3 to 5 days. The flood duration likely exceeds these values as peak discharge is unlikely to persist for the duration of drainage. Furthermore, it is probable that continual drainage from Lake Algar would have sustained flow for much longer. However, these estimates provide a minimum assessment of the flood duration.
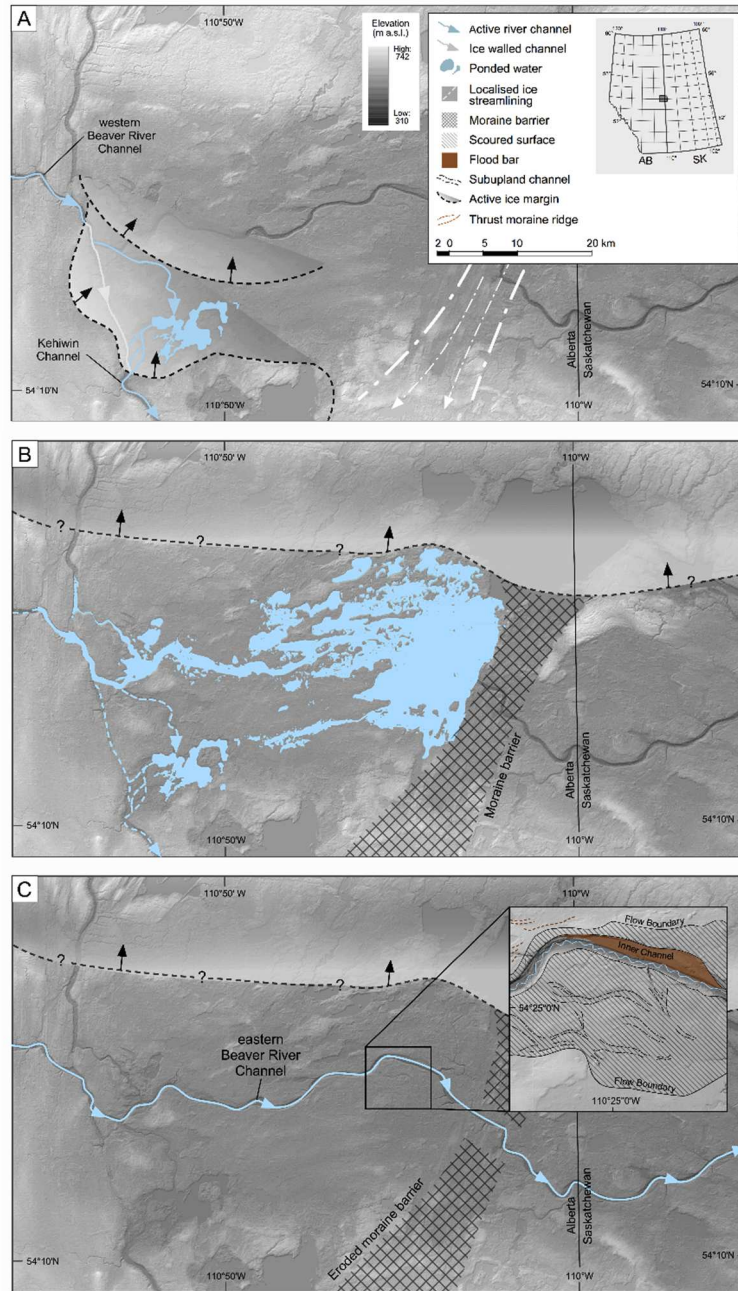
Figure 5.5: Reconstructed development sequence for the Beaver River Spillway. A. Initial southeastward drainage of glacial Lake Algar along the western Beaver River Spillway. Water would have initially flowed through an ice walled channel before entering the Kehiwin Channel. Easterly retreat of an ice lobe covering the lower Beaver River region allowed drainage in a progressively easterly direction though a network of meltwater channels. B. Continued northeastward retreat of ice allowed water to flow eastward, moraine barrier would then have blocked further eastward drainage and formed a short-lived ponded region. C. Once the water level overtopped the moraine barrier, progressive erosion of the spillway on both sides of the barrier occurred. Inset diagram shows the geomorphic imprint of the scoured surfaces and inner spillway channel.

5.6.3 Wider deglacial significance

Based on the regional chronology of Dyke et al., (2003), the Beaver River Valley would have been deglaciated between 13.9 and 13.3 ka BP (12-11.5 ^{14}C ka BP). Therefore, the region would have been ice free to allow the formation of the geomorphology and sedimentology described. We suggest that the timing of the flood falls between this age range. Furthermore, based on this age it is feasible that flood waters travelling down the Beaver River Spillway drained into Glacial Lake Meadow (Christiansen, 1979; Schreiner, 1983) potentially forming the delta recorded by Christiansen (1979). From here water was held in glacial Lake Meadow until the time the southwestern margin of the Laurentide Ice Sheet retreated allowing southeastern drainage of the lake through a complex of small spillways (Christiansen, 1979; Schreiner, 1983).

5.6.4 Significance of study

Well preserved sedimentological evidence associated with glacial lake outburst floods, as discussed in this study, is exceedingly rare within the Interior Plains. This study therefore has several implications for the analysis and reconstruction of local hydraulic variables and for the controls on outburst flood erosional and depositional processes. Hydraulic calculations demonstrate the limitations of using palaeohydraulic equations based on sediment particle measurements. We suggest that such equations should be used with caution in locations where high sediment loads are likely, as such conditions limit the application of these methods of estimating velocity and peak discharge. This is particularly important as we demonstrate that within an outburst flood, with spatially variable sediment loads, landforms with similar geomorphic expression can be produced in hyperconcentrated and fluid flows, but with sedimentary characteristics that are dramatically different.

Furthermore, HEC-RAS derived peak discharge estimates show a significant increase in the lower part of the spillway. Based on observed outburst floods (Bj*ö*rnsson, 1992; Kershaw et al., 2005) we would expect peak discharge to decrease in the spillway's lower reaches due to downstream discharge attenuation. While more work is required to fully understand the controls on outburst flood behaviour and hydraulics, these results

demonstrate the importance of external controls such as sediment supply on outburst flood evolution. These inferences concur with observations made in modern settings (O'Connor et al., 2001; Breien et al., 2008), where outburst floods overtopping moraines have been rapidly hyperconcentrated or evolved into debris flows. However, the uniqueness of the flowpath of the Beaver River Spillway, travelling through a region of thick, easily erodible material, provided the opportunity to observe how a single flood event can exhibit a range of flow conditions, with an associated sedimentological record.

5.7 Conclusions

We reconstruct the catastrophic drainage of glacial Lake Algar in north central Alberta based on the well preserved sedimentary record within the eastern Beaver River Spillway. Based on regional deglacial chronology (Dyke et al., 2003), we suggest the flood occurred between 13.9 and 13.3 ka BP. We estimate the peak discharge of the flood using a HECgeoRAS/HEC-RAS model in conjunction with PSIs. Modelling results indicate that peak discharge within the first 40 km (Reach 1) of the eastern Beaver River Spillway was approximately 14 000-21 000 m^3 s^{-1}. Within the 120 km long downstream reach (Reach 2), the peak discharge was estimated at 23 000-40 000 m^3 s^{-1} (n_{bulked} 18,000-26,000 m^3 s^{-1}). Based on lake volume estimates and the range of peak discharges from both reaches a minimum flood duration of 3-5 days is estimated. The downstream discharge increase coincides with a change in sediment composition of pendant bars. The increase in modelled peak discharge and compositional change of pendant bars occur downflow of the moraine barrier, which the spillway dissects. We suggest these changes, and increase in discharge estimates, result from sediment bulking of the flood flow due to the easily erodible nature of the moraine barrier, which produced differing hydraulics and associated sedimentology in close proximity from a single flood event.

5.8 References

Andriashek, L. D. and Fenton, M. M. 1989: *Quaternary Stratigraphy and Surficial Geology of the Sand River Area 73L.* Alberta Research Council, Edmonton.

Baker, V. R. 1973: Paleohydrology and sedimentology of lake Missoula flooding in eastern Washington. *Geological Society of America Special Paper, 144*, 1–79.

Beaney, C. L. 2002: Tunnel channels in southeast Alberta, Canada: evidence for catastrophic channelized drainage. *Quaternary International 90*, 67–74.

Bj*ö*rnsson, H. 1992: J*ö*kulhlaups in Iceland: prediction, characteristics and simulation. *Annales of Glaciology, 16*, 95–106.

Bretz, J. H., Smith, H. T. U. and Neff, G. E. 1956: Channeled scabland of Washington: New data and Interpretations. *Geological Society of America Bulletin, 67*, 957–1049.

Breien, H. De Blasio, F. V. Elverhoi, A. and Hoeg, K. 2008: Erosion and morphology of a debris flow caused by a glacial lake outburst flood, Western Norway. *Landslides, 5*, 271-280.

Broecker, W. S., Kennett, J., Flower, B., Teller, J., Trumbore, S., Bonani, G. and Wolfli, W. 1989: Routing of meltwater from the Laurentide Ice Sheet during the Younger Dryas cold episode. *Nature, 341*, 318-321.

Carling, P., Villanueva, I., Herget, J., Wright, N., Borodavko, P. and Morvan, H. 2010: Unsteady 1D and 2D hydraulic models with ice dam break for Quaternary megaflood, Altai Mountains, southern Siberia. *Global and Planetary Change, 70*, 24–34.

Carling, P. A. 2013: Freshwater megaflood sedimentation: What can we learn about generic processes? *Earth-Science Reviews, 125*, 87-113.

Christiansen, E. A. 1979: The Wisconsinan deglaciation, of southern Saskatchewan and adjacent areas. *Canadian Journal of Earth Sciences, 16*, 913–938.

Clark, P. U., Marshall, S. J., Clarke, G. K. C., Hostetler, S. W., Licciardi, J. M. and Teller, J. T. 2001: Freshwater forcing of abrupt climate change during the last glaciation. *Science, 293*, 283–287.

Costa, J. E. 1984: Physical geomorphology of debris flows. *In* Costa, J. E. and Fleisher, P. J. (eds.): *Developments and Applications of Geomorphology*, 268-317. Springer, New York.

Costa, J. E. 1983: Paleohydraulic reconstruction of flash-flood peaks from boulder deposits in the Colorado Front Range. *Geological Society of America Bulletin, 94*, 986–1004.

Cutler, P. M., Colgan, P. M. and Mickelson, D. M. 2002: Sedimentologic evidence for outburst floods from the Laurentide Ice Sheet margin in Wisconsin, USA: implications for tunnel channel formation. *Quaternary International, 90*, 23-40.

Dury, G. H. 1976: Discharge prediction, present and former, from channel dimensions. *Journal of Hydrology, 30*, 219-245.

Dyke, A. S., Moore, A. and Robertson, L. 2003: Deglaciation of North America. *Geological Survey of Canada, Open File 1574*.

Ferguson, R. I. 1994: Critical discharge for entrainment of poorly sorted gravel. *Earth Surface Processes and Landforms, 19,* 179–186.

Fisher, T. G. 1993: *Glacial Lake Agassiz: The N.W. outlet and paleoflood spillway, N.W. Saskatchewan and N.E. Alberta.* Ph.D. thesis. University of Calgary.

Fisher, T. G. and Lowell, T. V. 2017: Glacial geology and landforming events in the Fort McMurray region. *In* Ronaghan, B. (ed.): *Alberta's Lower Athabasca Plain: Archaeology and Paleoenvionments,* 45-68. Athabasca University Press, Alberta.

Fisher, T. G. and Smith, D. G. 1994: Glacial Lake Agassiz: its northwest maximum extent and outlet in Saskatchewan (Emerson phase). *Quaternary Science Reviews, 13*, 845–858.

Fisher, T. G., Smith, D. G. and Andrews, J. T. 2002: Preboreal oscillation caused by a glacial Lake Agassiz flood. *Quaternary Science Reviews, 21*, 873–878.

Fisher, T. G. and Taylor, L. D. 2002: Sedimentary and stratigraphic evidence for subglacial flooding south-central Michigan, USA. *Quaternary International, 90*, 87–115.

Fisher, T. G. and Waterson, N., Lowell, T. V. and Hajdas, I. 2009: Deglaciation ages and meltwater routing in the Fort McMurray region, northeastern Alberta and northwestern Saskatchewan, Canada. *Quaternary Science Reviews, 28*, 1608-1624.

Herget J. 2005: Reconstruction of ice-dammed lake outburst floods in the Altai mountains, Siberia. *Geological Society of America, Special Paper 386,* 118 pp.

Horritt, M. S. and Bates, P. D. 2002: Evaluation of 1D and 2D numerical models for predicting river flood inundation. *Journal of Hydrology, 268*, 87–99.

Hydrologic Engineering Center. 2001: HEC-RAS river analysis system. *Hydraulic Reference Manual version. 3.0. U.S. Army Corps of Engineering*. Davis, California. 46 pp.

Kehew, A. E. 1982: Catastrophic flood hypothesis for the origin of the Souris spillway, Saskatchewan and North Dakota. *Geological Society of America Bulletin, 93*, 1051-1058.

Kehew, A. E. 1993: Glacial-lake outburst erosion of the Grand Valley, Michigan, and impacts on glacial lakes in the Lake Michigan Basin. *Quaternary Research, 39*, 544–553.

Kershaw, J. A., Clague, J. J. and Evans, S. G. 2005: Geomorphic and sedimentological signature of a two-phase outburst flood from moraine-dammed Queen Bess Lake, British Columbia, Canada. *Earth Surface Processes and Landforms, 30,* 1–25.

Kehew, A. E. and Clayton, L. 1983: Late Wisconsinan floods and development of the Souris-Pembina spillway system in Saskatchewan, North Dakota and Manitoba. *In* Teller, J. T., and Clayton, Lee, (eds.): Glacial Lake Agassiz. *Geological Association of Canada Special Paper 26*, 187-209.

Kehew, A. E. and Lord, M. L. 1986: Origin and large-scale erosional features of glacial-lake spillways in the northern Great Plains. *Geological Society of America Bulletin, 97,* 162–177.

Kehew, A. E. and Lord, M. L. 1987: Glacial-lake outbursts along the mid-continent margins of the Laurentide Ice Sheet. *In* Mayer, L., Nash. D. (eds.) *Catastrophic flooding*, 95-120. Allen and Unwin, London.

Kehew, A. E. and Teller, J. T. 1994: Glacial-lake spillway incision and deposition of a coarse-grained fan near Waterous, Saskatchewan. *Canadian Journal of Earth Science, 31*, 544–553.

Komar, P. D. 1987: Selective gravel entrainment and the empirical evaluation of flow competence. *Sedimentology, 34*, 1165–1176.

Kozlowski, A. L., Kehew, A. E. and Brian, C. B. 2005: Outburst flood origin of the Central Kalamazoo River Valley, Michigan, USA. *Quaternary Science Reviews, 24*, 2354-2375.

Lord, M. L. and Kehew, A. E. 1987: Sedimentology and paleohydrology of glacial-lake outburst deposits in southeastern Saskatchewan and northwestern North Dakota. *Geological Society of America Bulletin, 99*, 663–673.

Maizels, J. K. 1991: Origin and evolution of Holocene sandurs in areas of Jokulhlaup drainage, south Iceland. *In* Maizels, J. K. and Caseldine, C. (eds.): *Environmental Change in Iceland: Past and Present,* 267–302. Kluwer, Dordrecht.

Maizels, J. 1997: Jokulhlaup deposits in proglacial areas. *Quaternary Science Reviews, 16,* 793–819.

Malde, H. E. 1968. The catastrophic late Pleistocene Bonneville flood in the Snake River Plain, Idaho. *US Geological Survey Professional Paper,* 595 pp.

Margold, M., Jansen, J. D., Codilean, A. T., Preusser, F., Gurinov, A. L., Fujioka, T. and Fink, D. 2018: Repeated megafloods from glacial Lake Vitim, Siberia, to the Arctic Ocean over the past 60,000 years. *Quaternary Science Reviews, 187*, 41–61.

Munro-Stasiuk, M. J., 1999: Evidence for water storage and drainage at the base of the Laurentide ice sheet, south-central Alberta, Canada. *Annals of Glaciology, 28*, 175–180.

O'Connor, J. E. 1993: Hydrology, hydraulics, and geomorphology of the Bonneville Flood. *Geological Society of America Special Paper 274*, 83-89.

O'Connor J. E, Hardison J. H. and Costa, J. E. 2001: Debris flows from failures of Neoglacial-age moraines in the Three Sisters and Mount Jefferson wilderness areas, Oregon. *US Geological Survey Professional Paper, 1606.*

Parker, G. 1990: Surface-based bedload transport relation for gravel rivers. *Journal of Hydraulic Research, 28,* 417-436.

Pierson, T. C. 1981: Dominant particle support mechanisms in debris flows at Mt. Thomas, New Zealand, and implications for flow mobility: *Sedimentology, 28*, 4940-4953.

Russell, A. J., Roberts, M. J., Fay, H., Marren, P. M., Cassidy, N. J., Tweed, F. S. and Harris, T. 2006: Icelandic jökulhlaup impacts: implications for ice-sheet hydrology, sediment transfer and geomorphology. *Geomorphology, 75*, 33-64.

Sjogren, D. B. and Rains, R. B., 1995: Glaciofluvial erosional morphology and sediments of the Coronation–Spondin Scabland, east-central Alberta. *Canadian Journal of Earth Sciences, 32*, 565–578.

Schreiner, B. T. 1983: Lake Agassiz in Saskatchewan, *In* Teller, J. T., and Clayton, L. (eds.) Glacial Lake Agassiz: *Geological Association of Canada Special Paper 25*, 75-96.

Smith, G. A. 1986: Coarse-grained nonmarine volcaniclastic sediment: Terminology and depositional Processes. *Geological Society of America Bulletin, 97*, 1-10.

Teller, J. T., Leverington, D. W. and Mann, J. D. 2002: Freshwater outbursts to the oceans from glacial Lake Agassiz and their role in climate change during the last deglaciation. *Quaternary Science Reviews, 21*, 879–887.

Thompson, S. M. and Campbell, P. L. 1979: Hydraulics of a large channel paved with boulders. *Journal of Hydraulic Research, 17*, 341-354.

Todd, S. P. 1989: Stream-driven, high-density gravelly traction carpets: possible deposits in the Trabeg Conglomerate Formation, SW Ireland and some theoretical considerations of their origin. *Sedimentology, 36*, 513-530.

Travis, B., Teal, M. and Gusman, J. 2012: Best Methods and Inherent Limitations of Bulked Flow Modeling with HEC-RAS. Conference. Proceedings of the 2012 World Environmental and Water Resources Conference. Albuquerque, New Mexico.

Utting, D. J., Atkinson, N. and Pawley, S. 2015: Reconstruction of proglacial lakes in Alberta. *Canadian Quaternary Association Conference.* St. John's, Canada.

Waitt, R. B. 1980: About 40 last-glacial Lake Missoula jokulhlaups through southern Washington. *Journal of Geology, 88*, 653-679.

Waitt, R. B. 1985: Case for periodic, colossal jókulhlaups from glacial Lake Missoula. *Geological Society of America Bulletin, 95*, 1271-1286.

Williams, G. P. 1983: Paleohydrological methods and some examples from Swedish fluvial environments I: cobble and boulder deposits. *Geografiska Annaler, 65*, 227–243.

CHAPTER 6: CONCLUSIONS

To improve understanding of the SWLIS this thesis has examined the (i) timing (ii) dynamics and (iii) meltwater discharge of this region during the last deglaciation. This chapter will provide a synthesis of the data reported in previous chaptered and highlight key areas for future research.

This thesis has provided a reconstruction of the SWLIS using direct dating methods and detailed mapping techniques. Chapter 2 provided the foundation for this work and presented a 1:100,000 scale glacial geomorphology of the interior SWLIS. Chapter 3 documents the results of a ^{10}Be direct dating campaign for the region constraining the timing of deglaciation and presenting ice sheet retreat rates. Chapter 4 builds on these previous chapters but drawing together the geomorphic imprint of the interior SWLIS and previously published ice dynamic reconstructions from the ice sheets' peripheral regions to reconstruct the dynamic behaviour of the SWLIS. These data were then placed into a temporal context using the results of Chapter 3. Chapter 5 draws on conclusions from Chapter 4 by investigating the meltwater discharge of the SWLIS through a case study of a glacial lake outburst flood in central Alberta. This Chapter highlighted the lack of sedimentological and geomorphic investigation surrounding the rich meltwater channel record throughout the Interior Plains and demonstrated both the approach and the significance of reconstructing the meltwater discharge associated with these features.

6. 1 Chapter summaries

Chapter 2 presents a detailed geomorphic map for the interior portion of the SWLIS. Remote sensing of 1-arc (~30 m resolution) Shuttle Radar Topography Mission digital elevation models over an area of approximately 150,000 km^2 were used as the primary data source for landform identification. This geomorphic mapping depicted a high density of glacial geomorphology. Multiple generations of glacial landforms, many of which crosscut, suggested the region have undergone several shifts in ice flow orientation during the last deglaciation. This map also identified many previously unmapped deglacial landforms, glacial lake strandlines and the first detailed mapping of the previously proposed Younger Dryas position of the SWLIS, the Cree Lake Moraine.

Chapter 3 presents a database of 20 new and 12 previously published [10]Be surface exposure ages from glacial erratics spanning the SWLIS. Ages were collected along a ~1200 km transect beginning at the region of convergence between the CIS and LIS and extending to its proposed Younger Dryas position. Surface exposure dates were combined with pre-existing luminescence and high quality minimum radiocarbon chronologies, exclusive of dates on bulk sediments, terrestrial shells or mixed assemblages, to provide an updated chronology for the retreat of the SWLIS. Our compiled dataset shows these diverse chronometers provide an internally consistent retreat record. These data indicates that initial detachment of the southwestern Laurentide Ice Sheet, from its convergence with the CIS, occurred at ~15 ka BP, concurrent with, or possibly somewhat before the abrupt warming at the onset of the Bølling-Allerød, and retreated >1200 km to its Younger Dryas position in ≤ 2500 yrs. Our data also indicate that the Cree Lake Moraine is the Younger Dryas position for this sector of the LIS, and suggested that the LIS likely stabilised at this position for >1000 yrs.

Chapter 4 built on the geomorphic mapping in chapter 1, in combination with pre-existing mapping within the peripherical regions of the SWLIS, to reconstruct ice flow dynamics. Identified ice flow dynamics were then embedded into the deglaciation of the SWLIS using the ice margin chronology identified in Chapter 3 providing a dynamical reconstruction of the SWLIS. Our reconstruction builds on the previously identified complex pattern of ice stream behaviour characterised by substantial flow switches. Using the new chronological controls on the ice margin retreat (Chapter 3) this study indicates that the SWLIS underwent ice sheet scale reorganisation at least three times in ~2500 yrs. These rapid, decadal to centennial, changes in ice stream orientations demonstrate both, how ice streams can influence an ice sheet's broader response to external climate forcing, and how ice sheets, through changes to ice flow regime, are highly sensitive to rapid climate change.

Throughout this thesis the deglaciation of the SWLIS has been examined in terms of its ice retreat rate and dynamics. Chapter 5 highlights the resulting meltwater discharge associated with rapid deglaciation of the region by reconstructing a large glacial lake outburst flood in north central Alberta. Geomorphic and sedimentological evidence as well as hydraulic

modelling of the Beaver River Spillway indicates it formed catastrophically immediately following deglaciation of the region. Modelling results show that peak discharge within Beaver River Spillway was approximately 14 000–26 000 m³ and maintained a minimum flow duration of ~3-5 days. This case study demonstrates the catastrophic nature of meltwater drainage from the SWLIS and also demonstrates the role of easily erodible glacial sediment as a primary control on meltwater channel evolution and morphology within the Canadian Prairies.

6.2 Suggestions for future research

The research presented in this thesis has provided several advances in our understanding of the SWLIS's deglaciation from which multiple directions for future research are apparent. Below I highlight some key areas that future work might address:

Southwestern Laurentide Ice Sheet sea level contribution
The new cosmogenic database and substantially increased retreat rates for the SWLIS presented in this thesis provide an opportunity to explore the meltwater equivalent sea level contribution of this sector of the ice sheet. Given retreat rates calculated in Chapter 3 are almost double those previously presented (see Dyke et al., 2003) it is likely SWLIS sea level equivalent contribution is substantially higher. As complete retreat of the SWLIS occurs over ≤ 2500 yrs rather than a >4000 year period, as previously proposed period, this sectors' contribution to sea level rise during the Bølling-Allerød may have been considerable more significant on a global scale. Previous ice sheet numerical models (e.g.Peltier et al 2015; Lambeck et al., 2017) are constructed in part using the ice sheet chronology of Dyke et al. (2003), thus integrating the chronology presented in Chapter 3 into these models would allow a more updated representation of ice sheet mass loss during deglaciation and, specifically the Bølling-Allerød contribution to be assessed.

While integration of new chronology into ice sheet models allows the timing of ice flow dynamics to be assessed, it is also important to consider the uncertainly associated with this chronology. As indicated in Chapter 3 compilation of available high quality

cosmogenic, radiocarbon and luminescence dates show a consistent picture of retreat that is only apparent when the associated uncertainties of these ages are considered. However, given the uncertainly associated with these chronometers range from ~200-800 yrs. it is more appropriate to produce a range of possible ice margin positions rather than a single discrete margin position. This would permit a minimum and maximum time period over which deglaciation could have taken place to be modelled and thus be more representative of the uncertainty of the deglacial ice margin chronology.

Improved dating of ice streaming operation, switching and shutdown

As has been demonstrated in Chapter 4, understanding the dynamics of ice streaming within the SWLIS is critical to explaining the ice sheets' deglacial behaviour. Constraining the time interval over which these ice streams were active is thus key to understanding the internal dynamics of the ice sheet. At present, we have indirectly dated their operation using estimates of margin position and ice thickness to infer the activity of an ice stream. However, if we want to assess the link between ice streaming activity and abrupt climate fluctuations i.e. the Bølling-Allerød a concerted effort to specifically date palaeo-ice stream tracks is needed.

Reproducing palaeo-ice stream dynamics in numerical models

Given the importance of internal controls in modulating the external climatically driven retreat rates within the SWLIS, it is clear replicating this behaviour and integrating the ice stream response is important. Much progress has recently been made in modelling the behaviour of palaeo and modern ice streaming. For the Antarctic ice sheet, Golledge et al., (2013) have successfully compared numerical and empirically derived ice stream locations. At a continental scale these ice sheet models are able to capture the complexity of modern day ice streams. For the LIS similar advances have been made. Stokes and Tarasvov (2010) compared model output against a simplified inventory of ice streams and found that major topographically controlled ice stream were reproduced. However their model was unable to reproduce many terrestrially terminating ice streams such has those associated with LGM ice streaming in the SWLIS. The most likely reason for these unrepresented ice streams is the inability of present models to integrate the role of subglacial hydrology and

substrate changes. This highlights the need for better integration of internal controls and thus is a key area for future work.

Younger Dryas behaviour

This thesis has provided the first steps in constraining the Younger Dryas position of the LIS within western North America. However, at present the LIS reaction to Younger Dryas cooling has not yet been described in detail at the ice sheet scale. Dyke et al. (2003) placed the formation of some of the major moraine system, which occur close to the geological transition to the Canadian Shield boundary, in connection with the Younger Dryas. Additionally, they also attributed several readvances to Younger Dryas cooling. Nevertheless, the constraints on the ice sheet chronology in many of these locations are limited to a few minimum limiting radiocarbon dates. While it is plausible that many of these large moraines systems are in fact of Younger Dryas age, a comprehensive dating project is needed to enhance our understand of the dynamic response of the LIS to this period of cooling.

Of interest would be the north eastern LIS margin. North of the Cree Lake Moraine an ice margin parallel with the Canadian Shield boundary has been previously suggested. Comprehensive dating along this isochrone would allow a more complete understanding of the dynamics of the LIS during this period.

Ice redevelopment during the Younger Dryas
Situated on multiple topographic highs, within the previously glaciated SWLIS, this study has recorded the re-establishment of several local plateau ice fields. Based on the morpho-stratigraphic signature of landforms on these uplands we suggest these dispersal centres were active after their surrounding valleys were ice free. Though no chronologic control directly dates the timing of these dispersal centres, based on their location compared to regional deglacial isochrones we suggest dispersal centres may have been a localised response to Younger Dryas cooling. Given the absence of research surrounding these features in a SWLIS context, a logical next step would be to constrain the timing of their formation and the climatic conditions under which they could have been sustained.

6.3 References

Dyke, A. S., Moore, A. and Robertson, L. 2003: Deglaciation of North America. *Geological Survey of Canada, Open File 1574.*

Golledge, N.R., Levy, R.H., McKay, R.M., Fogwill, C.J., White, D.A., Graham, A.G.C., Smith, J.A., Hillengrand, C.-D., Licht, K.J., Denton, G.H., Ackert Jr., R.P., Maas, S.M. and Hall, B.L. 2013: Glaciology and geological signature of the Last Glacial Maximum Antarctic ice sheet. *Quaternary Science Reviews 78,* 225-247.

Lambeck, K., Purcell, A. and Zhao, S. 2017: The North American Late Wisconsin ice sheet and mantle viscosity from glacial rebound analyses. *Quaternary Science Reviews*, *158*, 172-210.

Peltier, W.R., Argus, D.F. and Drummond, R. 2015: Space geodesy constrains ice-age terminal deglaciation: the global ICE-6G_C (VM5a) model. *Journal of Geophysical Research, 120,* 450-487.

Stokes, C. R. and Tarasov, L. 2010: Ice streaming in the Laurentide Ice Sheet: A first comparison between data-calibrated numerical model output and geological evidence. *Geophysical Research Letters*, *37*(1).

Bibliography

Alley, R. B. and Bindschadler, R. A. 2001: The West Antarctic ice sheet: behavior and environment. *American Geophysical Union.*

Alley, R.B., Clark, P.U., Huybrechts, P. and Joughin, I. 2005: Ice-sheet and sea-level changes. *Science 310*, 456-460.

Andriashek, L. D. and Atkinson, N. 2007: *Buried channels and glacial-drift aquifers in the Fort McMurray region, northeast Alberta*. Alberta Energy and Utilities Board.

Andriashek, L. D. and Barendregt, R. W. 2017: Evidence for Early Pleistocene glaciation from borecore stratigraphy in north-central Alberta, Canada. *Canadian Journal of Earth Sciences*, *54*(4), 445-460.

Andriashek, L. D. and Fenton, M. M. 1989: *Quaternary Stratigraphy and Surficial Geology of the Sand River Area 73L.* Alberta Research Council, Edmonton.

Atkinson, N., Pawley, S. and Utting, D. J. 2016: Flow-pattern evolution of the Laurentide and Cordilleran ice sheets across west-central Alberta, Canada: implications for ice sheet growth, retreat and dynamics during the last glacial cycle. *Journal of Quaternary Science*, *31*(7), 753-768.

Atkinson, N., Uttings, D. J and Pawley, S. P. 2014b: Landform signature of the Laurentide and Cordilleran ice sheet across Alberta during the last glaciation. *Canadian Journal of Earth Sciences, 51,* 1067-1083.

Atkinson, N., Uttings, D. J and Pawley, S. P. 2014a: *Glacial Landforms of Alberta. Alberta Geological Survey,* AER/AGS, Map 604.

Atkinson, N., Uttings, D. J. and Pawley, S. P. 2014: *Glacial Landforms of Alberta. Alberta Geological Survey,* AER/AGS, Map 604.

Baker, V. R. 1973: Paleohydrology and sedimentology of lake Missoula flooding in eastern Washington. *Geological Society of America Special Paper, 144*, 1–79.

Barber, D.C., Dyke, A., Hillaire-Marcel, C., Jennings, A.E., Andrews, J.T., Kerwin, M.W., Bilodeau, G., McNeely, R., Southon, J., Morehead, M.D., Gagnon, J.-M. 1999: Forcing of the cold event of 8,200 years ago by catastrophic drainage of Laurentide lakes. *Nature 400*, 344-348.

Batchelor, C. L., Margold, M., Krapp, M., Murton, D. K., Dalton, A. S., Gibbard, P. L., and Manica, A. 2019: The configuration of Northern Hemisphere ice sheets through the Quaternary. *Nature communications*, *10*(1), 1-10.

Beaney, C. L. 2002: Tunnel channels in southeast Alberta, Canada: evidence for catastrophic channelized drainage. *Quaternary International 90*, 67–74.

Bj*ö*rnsson, H. 1992: J*ö*kulhlaups in Iceland: prediction, characteristics and simulation. *Annales of Glaciology, 16*, 95–106.

Borchers, B., Marrero, S., Balco, G., Caffee, M., Goehring, B., Lifton, N., Nishiizumi, K., Phillips, F., Schaefer, J. and Stone, J. 2016: Geological calibration of spallation production rates in the CRONUS-Earth project. *Quaternary Geochronology 31,* 188–198.

Breckenridge, A. 2015: The Tintah-Campbell gap and implications for glacial Lake Agassiz drainage during the Younger Dryas cold interval. *Quaternary Science Reviews, 117,* 124-134.

Breien, H. De Blasio, F. V. Elverhoi, A. and Hoeg, K. 2008: Erosion and morphology of a debris flow caused by a glacial lake outburst flood, Western Norway. *Landslides, 5*, 271-280.

Bretz, J. H., Smith, H. T. U. and Neff, G. E. 1956: Channeled scabland of Washington: New data and Interpretations. *Geological Society of America Bulletin, 67*, 957–1049.

Broecker, W. S., Kennet, J., Flower. R, B., Teller, J., Trumbore, S., Bonani, G. and Wolfi, W. 1989: Routing of meltwater from the Laurentide Ice Sheet during the Younger Dryas cold episode. *Nature, 341,* 318-321.

Campbell, J. E. 1988: *Surficial Geology of the Buffalo Narrows Area (73N) Saskatchewan.* Saskatchewan Research Council, Sedimentary Resources, Map 1:250,000 scale.

Campbell, J. E. 2006: *Fond-du-Lac Project: Surficial Geology of the Western Fond-du-Lac Area, South-Central Beaverlodge Domain (Part of NTS 74O/5 and 6).* 1:50,000 scale preliminary map with Summary of Investigations 2006, Volume 2, Saskatchewan Geological Survey, Saskatchewan Industry and Resources, Miscellaneous Report 2006-4.2.

Campbell, J. E. 2007: *Quaternary Investigations in the Fond-du-Lac Area (part of NTS 74O/6 and /7), Southeast Beaverlodge Domain (Fond-du-Lac Project).* 1:50,000 scale preliminary map with Summary of Investigations 2007, Volume 2, Saskatchewan Geological Survey, Saskatchewan Industry and Resources, Miscellaneous Report 2007-4.2.

Campbell, J. E., Ashton. K. E, and Knox, B. 2006: *Fond-du-Lac Project: Ice Flow Indicators, Western Fond-du-Lac Area, South Central Beaverlodge Domain (Part of NTS 74O/5 and 6).* 1:50,000 scale preliminary map with Summary of Investigations 2006, Volume 2, Saskatchewan Geological Survey, Saskatchewan Industry and Resources, Miscellaneous Report 2006-4.2.

Carling, P. A. 2013: Freshwater megaflood sedimentation: What can we learn about generic processes? *Earth-Science Reviews, 125*, 87-113.

Carling, P., Villanueva, I., Herget, J., Wright, N., Borodavko, P. and Morvan, H. 2010: Unsteady 1D and 2D hydraulic models with ice dam break for Quaternary megaflood, Altai Mountains, southern Siberia. *Global and Planetary Change, 70*, 24–34.

Carlson, A. E. and Clark, P. U. 2012: Ice sheet sources of sea level rise and freshwater discharge during the last deglaciation. *Reviews of Geophysics*, *50*(4).

Carlson, A. E., and Winsor, K. 2012: Northern Hemisphere ice-sheet responses to past climate warming. *Nature Geoscience* 5(9), 607-613.

Christiansen, E. A. 1979: The Wisconsinan deglaciation, of southern Saskatchewan and adjacent areas. *Canadian Journal of Earth Sciences, 16*, 913-938.

Clark, P. U., Alley, R. B. and Pollard, D. 1999: Northern Hemisphere ice-sheet influences on global climate change. *Science*, *286*(5442), 1104-1111.

Clark, P. U., and Tarasov, L. 2014: Closing the sea level budget at the Last Glacial Maximum. *Proceedings of the National Academy of Sciences*, *111*(45), 15861-15862.

Clark, P. U., Marshall, S. J., Clarke, G. K. C., Hostetler, S. W., Licciardi, J. M. and Teller, J. T. 2001: Freshwater forcing of abrupt climate change during the last glaciation. *Science, 293*, 283–287.

Clark, P.U., Dyke, A.S., Shakun, J.D., Carlson, A.E., Clark, J., Wohlfarth, B., Mitrovica, J.X., Hostetler, S.W. and McCabe, A. 2009: The Last Glacial Maximum. *Science* 325, 710-714.

Costa, J. E. 1983: Paleohydraulic reconstruction of flash-flood peaks from boulder deposits in the Colorado Front Range. *Geological Society of America Bulletin, 94*, 986–1004.

Costa, J. E. 1984: Physical geomorphology of debris flows. *In* Costa, J. E. and Fleisher, P. J. (eds.): *Developments and Applications of Geomorphology*, 268-317. Springer, New York.

Cutler, P. M., Colgan, P. M. and Mickelson, D. M. 2002: Sedimentologic evidence for outburst floods from the Laurentide Ice Sheet margin in Wisconsin, USA: implications for tunnel channel formation. *Quaternary International, 90*, 23-40.

Dalton A.S., Margold M., Stokes C.R.; Tarasov L., Dyke A. S., Adams R. S., Allard S., Arends H. E., Atkinson N., Attig J. W., Barnett P. J., Barnett R. L.., Batterson M., Bernatchez P., Borns H. W., Breckenridge A., Briner J. P., Brouard E., Campbell J. E., Carlson A. E., Clague J. J., Curry B. B., Daigneault R., Dubé-Loubert H., Easterbrook D. J., Franzi D. A., Friedrich H. G., Funder S., Gauthier M. S., Gowan A. S., Harris K. L., Hétu B., Hooyer T. S., Jennings C.E., Johnson M. D., Kehew A. E., Kelley S. E., Kerr D., King E. L., Kjeldsen K. K., Knaeble A. R., Lajeunesse P., Lakeman T. R., Lamothe M., Larson P., Lavoie M., Loope H. M., Lowell T. V., Lusardi B. A., Manz L., McMartin I.,. Nixon C. F, Occhietti S., Parkhill M. A., Piper D. J.W., Pronk A. G., Richard P. J.H., Ridge J. C., Ross M., Roy M., Seaman A., Shaw J., Stea R. R., Teller J. T., Thompson W. B., Thorleifson L., Utting D. J., Veillette J. J., Ward B. C., Weddle T. K. and Wright H. E. 2020: An updated radiocarbon-based ice margin chronology for the last deglaciation of the North American Ice Sheet Complex. *Quaternary Science Reviews.* 234 (106223).

Davies, B. J., Livingstone, S. J., Roberts, D. H., Evans, D. J. A., Gheorghiu, D. M. and Ó Cofaigh, C. 2019: Dynamic ice stream retreat in the central sector of the last British-Irish Ice Sheet. *Quaternary Science Reviews*, *225*, 105989.

De Angelis, H. and Kleman, J. 2008: Palaeo-ice-stream onsets: examples from the north-eastern Laurentide Ice Sheet. *Earth Surface Processes and Landforms: The Journal of the British Geomorphological Research Group*, *33*(4), 560-572.

Dury, G. H. 1976: Discharge prediction, present and former, from channel dimensions. *Journal of Hydrology, 30*, 219-245.

Dyke, A. S. and Morris, T. F. 1988: Drumlin fields, dispersal trains, and ice streams in Arctic Canada. *Canadian Geographer, 32,* 86-90.

Dyke, A. S., Andrews, J. T., Clark, P. U., England, J. H., Miller, G. H., Shaw, J. and Veillette, J. J. 2002: The Laurentide and Innuitian ice sheets during the last glacial maximum. *Quaternary Science Reviews*, *21*(1-3), 9-31.

Dyke, A. S., Moore, A, and Robertson, L. 2003: Deglaciation of North America. *Geological Survey of Canada, Open File 1574.*

Dyke, A.S. and Prest, V.K. 1987: Late Wisconsinan and Holocene retreat of the Laurentide Ice Sheet. Geological Survey of Canada. Map 1702A.

Dyke, A.S., Moore, A. and Robertson, L. 2003: *Deglaciation of North America.* Geological Survey of Canada, Ottawa.

Evans, D. J. A., Clark, C. D. and Rea, B. R. 2008: Landform and sediment imprints of fast glacier flow in the southwest Laurentide Ice Sheet. *Journal of Quaternary Science, 23,* 249-272.

Evans, D. J. A., Young, N. J. P. and Ó Cofaigh, C. 2014: Glacial geomorphology of terrestrial-terminating fast flow lobes/ice stream margins in the southwest Laurentide Ice Sheet. Geomorphology, 204, 86-113

Evans, D.J.A. 2000: Quaternary geology and geomorphology of the Dinosaur Provincial Park area and surrounding plains, Alberta, Canada: the identification of former glacial lobes, drainage diversions and meltwater flood tracks. Quaternary Science Reviews, 19 (10), 931–958.

Evans, D.J.A. 2005: The glacier-marginal landsystems of Iceland. *Iceland: Modern processes and past environments*, 93-126.

Evans, D.J.A., Hiemstra, J. F., Boston, C. M., Leighton, I., Ó Cofaigh, C. and Rea, B. R. 2012: Till stratigraphy and sedimentology at the margins of terrestrially terminating ice streams: case study of the western Canadian prairies and high plains. *Quaternary Science Reviews*, *46*, 80-125.

Evans, D.J.A., Young, N. J. and Ó Cofaigh, C. 2014: Glacial geomorphology of terrestrial-terminating fast flow lobes/ice stream margins in the southwest Laurentide Ice Sheet. *Geomorphology*, *204*, 86-113.

Ferguson, R. I. 1994: Critical discharge for entrainment of poorly sorted gravel. *Earth Surface Processes and Landforms, 19,* 179–186.

Fisher, T. G. 1993: *Glacial Lake Agassiz: The N.W. outlet and paleoflood spillway, N.W. Saskatchewan and N.E. Alberta.* Ph.D. thesis. University of Calgary.

Fisher, T. G. and Lowell, T. V. 2017: Glacial geology and landforming events in the Fort McMurray region. *In* Ronaghan, B. (ed.): *Alberta's Lower Athabasca Plain: Archaeology and Paleoenvionments,* 45-68. Athabasca University Press, Alberta.

Fisher, T. G. and Smith, D. G. 1994: Glacial Lake Agassiz: its northwest maximum extent and outlet in Saskatchewan (Emerson phase). *Quaternary Science Reviews, 13*, 845–858.

Fisher, T. G. and Taylor, L. D. 2002: Sedimentary and stratigraphic evidence for subglacial flooding south-central Michigan, USA. *Quaternary International, 90*, 87–115.

Fisher, T. G. and Waterson, N., Lowell, T. V. and Hajdas, I. 2009: Deglaciation ages and meltwater routing in the Fort McMurray region, northeastern Alberta and northwestern Saskatchewan, Canada. *Quaternary Science Reviews, 28*, 1608-1624.

Fisher, T. G., Smith, D. G. and Andrews, J. T. 2002: Preboreal oscillation caused by a glacial Lake Agassiz flood. *Quaternary Science Reviews, 21*, 873–878.

Fisher, T. G., Waterson, N., Lowell, T.V. and Hajdas, I. 2009: Deglaciation ages and meltwater routing in the Fort McMurray region, northeastern Alberta and northwestern Saskatchewan, Canada. *Quaternary Science Reviews, 28,* 1608-1624.

Froese, D. F., Young, J. M., Norris, S, L. and Margold, M. 2019: Availability and viability of the ice-free corridor and pacific coast routes for the peopling of the Americas. SAA Archaeological Record. 19, 27-33.

Golledge, N. R., Kowalewski, D. E., Naish, T. R., Levy, R. H., Fogwill, C. J., and Gasson, E. G. 2015: The multi-millennial Antarctic commitment to future sea-level rise. *Nature*, *526*(7573), 421-425.

Golledge, N. R., Kowalewski, D. E., Naish, T. R., Levy, R. H., Fogwill, C. J. and Gasson, E. G. 2015: The multi-millennial Antarctic commitment to future sea-level rise. *Nature*, *526*(7573), 421-425.

Golledge, N.R., Levy, R.H., McKay, R.M., Fogwill, C.J., White, D.A., Graham, A.G.C., Smith, J.A., Hillengrand, C.-D., Licht, K.J., Denton, G.H., Ackert Jr., R.P., Maas, S.M. and Hall, B.L. 2013: Glaciology and geological signature of the Last Glacial Maximum Antarctic ice sheet. *Quaternary Science Reviews 78,* 225-247.

Greenwood, S. L. and Clark, C. D. 2009: Reconstructing the last Irish Ice Sheet 2: a geomorphologically-driven model of ice sheet growth, retreat and dynamics. *Quaternary Science Reviews*, *28*(27-28), 3101-3123.

Gregoire, L. J., Otto-Bliesner, B., Valdes, P. J. and Ivanovic, R. 2016: Abrupt Bølling warming and ice saddle collapse contributions to the Meltwater Pulse 1a rapid sea level rise. *Geophysical Research Letters*, *43*(17), 9130-9137.

Gregoire, L. J., Payne, A. J. and Valdes, P. J. 2012: Deglacial rapid sea level rises caused by ice-sheet saddle collapses. *Nature*, *487*(7406), 219-222.

GSC Geological Survey of Canada 2008: Geoscience Data Reposi- tory. Available at: http://gdr.nrcan.gc.ca/index_e.php. Natural Resources Canada, Ottawa

Hanson, M. A. 2014: *Ice-flow indicator map, Pine Channel and Fond du Lac River area (parts of NTS 74O01, 02, 07 and 08).* 1:50,000 scale preliminary map with Summary of

Investigations 2014, Volume 2, Saskatchewan Geological Survey, Saskatchewan Ministry of the Economy, Miscellaneous Report 2014-4.2.

Hanson, M. A. 2015a: *Ice-flow indicator map, Pine Channel and Fond du Lac River areas (parts of NTS 74O01, 02, 07, and 08, and 74P05, and 06).* 1:50,000 scale preliminary map with Summary of Investigations 2015, Volume 2, Saskatchewan Geological Survey, Saskatchewan Ministry of the Economy, Miscellaneous Report 2015-4.2.

Hanson, M. A. 2015b: *Preliminary ice-flow indicator mapping, Fond du Lac River area, southern Tantato Domain and northern Athabasca Basin, Saskatchewan.* 1:50,000 scale preliminary map with Summary of Investigations 2015, Volume 2, Saskatchewan Geological Survey, Saskatchewan Ministry of the Economy, Miscellaneous Report 2015-4.2.

Hanson, M. A. 2015c: *Surficial Geology of the West Fond du Lac River area (parts of NTS 74O01, 02, 07 and 08).* 1:50,000 scale preliminary map with Summary of Investigations 2015, Volume 2, Saskatchewan Geological Survey, Saskatchewan Ministry of the Economy, Miscellaneous Report 2015-4.3.

Herget J. 2005: Reconstruction of ice-dammed lake outburst floods in the Altai mountains, Siberia. *Geological Society of America, Special Paper 386,* 118 pp.

Hodgson, D. A. 1994: Episodic ice streams and ice shelves during retreat of the northwestern most sector of the Late Weichselian Laurentide Ice Sheet over the central Canadian Arctic Archipelago. *Boreas, 23,* 14-28.

Horritt, M. S. and Bates, P. D. 2002: Evaluation of 1D and 2D numerical models for predicting river flood inundation. *Journal of Hydrology, 268*, 87–99.

Hughes, A. L., Clark, C. D. and Jordan, C. J. 2014: Flow-pattern evolution of the last British Ice Sheet. *Quaternary Science Reviews*, *89*, 148-168.

Hydrologic Engineering Center. 2001: HEC-RAS river analysis system. *Hydraulic Reference Manual version. 3.0. U.S. Army Corps of Engineering*. Davis, California. 46 pp.

Ives, J. W., Froese, D., Supernant, K. and Yanicki, G. 2013: Vectors, vestiges and Valhallas: Rethinking the corridor. *Paleoamerican odyssey*, 149-169.

Kehew, A. E. 1982: Catastrophic flood hypothesis for the origin of the Souris spillway, Saskatchewan and North Dakota. *Geological Society of America Bulletin, 93*, 1051-1058.

Kehew, A. E. 1993: Glacial-lake outburst erosion of the Grand Valley, Michigan, and impacts on glacial lakes in the Lake Michigan Basin. *Quaternary Research, 39*, 544–553.

Kehew, A. E. and Clayton, L. 1983: Late Wisconsinan floods and development of the Souris-Pembina spillway system in Saskatchewan, North Dakota and Manitoba. *In* Teller, J. T., and Clayton, Lee, (eds.): Glacial Lake Agassiz. *Geological Association of Canada Special Paper 26*, 187-209.

Kehew, A. E. and Lord, M. L. 1986: Origin and large-scale erosional features of glacial-lake spillways in the northern Great Plains. *Geological Society of America Bulletin, 97,* 162–177.

Kehew, A. E. and Lord, M. L. 1987: Glacial-lake outbursts along the mid-continent margins of the Laurentide Ice Sheet. *In* Mayer, L., Nash. D. (eds.) *Catastrophic flooding*, 95-120. Allen and Unwin, London.

Kehew, A. E. and Teller, J. T. 1994: Glacial-lake spillway incision and deposition of a coarse-grained fan near Waterous, Saskatchewan. *Canadian Journal of Earth Science, 31*, 544–553.

Kershaw, J. A., Clague, J. J. and Evans, S. G. 2005: Geomorphic and sedimentological signature of a two-phase outburst flood from moraine-dammed Queen Bess Lake, British Columbia, Canada. *Earth Surface Processes and Landforms, 30,* 1–25.

Kleman, J. and Borgström, I. 1996: Reconstruction of palaeo-ice sheets: the use of geomorphological data. *Earth surface processes and landforms*, *21*(10), 893-909.

Kleman, J., Hättestrand, C., Borgström, I. and Stroeven, A. 1997: Fennoscandian palaeoglaciology reconstructed using a glacial geological inversion model. *Journal of glaciology*, *43*(144), 283-299.

Kleman, J., Jansson, K., De Angelis, H., Stroeven, A. P., Hatterstrand, C., Alm G. and Glasser, N.F. 2010: North American ice sheet build-up during the last glacial cycle, 115-21 kyr. *Quaternary Science Reviews, 29,* 2036-2051.

Komar, P. D. 1987: Selective gravel entrainment and the empirical evaluation of flow competence. *Sedimentology, 34*, 1165–1176.

Kozlowski, A. L., Kehew, A. E. and Brian, C. B. 2005: Outburst flood origin of the Central Kalamazoo River Valley, Michigan, USA. *Quaternary Science Reviews, 24*, 2354-2375.

Lambeck, K., Purcell, A. and Zhao, S. 2017: The North American late Wisconsin ice sheet and mantle viscosity from glacial rebound analyses. *Quaternary Science Reviews,* 158, 172–210.

Landvik, J. Y., Alexanderson, H., Henriksen, M. and Ingólfsson, Ó. 2014: Landscape imprints of changing glacial regimes during ice-sheet build-up and decay: a conceptual model from Svalbard. *Quaternary Science Reviews*, *92*, 258-268.

Lifton, N., Sato, T. and Dunai, T. J. 2014: Scaling in situ cosmogenic nuclide production rates using analytical approximations to atmospheric cosmic-ray fluxes. *Earth and Planetary Science Letters*, *386*, 149-160.

Lord, M. L. and Kehew, A. E. 1987: Sedimentology and paleohydrology of glacial-lake outburst deposits in southeastern Saskatchewan and northwestern North Dakota. *Geological Society of America Bulletin, 99*, 663–673.

Maizels, J. 1997: Jokulhlaup deposits in proglacial areas. *Quaternary Science Reviews, 16,* 793–819.

Maizels, J. K. 1991: Origin and evolution of Holocene sandurs in areas of Jokulhlaup drainage, south Iceland. *In* Maizels, J. K. and Caseldine, C. (eds.): *Environmental Change in Iceland: Past and Present,* 267–302. Kluwer, Dordrecht.

Malde, H. E. 1968. The catastrophic late Pleistocene Bonneville flood in the Snake River Plain, Idaho. *US Geological Survey Professional Paper,* 595 pp.

Margold, M., Gosse, J. C., Hidy, A. J., Woywitka, R. J., Young, J. M. and Froese, D. 2019: Beryllium-10 dating of the Foothills Erratics Train in Alberta, Canada, indicates detachment of the Laurentide Ice Sheet from the Rocky Mountains at~ 15 ka. *Quaternary Research 92*(2), 469-482.

Margold, M., Jansen, J. D., Codilean, A. T., Preusser, F., Gurinov, A. L., Fujioka, T. and Fink, D. 2018: Repeated megafloods from glacial Lake Vitim, Siberia, to the Arctic Ocean over the past 60,000 years. *Quaternary Science Reviews, 187*, 41–61.

Margold, M., Stokes, C. R. and Clark, C. D. 2015a: Ice streams in the Laurentide Ice Sheet: identification, characteristics and comparison to modern ice sheets. *Earth Science Reviews, 143,* 117-146.

Margold, M., Stokes, C. R. and Kleman, J. 2015b: Ice streams in the Laurentide Ice Sheet: a new mapping inventory. *Journal of Maps, 11,* 380-395.

Margold, M., Stokes, C. R. and Clark, C. D. 2018: Reconciling records of ice streaming and ice margin retreat to produce a palaeogeographic reconstruction of the deglaciation of the Laurentide Ice Sheet. *Quaternary Science Reviews, 189*, 1-30.

Menounos, B., Goehring, B. M., Osborn, G., Margold, M., Ward, B., Bond, J. and Caffee, M. W. 2017: Cordilleran Ice Sheet mass loss preceded climate reversals near the Pleistocene Termination. *Science*, *358*(6364), 781-784.

Moran, S. R., Clayton, L., Hooke, R. L., Fenton, M. M. and Aandriashek, L. D. 1980: Glacier-bed landforms of the prairie region of North America. *Journal of Glaciology, 25,* 457-476.

Munro-Stasiuk, M. J., 1999: Evidence for water storage and drainage at the base of the Laurentide ice sheet, south-central Alberta, Canada. *Annals of Glaciology, 28*, 175–180.

Munyikwa, K., Feathers, J.K., Rittenour, T.M. and Shrimpton, H.K. 2011: Constraining the late Wisconsinan retreat of the Laurentide ice sheet from western Canada using luminescence ages from post-glacial aeolian dunes. Quaternary Geochronology 6, 407–422.

Munyikwa, K., Rittenour, T. M. and Feathers, J. K. 2017: Temporal constraints for the Late Wisconsinan deglaciation of western Canada using eolian dune luminescence chronologies from Alberta. *Palaeogeography, palaeoclimatology, palaeoecology*, *470*, 147-165.

Murton, J. B., Bateman, M. D., Dallimore, S. R., Teller, J. T. and Yang, Z. 2010: Identification of Younger Dryas outburst flood path from Lake Agassiz to the Arctic Ocean. *Nature*, *464*(7289), 740-743.

Norris. S. L., Margold, M. and Froese, D. G. 2017: Glacial landforms of northwest Saskatchewan. *Journal of Maps*. 13:2, 600-607.

Ó Cofaigh, C., Evans, D. J. A. and Smith, R. 2010: Large-scale reorganization and sedimentation of terrestrial ice streams during late Wisconsinan Laurentide Ice Sheet deglaciation. *Geological Society of America 122*, 743-756.

O'Connor J. E, Hardison J. H. and Costa, J. E. 2001: Debris flows from failures of Neoglacial-age moraines in the Three Sisters and Mount Jefferson wilderness areas, Oregon. *US Geological Survey Professional Paper, 1606.*

O'Connor, J. E. 1993: Hydrology, hydraulics, and geomorphology of the Bonneville Flood. *Geological Society of America Special Paper 274*, 83-89.

Peltier, W.R., Argus, D.F. and Drummond, R. 2015: Space geodesy constrains ice-age terminal deglaciation: the global ICE-6G_C (VM5a) model. *Journal of Geophysical Research, 120,* 450-487.

Pierson, T. C. 1981: Dominant particle support mechanisms in debris flows at Mt. Thomas, New Zealand, and implications for flow mobility: *Sedimentology, 28*, 4940-4953.

Prest, V. K. 1968: *Nomenclature of moraines and ice-flow features as applied to the glacial map of Canada* (p. 32). Department of Energy, Mines and Resources.

Prest, V. K., Grant, D. R. and Rampton, V. N. 1968: *Glacial map of Canada.* Geological Survey of Canada, Map 1253A.

Rasmussen, S. O., Andersen, K. K., Svensson, A. M., Steffensen, J. P., Vinther, B. M., Clausen, H. B. and Bigler, M. 2006: A new Greenland ice core chronology for the last glacial termination. *Journal of Geophysical Research: Atmospheres*, *111*(D6).

Rignot, E., and Thomas, R. H. 2002: Mass balance of polar ice sheets. *Science*, *297*(5586), 1502 1506.

Rignot, E., Bamber, J. L., Van Den Broeke, M. R., Davis, C., Li, Y., Van De Berg, W. J., and Van Meijgaard, E. 2008: Recent Antarctic ice mass loss from radar interferometry and regional climate modelling. *Nature Geoscience 1*(2), 106-110.

Rignot, E., Velicogna, I., van den Broeke, M.R., Monaghan, A. and Lenaerts, J.T.M. 2011: Acceleration of the contribution of the Greenland and Antarctic ice sheets to sea level rise. *Geophysical Research Letters 38*, L05503.

Ritz, C., Edwards, T. L., Durand, G., Payne, A. J., Peyaud, V., and Hindmarsh, R. C. 2015: Potential sea-level rise from Antarctic ice-sheet instability constrained by observations. *Nature 528*(7580), 115-118.

Ross, M., Campbell, J.E., Parent, M. and Adams, R.S. 2009: Palaeo-ice streams and the subglacial landscape mosaic of the North American mid-continental prairies. *Boreas* 38, 421–439.

Russell, A. J., Roberts, M. J., Fay, H., Marren, P. M., Cassidy, N. J., Tweed, F. S. and Harris, T. 2006: Icelandic jökulhlaup impacts: implications for ice-sheet hydrology, sediment transfer and geomorphology. *Geomorphology, 75*, 33-64.

Schreiner, B. I. 1984a: *Quaternary geology of the Precambrian Shield, Saskatchewan.* Saskatchewan Energy and Mines, Report 221.

Schreiner, B. I. 1984b: *Quaternary geology of the Ile-a-la-Crosse area (NTS 73O).* Saskatchewan Energy and Mines, Open File Rep. 84-5.

Schreiner, B. I. 1984c: *Quaternary geology of the Mudjatik area (NTS 74B).* Saskatchewan Energy and Mines, Open File Rep. 84-8.

Schreiner, B. I. 1984d*: Quaternary geology of the La Loche area (NTS 74C).* Saskatchewan Energy and Mines, Open File Rep. 84-9.

Schreiner, B. I. 1984e: *Quaternary geology of the Cree Lake area (NTS 74G).* Saskatchewan Energy and Mines, Open File Rep. 84-12.

Schreiner, B. I. 1984f: *Quaternary geology of the Lloyd Lake area (NTS 74F).* Saskatchewan Energy and Mines, Open File Rep. 84-13.

Schreiner, B. I. 1984g: *Quaternary geology of the Livingstone Lake area (NTS 74J).* Saskatchewan Energy and Mines, Open File Rep. 84-16.

Schreiner, B. I. 1984h: *Quaternary geology of the William River area (NTS 74K).* Saskatchewan Energy and Mines, Open File Rep. 84-17.

Schreiner, B. I. 1984i: *Quaternary geology of the Fond-du-Lac area (NTS 74O).* Saskatchewan Energy and Mines, Open File Rep. 84-20.

Schreiner, B. I. 1984j: *Quaternary geology of the Tazin Lake area (NTS 74N).* Saskatchewan Energy and Mines, Open File Rep. 84-21.

Schreiner, B. T. 1983: Lake Agassiz in Saskatchewan, *In* Teller, J. T., and Clayton, L. (eds.) Glacial Lake Agassiz: *Geological Association of Canada Special Paper 25*, 75-96.

Scott, B. P. 1965: *Geology of the Upper Clearwater Area. Saskatchewan Energy and Mines.* Open File Report 85-2.

Shaw, J., Sharpe, D., and Harris, J. 2010: A flowline map of glaciated Canada based on remote sensing data. *Canadian Journal of Earth Sciences, 47*, 89-101.

Simpson, M. A. 1988: *Surficial geology of the Ile-a-la-Crosse Area (73O) Saskatchewan.* Saskatchewan Research Council, Sedimentary Resources, Map 1:250,000 scale.

Simpson, M. A. 1997: *Surficial geology map of Saskatchewan. Saskatchewan Energy and Mines/ Saskatchewan Research Council.* Map 1:1000,000 scale.

Sjogren, D. B. and Rains, R. B., 1995: Glaciofluvial erosional morphology and sediments of the Coronation–Spondin Scabland, east-central Alberta*. Canadian Journal of Earth Sciences, 32*, 565–578.

Slimmon, W. L. 2011: *Geological Atlas of Saskatchewan; Saskatchewan.* Ministry of Energy and Resources, Miscellaneous Report, 2011-7 CD_ROM, version 14, URL: http://www.infomaps.gov.sk.ca/website/SIR_Geological_Atlas/SK.

Smith, D. G. and Fisher, T. G. 1993: Glacial Lake Agassiz: The northwestern outlet and paleoflood. *Geology*, *21*(1), 9-12.

Smith, G. A. 1986: Coarse-grained nonmarine volcaniclastic sediment: Terminology and depositional Processes. *Geological Society of America Bulletin, 97*, 1-10.

Smith, M. J. and Clark, C. D. 2005: Methods for the visualization of digital elevation models for landform mapping. *Earth Surface Processes and Landforms, 30*, 885-900.

Stokes, C. R. and Clark, C. D. 2002: Ice Stream Shear Margin Moraines'. *Earth Surface Processes and Landforms, 27,* 547-558.

Stokes, C. R. and Tarasov, L. 2010: Ice streaming in the Laurentide Ice Sheet: A first comparison between data-calibrated numerical model output and geological evidence. *Geophysical Research Letters*, *37*(1).

Stokes, C. R., and Clark, C. D. 2002: Are long subglacial bedforms indicative of fast ice flow?. *Boreas*, *31*(3), 239-249.

Stokes, C. R., Margold, M., Clark. C. D. and Tarasov, L. 2016: Ice stream activity scaled to ice sheet volume during Laurentide Ice Sheet deglaciation. *Nature, 530,* 322-326.

Stokes, C.R., Tarasov, L., Blomdin, R., Cronin, T., Fisher, T.G., Gyllencreutz, R., Tarasov, L. and Peltier, W.R. 2005: Arctic freshwater forcing of the Younger Dryas cold reversal. *Nature 435*, 662-665.

Tarasov, L., Dyke, A.S., Neal, R.M. and Peltier, W.R. 2012: A data-calibrated distribution of deglacial chronologies for the North American ice complex from glaciological modelling. *Earth and Planetary Science Letters 315*, 30-40.

Teller, J. T. and Clayton, L. (eds). 1983: Glacial Lake Agassiz. *Geological Association of Canada, Special Paper 26,* 117-131.

Teller, J. T. and Leverington, D. W. 2004: Glacial Lake Agassiz: a 5000 yr history of change and its relationship to the d18O record of Greenland. *Geological Society of America Bulletin, 116,* 729-742.

Teller, J. T., Leverington, D. W. and Mann, J. D. 2002: Freshwater outbursts to the oceans from glacial Lake Agassiz and their role in climate change during the last deglaciation. *Quaternary Science Reviews, 21*, 879–887.

Thompson, S. M. and Campbell, P. L. 1979: Hydraulics of a large channel paved with boulders. *Journal of Hydraulic Research, 17*, 341-354.

Todd, S. P. 1989: Stream-driven, high-density gravelly traction carpets: possible deposits in the Trabeg Conglomerate Formation, SW Ireland and some theoretical considerations of their origin. *Sedimentology, 36*, 513-530.

Travis, B., Teal, M. and Gusman, J. 2012: Best Methods and Inherent Limitations of Bulked Flow Modeling with HEC-RAS. Conference. Proceedings of the 2012 World Environmental and Water Resources Conference. Albuquerque, New Mexico.

Utting, D. J., Atkinson, N. and Pawley, S. 2015: Reconstruction of proglacial lakes in Alberta. *Canadian Quaternary Association Conference.* St. John's, Canada.

W.R., Peteet, D.M., Piper, D.J.W., Preusser, F., Renssen, H., Roberts, D.H., Roche,
Waitt, R. B. 1980: About 40 last-glacial Lake Missoula jokulhlaups through southern Washington. *Journal of Geology, 88*, 653-679.

Waitt, R. B. 1985: Case for periodic, colossal jókulhlaups from glacial Lake Missoula. *Geological Society of America Bulletin, 95*, 1271-1286.

Williams, G. P. 1983: Paleohydrological methods and some examples from Swedish fluvial environments I: cobble and boulder deposits. *Geografiska Annaler, 65*, 227–243.

Wolfe, S., Huntley, D. and Ollerhead, J. 2004: Relict late Wisconsinan dune fields of the northern Great Plains, Canada. Géographie physique et Quaternaire 58, 323–336.

Young, R. R., Burns, J. A., Smith, D. G., Arnold, L. D. and Rains, R. B. 1994: A single, late Wisconsin, Laurentide glaciation, Edmonton area and southwestern Alberta. *Geology*, *22*(8), 683-686.
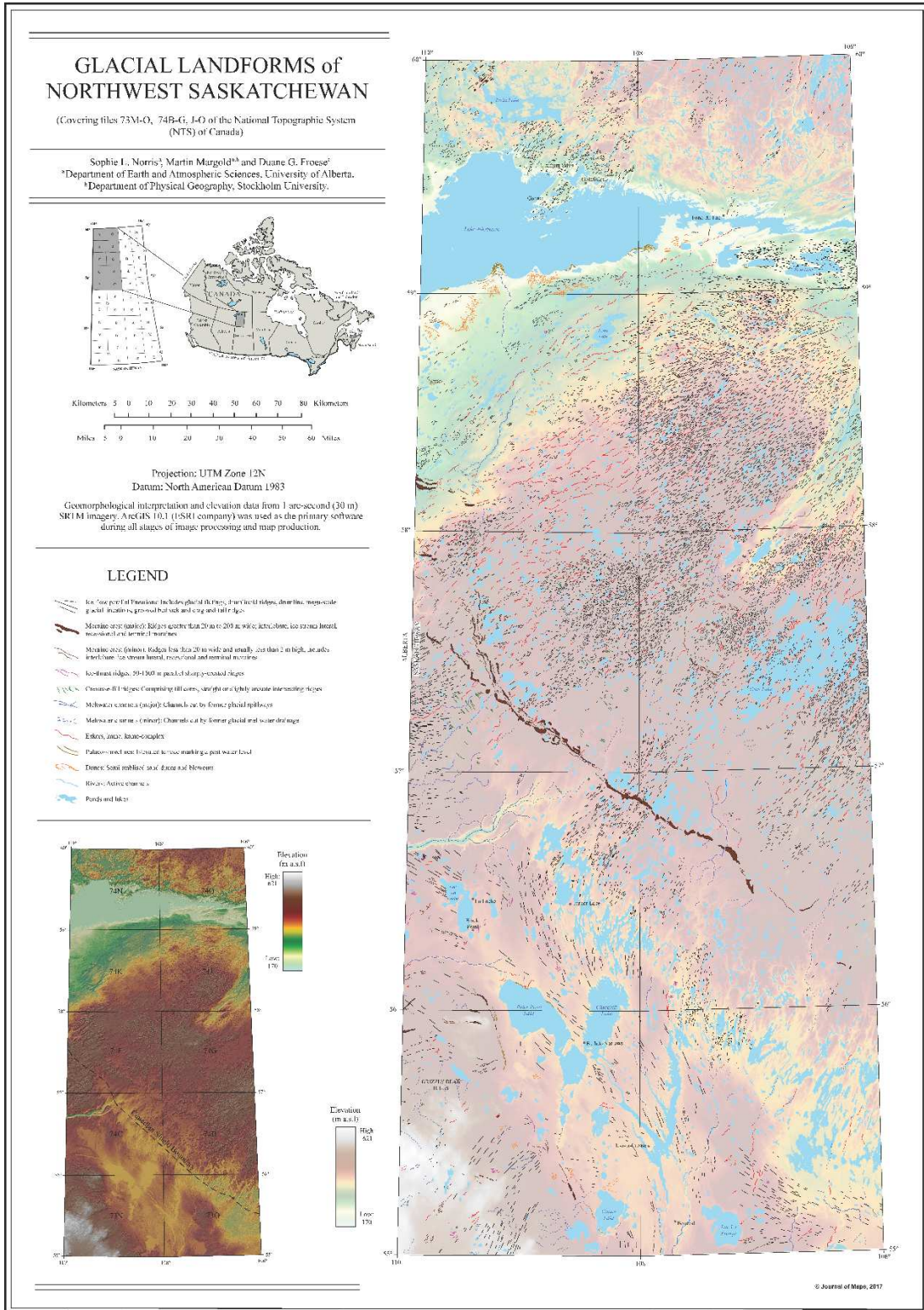
Figure SA1: Glacial landforms of northeast Alberta and northwest Saskatchewan.

APPENDIX B: SUPPORTING INFORMATION FOR CHAPTER 3

Cosmogenic nuclide exposure dating

Laboratory methods

Samples were collected for exposure dating with a diamond blade concrete saw or hammer and chisel. All samples were prepared as BeO targets at CRISDal Lab, Dalhousie University. To facilitate isolation of sufficient quartz, the following laboratory techniques were employed.

The samples were cleaned, crushed, and ground, and the 250-355 mm fraction was rinsed, leached in aqua regia (2 hours), and etched in HF, before mineral separation using combinations of froth flotation, Frantz magnetic separation, air abrasion, heavy liquids, and controlled digestions of non-quartz phases using hydrofluoric or hexafluorosilicic acids. When the quartz concentration was sufficiently pure (as determined optically and with <100 ppm Al and Ti as determined on a 1 g aliquot with the lab's ICP-OES), approximately 35 wt% of the dried quartz concentrate was removed in an ultrasonic bath with dilute HF as per Kohl and Nishiizumi (1992). The samples were spiked with approximately 240 µg of the lab's $BeCl_2$ carrier ('Be-Carrier-31-28Sept2012'; prepared from a deeply mined Ural Mountain phenacite with $^{10}Be/^9Be$ below 1 x 10-16), and were digested in a $HF-HNO_3$ mixture, evaporated twice in perchloric acid, and treated with anion and cation column chemistry to isolate the Be^{2+}. After acidifying with perchloric and nitric acid to remove residual B, $Be(OH)_2$ was precipitated using ultrapure ammonia gas, transferred to a cleaned boron-free quartz vial and carefully calcined in a Bunsen burner flame to a white oxide for over three minutes. The BeO's were powdered, mixed 2:3 by volume with high purity niobium powder (325 mesh), and packed into stainless steel cathodes for $^{10}Be/^9Be$ measurement at the Center for Accelerator Mass Spectrometry, Lawrence Livermore National Lab (CAMS-LLNL). These measurements were made against the 07KNSTD3110 standard with a known ratio of $^{10}Be/^9Be$=2850x10-15 (Nishiizumi et al. 2007). Process blanks were also analysed and used to subtract ^{10}Be

introduced during target preparation and analysis. For all samples, this correction was less than 1% of the adjusted ^{10}Be values.

Age calculation

Exposure ages were calculated using the CRONUS-Earth Online Calculator (Balco et al., 2008; v3.0; constrants 3.0.3) using the default calibration set of Borchers et al. (2016) and the time dependent 'LSDn' production scaling scheme of Lifton et al., (2014). Utilizing other scaling schemes or production rates does not alter our conclusions as the ages are within the internal uncertainty of our reported ages. We report exposure ages with no correction for snow shielding and with a zero erosion rate. The region has low winter precipitation average and sample boulders are large and situated on open plains or ridge tops, therefore we would expect boulders to be adequately windswept of snow. Additionally, due to the highly resistant nature of erratic's rock type, and a sampling strategy that avoids surfaces with evidence of erosion, we assume surface erosion to be less than a few mm since deposition.

Glacial isostatic adjustment (GIA) of the region, resulting from the depression of the lands surface by a >1.5 km thick continental ice sheet (Lambeck et al., 2017), affects the elevation and thus measured nuclide concentration of our samples. We apply a GIA correction using the Lambeck et al. (2017) ice sheet reconstruction. We also obtain GIA from Gowan et al. (2016) and Ice 5G (Peltier, 2015) however favor that of Lambeck et al. (2017) due to its higher spatial and/or temporal resolution. We calculate the elevation for each sample site at 500 yr intervals, from ice free conditions within the model to 0 yrs, using Lambeck et al's. (2017) dRSL data. Based on 500 yr interval elevations we calculate a mean dRSL for each sample site. We then adjust the modern elevation of our sample sites by the mean dRSL elevation. This GIA correction makes ages 4-6% older than uncorrected ages.

Compilation of pre-existing chronology

We compile a dataset of pre-existing luminescence, ^{10}Be surface exposure ages and 'high quality' minimum radiocarbon chronologies. Individual dates are summarised in table SB3.

Pre-existing ^{10}Be surface exposure ages are limited to a single study in the region. 16 glacial erratic boulders that mark the zone of convergence of the Laurentide and Cordilleran Ice sheets have been recently re-dated (Margold et al., 2019) using ^{10}Be surface exposure ages. Of the 16 boulders dated, 12 accurately constrain the age of decoupling of the two ice sheets and are used by the original authors to provide a weighted mean age, including propagated uncertainty, of 14,900 ± 900 cal yr BP. We present these dates at one standard deviation uncertainty consistent with our samples.

Optically stimulated luminescence (OSL) and infrared stimulated luminescence (IRSL), from eolian sands have been previously used to constrain deglaciation within the study region (Wolfe et al., 2004; Munyikwa et al., 2011, 2017). We collate dates and group them into sites within 40km and present the oldest reliable sites where several exist within a 40 km region *(40 km region is equal to maximum size of a single sand dune field)*. We remove outliers proposed by the original authors and present dates with one standard deviation uncertainty.

A large number of radiocarbon dates have been used to constrain the deglaciation of the southwestern sector of the LIS. We focus on 'high quality' minimum limiting radiocarbon chronologies and present the five oldest reliable dates in each location. We exclude dates on bulk sediments, terrestrial shells or mixed assemblages. Where available Accelerator Mass Spectrometry (AMS) radiocarbon dates are prioritized over radiometric (conventional) dating methods. In cases of bone, ultrafiltered collagen samples, where available, are prioritized. We remove outliers proposed by the original authors or where later data complications make clear arguments for the exclusion of single unreproduced dates. Radiocarbon dates are recalibrated using IntCal13 (Reimer et al., 2013) and presented at two standard deviation uncertainty.

Table SB1. Cosmogenic ^{10}Be sample details and modelled surface exposure ages

Laboratory no.	Sample ID	Latitude (DD)	Longitude (DD)	Modern elevation (m a.s.l.)	Palaeo-elevation (m a.s.l.)	Boulder height (m)	Sample thickness (cm)	Quartz Mass (g)	Be carrier mass (g)	^{10}Be/^{9}Be (10^{-14})	^{10}Be ± 1σ (atoms g^{-1} SiO$_2$)	^{10}Be age[a] (ka)	^{10}Be age[b] (ka)	^{10}Be age[c] (ka)
Pine Lake Moraine														
JG3829	PL-SN-01	52.1622	-113.51281	927	897	0.7	2	20.201	0.2504	6.56	56602 ± 1607	5.8 ± 0.2	6.0 ± 0.2	6.0 ± 0.2
JG3830	PL-SN-02	52.1622	-113.51274	927	897	0.8	2	20.0614	0.2103	7.51	54769 ± 1976	5.7 ± 0.2	5.8 ± 0.2	5.8 ± 0.2
JG3831	PL-SN-03	52.1621	-113.51276	926	896	1.6	2	25.0204	0.8262	13.16	80616 ± 1695	8.3 ± 0.2	8.5 ± 0.2	8.4 ± 0.2
JG3832	PL-SN-05	52.1607	-113.54400	976	949	0.8	2	25.198	0.8199	21.60	130685 ± 2587	12.9 ± 0.3	13.2 ± 0.3	13.2 ± 0.3
Beaver River Region														
JG3826	ML-BR-01	54.2769	-109.05209	496	469	0.7	3	20.028	0.208	12.48	90900 ± 2205	13.5 ± 0.3	13.9 ± 0.3	13.9 ± 0.3
JG3827	ML-BR-02	54.2770	-109.05213	492	465	0.8	2.5	20.0498	0.2109	11.93	88020 ±2402	13.1 ± 0.4	13.4 ± 0.4	13.4 ± 0.4
JG3612	ML-BR-03	54.276979	-109.053532	492	465	1	3	30.072	0.2087	17.78	87398 ± 1848	13.1 ± 0.3	13.4 ± 0.3	13.4 ± 0.3
JG3613	ML-BR-04	54.276866	-109.054023	501	474	1.3	3	27.664	0.1994	18.03	92033 ± 1943	13.6 ± 0.3	14.0 ± 0.3	14.0 ± 0.3
JG3614	ML-BR-06	54.316897	-109.52475	490	463	1	3	20.207	0.212	12.04	85866 ± 1965	12.9 ± 0.3	13.2 ± 0.3	13.2 ± 0.3
JG3828	ML-BR-07	54.3179	-109.52480	526	499	1.6	3	20.0501	0.211	11.85	87450 ±2179	12.7 ± 0.3	13.0 ± 0.3	13.0 ± 0.3
Clearwater Lower Athabasca Spillway														
JG3602	CLM-S-02	56.834014	-109.076727	455	405	0.8	2.5	15.218	0.206	11.62	106578 ± 2095	16.3 ± 0.3	17.1 ± 0.3	16E-.9 ± 0.3
JG3603	CLM-S-03	56.834409	-109.076172	457	407	0.7	3.5	20.2939	0.2065	9.71	69762 ± 1890	10.7 ± 0.3	11.2 ± 0.3	11.0 ± 0.3
JG3604	CLM-S-04	56.9179	-108.97747	432	379	1	3	20.299	0.2064	11.24	80821 ± 2165	12.6 ± 0.3	13.3 ± 0.4	13.2 ± 0.4
JG3605	CLM-S-05	56.91788	-108.978	425	372	0.5	2	27.6148	0.2134	16.56	90659 ± 1910	14.2 ± 0.3	14.9 ± 0.3	14.7 ± 0.3
JG3606	CLM-S-06	56.91793	-108.97805	425	372	0.5	2.5	20.188	0.2070	10.99	79711 ± 1897	12.5 ± 0.3	13.2 ± 0.3	13.0 ± 0.3
Cree Lake Moraine														
JG3607	CLM-Mr-01	57.52343	-109.31159	566	502	1.2	1.5	30.0719	0.2141	16.63	83839 ± 1766	11.4 ± 0.3	12.1 ± 0.3	11.9 ± 0.3
JG3608	CLM-Mr-03	57.52338	-109.31061	569	505	0.7	1.5	27.566	0.2022	17.04	88465 ± 1866	12.0 ± 0.3	12.7 ± 0.3	12.6 ± 0.3
JG3609	CLM-Mr-04	57.34907	-109.22395	554	497	0.5	2	20.2944	0.2059	14.08	101095 ± 2170	14 .0 ± 0.3	14.7 ± 0.3	14.6 ± 0.3
JG3610	CLM-Mr-05	57.35009	-109.22413	562	505	0.5	1.5	30.0501	0.2067	18.61	90668 ± 1868	12.4 ± 0.3	13.1 ± 0.3	12.9 ± 0.3
JG3611	CLM-Mr-13	57.52379	-109.31047	573	509	0.3	2	30.1446	0.2076	17.11	83457 ± 1758	11.3 ± 0.2	12.0 ± 0.3	11.8 ± 0.2
Upper Cree Lake Moraine- East														
JG3615	UCLM-E-03	58.4685	-110.1993	285	210	1.6	4	27.5495	0.1992	11.59	59225 ± 1336	10.7 ± 0.2	11.6 ± 0.3	11.2 ± 0.3

JG3616	UCLM-E-04	58.4688	-110.2	281	206	1	4	30.0464	0.2061	12.12	58797 ± 1336	10.7 ± 0.2	11.5 ± 0.3	11.2 ± 0.3
JG3617	UCLM-E-05	58.4678	-110.1981	283	208	1.3	4	27.5301	0.2004	16.15	83232 ± 1761	15.1 ± 0.3	16.3 ± 0.3	15.9 ± 0.3
Upper Cree Lake Moraine- West														
JG3618	UCLM-W-06	58.1798	-110.431	315	253	0.6	4	30.0209	0.2088	14.99	73800 ± 1839	13.0 ± 0.3	13.8 ± 0.3	13.5 ± 0.3
JG3619	UCLM-W-07	58.1807	-110.4298	344	282	1	4	27.5892	0.2035	12.82	66875 ± 1412	11.4 ± 0.2	12.1 ± 0.3	11.9 ± 0.3
JG3620	UCLM-W-08	58.1807	-110.4296	335	273	1.3	4	27.5556	0.2132	12.22	66859 ± 1432	11.5 ± 0.2	12.3 ± 0.3	12.0 ± 0.3

Notes: Rock density for all samples is 2.6 g cm^{-3}; no shielding correction applied to samples; exposure ages were calculated using the online calculator formerly known as CRONUS (Balco et al., 2008; v3.0; constants 3.0.3)

[a] Ages calculated using the CRONUS default production rate (Borchers et al., 2016) , Lm scaling (Lal, 1991/Stone, 2000) and modern day elevations

[b] Ages calculated using the CRONUS default production rate (Borchers et al., 2016) , Lm scaling (Lal, 1991/Stone, 2000) and glacioisostatic palaeo-elevations.

[c] Ages calculated using the CRONUS default production rate (Borchers et al., 2016), LSDn scaling (Lifton et al., 2014) and glacioisostatic palaeo-elevations.

Table SB2. Summary statistics for [10]Be surface-exposure age distributions.

Data Set	N	$N_{removed}$	Mean age (ka)	±1σ (ka)	Propagated uncertainty (ka)	Error-weighted mean (ka)	Error-weighted uncertainty (ka)	Standard error of the mean (ka)	Median age (ka)	χ^2 calculated	χ^2 expected (95%)	χ^2 test (Pass/Fail)
UCLM-E (outliers)	3	-	12.8	2.7	1.6	12.3	0.2	1.6	11.2	11.63	5.99	Fail
UCLM-E (no outliers)	2	1	11.2	0.03	0.7	11.2	0.2	0.02	11.2	0.0008	3.84	Pass
UCLM-W (no outliers)	3	-	12.5	0.9	0.9	12.3	0.2	0.5	12.0	1.41	5.99	Pass
CLM (no outliers)	5	-	12.7	1.1	0.9	12.6	0.1	0.5	12.6	3.93	9.49	Pass
CLAS (outliers)	5	-	13.8	2.2	1.3	13.6	0.1	1.0	13.1	13.82	9.49	Fail
CLAS (no outliers)	4	1	13.0	1.5	1.1	12.9	0.2	0.8	13.1	6.83	7.82	Pass
BR (no outliers)	6	-	13.5	0.4	0.8	13.5	0.1	0.2	13.4	0.94	11.07	Pass

Table SB3**.** Synthesis of existing ^{10}Be surface exposure ages, luminescence and minimum-limiting radiocarbon chronologies.

Table DR3. Synthesis of existing 10Be surface exposure ages, luminescence and minimum-limiting radiocarbon chronologies.

Sample ID	Locality (Fig. 1 Location)	Location Desciption	Latitude (DD)	Longitude (DD)	Method	Dated Material	14C age (years)	14C error (years)	2σ lower (years)	2σ upper (years)	Age (years)	1σ uncertainty (years)	Reference	Comment
ALT-MM-15-09	A	Foothills Erratics Train, AB	50.1366	-113.7574	CN	Quartzite erratic	-	-	-	-	169,500	11,200	Margold et al., 2019	regarded anomolous by author
ALT-MM-15-14	A	Foothills Erratics Train, AB	52.1750	-114.8700	CN	Quartzite erratic	-	-	-	-	22,400	1,600	Margold et al., 2019	regarded anomolous by author
ALT-MM-15-01	A	Foothills Erratics Train, AB	49.1003	-112.2226	CN	Granite erratic	-	-	-	-	17,700	1,200	Margold et al., 2019	not shield origin, regarded anomolous by author
ALT-MM-15-16	A	Foothills Erratics Train, AB	53.3807	-116.7881	CN	Quartzite erratic	-	-	-	-	16,300	1,100	Margold et al., 2019	
ALT-MM-15-10	A	Foothills Erratics Train, AB	50.3062	-113.8719	CN	Quartzite erratic	-	-	-	-	15,600	1,000	Margold et al., 2019	
ALT-MM-15-04	A	Foothills Erratics Train, AB	49.9625	-113.6892	CN	Quartzite erratic	-	-	-	-	15,500	1,000	Margold et al., 2019	
ALT-MM-15-15	A	Foothills Erratics Train, AB	52.1873	-114.8820	CN	Quartzite erratic	-	-	-	-	15,200	1,000	Margold et al., 2019	
ALT-MM-15-08	A	Foothills Erratics Train, AB	50.1025	-113.7862	CN	Quartzite erratic	-	-	-	-	15,100	1,000	Margold et al., 2019	
ALT-MM-15-05	A	Foothills Erratics Train, AB	49.9555	-113.8373	CN	Quartzite erratic	-	-	-	-	15,000	1,000	Margold et al., 2019	
ALT-MM-15-02	A	Foothills Erratics Train, AB	49.7785	-113.6514	CN	Quartzite erratic	-	-	-	-	14,700	1,000	Margold et al., 2019	
ALT-MM-15-03	A	Foothills Erratics Train, AB	49.7783	-113.6511	CN	Quartzite erratic	-	-	-	-	14,700	1,000	Margold et al., 2019	
ALT-MM-15-13	A	Foothills Erratics Train, AB	51.6350	-114.4786	CN	Quartzite erratic	-	-	-	-	14,600	1,000	Margold et al., 2019	
ALT-MM-15-12	A	Foothills Erratics Train, AB	50.5313	-114.1399	CN	Quartzite erratic	-	-	-	-	14,500	1,000	Margold et al., 2019	
ALT-MM-15-07	A	Foothills Erratics Train, AB	49.9559	-113.8358	CN	Quartzite erratic	-	-	-	-	14,300	900	Margold et al., 2019	
ALT-MM-15-11	A	Foothills Erratics Train, AB	50.3087	-113.8721	CN	Quartzite erratic	-	-	-	-	14,200	900	Margold et al., 2019	
ALT-MM-15-06	A	Foothills Erratics Train, AB	49.9559	-113.8361	CN	Quartzite erratic	-	-	-	-	8,200	500	Margold et al., 2019	regarded anomolous by author
UCIAMS-127348	B	Wally's Beach, AB	49.3386	-113.1445	C14	Bone (Equua conversidens)	11470	35	13430	13230	-	-	Waters et al., 2014	Ultrafiltered Collagen
UCIAMS-116400	B	Wally's Beach, AB	49.3386	-113.1445	C14	Bone (Equua conversidens)	11465	40	13420	13210	-	-	Waters et al., 2014	Ultrafiltered Collagen
UCIAMS-127352	B	Wally's Beach, AB	49.3386	-113.1445	C14	Bone (Equua conversidens)	11475	30	13420	13250	-	-	Waters et al., 2014	Ultrafiltered Collagen
UCIAMS-127350	B	Wally's Beach, AB	49.3386	-113.1445	C14	Bone (Equua conversidens)	11460	30	13410	13220	-	-	Waters et al., 2014	Ultrafiltered Collagen
UCIAMS-127355	B	Wally's Beach, AB	49.3386	-113.1445	C14	Bone (Equua conversidens)	11465	30	13410	13240	-	-	Waters et al., 2014	Ultrafiltered Collagen
UCIAMS-127351	B	Wally's Beach, AB	49.3386	-113.1445	C14	Bone (Equua conversidens)	11440	30	13380	13190	-	-	Waters et al., 2014	Ultrafiltered Collagen
UCIAMS-127353	B	Wally's Beach, AB	49.3386	-113.1445	C14	Bone (Equua conversidens)	11440	30	13380	13190	-	-	Waters et al., 2014	Ultrafiltered Collagen
TO-8972	B	Wally's Beach, AB	49.3167	-113.1500	C14	Bone (Rangifer tarandus)	11350	80	13360	13060	-	-	Morlan database (unpublished); cited in Dyke et al., 2003	
UCIAMS-127354	B	Wally's Beach, AB	49.3386	-113.1445	C14	Bone (Equua conversidens)	11430	30	13360	13170	-	-	Waters et al., 2014	Ultrafiltered Collagen
TO-7696	B	Wally's Beach, AB	49.3167	-113.1500	C14	Bone (Equus conversidens)	11330	80	13340	13050	-	-	Hall, 1999; cited in Dyke et al., 2003	
UCIAMS-127347	B	Wally's Beach, AB	49.3386	-113.1445	C14	Bone (Equua conversidens)	11425	30	13340	13160	-	-	Waters et al., 2014	Ultrafiltered Collagen
UCIAMS-127349	B	Wally's Beach, AB	49.3386	-113.1445	C14	Bone (Equua conversidens)	11410	30	13320	13150	-	-	Waters et al., 2014	Ultrafiltered Collagen
UCIAMS-127373	B	Wally's Beach, AB	49.3386	-113.1445	C14	Bone (Bootherium bombifrons)	11320	30	13260	13080	-	-	Waters et al., 2014	
OxA-14273	C	Vauxhall, AB	50.0830	-112.0000	C14	Bone (Eques cf. E. conversidens)	11620	150	13760	13150	-	-	Burns, 2010	Ultrafiltered Collagen
BSG-2143	C	Vauxhall, AB	50.0830	-112.0000	C14	Bone (camelops cf. hestermus)	10708	100	12770	12420	-	-	Burns, 2010	
RL-757	D	Calgary Region, AB	51.1700	-114.4200	C14	Bone (Bison)	11300	290	13750	12690	-	-	Wilson & Churcher, 1978; cited in Dyke et al., 2003	
GSC-613	D	Calgary Region, AB	50.9625	-114.0170	C14	Bone (unspecified)	11370	170	13560	12860	-	-	Wilson and Churcher, 1978; Wilson et al., 2008	
TO-7694	D	Calgary Region, AB	50.9625	-114.0170	C14	Bone (Bison)	11290	80	13310	13020	-	-	Wilson et al., 2008	
GSC-989	D	Calgary Region, AB	50.9625	-114.0170	C14	Bone (unspecified)	11100	160	13260	12710	-	-	Stalker, 1968; cited in Dyke et al., 2003	
GSC-612	D	Calgary Region, AB	51.1806	-114.4630	C14	Bone (Unspecified)	10760	160	13060	12190	-	-	Burns, 1996; cited in Dyke et al., 2003	
BSG-2141	D	Calgary Region, AB	51.0870	-114.1710	C14	Bone (Mammuthus sp.)	10743	100	12830	12420	-	-	Burns, 2010	
GSC-3065	D	Calgary Region, AB	50.9625	-114.0170	C14	Bone (Bison)	10200	280	12690	11180	-	-	Blake 1986; Wilson 1983; cited in Dyke et al., 2003	
TO-7695	D	Calgary Region, AB	50.9625	-114.0170	C14	Bone (Bison)	10090	70	11990	11340	-	-	Wilson et al., 2008	
OxA-11622	D	Calgary Region, AB	51.1230	-114.2470	C14	Bone (Bison)	7475	45	8380	8190	-	-	Shapiro et al., 2004	
OxA-11583	D	Calgary Region, AB	51.1230	-114.2470	C14	Bone (Bison)	7310	45	8200	8010	-	-	Shapiro et al., 2004	
OxA-11585	D	Calgary Region, AB	51.1230	-114.2470	C14	Bone (Bison)	6775	40	7680	7570	-	-	Shapiro et al., 2004	
SFU-0-264	E	Edson, AB	53.4919	-116.6250	OSL/IRSL	Sand	-	-	-	-	14,000	800	Wolfe et al., 2004	
SFU-0-274	F	Lodgepole, AB	53.1150	-115.2442	OSL/IRSL	Sand	-	-	-	-	14,100	1,800	Wolfe et al., 2004	
OxA-11274	G	Chetwynd, AB	55.6830	-121.6300	C14	Bone (Bison)	11240	70	13280	12980	-	-	Shapiro et al., 2004	Ultrafiltered Collagen

Lab ID		Location	Latitude	Longitude	Method	Material	Age	±	Cal max	Cal min	OSL	±	Reference	Notes
AA43652	H	Bear Flat, AB	56.2740	-121.2290	C14	Bone (Taiga vole)	12567	49	15150	14560	-	-	Hebda et al., 2008	Froese et al (2018) regarded as anomolous
AA46353	H	Bear Flat, AB	56.2740	-121.2290	C14	Bone (Taiga vole)	11507	52	13470	13250	-	-	Hebda et al., 2008	
OxA-31358	I	Charlie Lake, BC	56.3370	-120.9950	C14	Plant (unidentified)	10635	50	12720	12440	-	-	Pederson et al., 2016	
OxA-12085	I	Charlie Lake, BC	56.2728	-120.9442	C14	Bone (Bison)	10505	45	12640	12190	-	-	Shapiro et al., 2004	
UCIAMS 142221	I	Charlie Lake, BC	56.2728	-120.9442	C14	Bone (Bison)	10440	40	12530	12120	-	-	Heintzman et al., 2016	Ultrafiltered Collagen
UCIAMS-11346	I	Charlie Lake, BC	56.2728	-120.9442	C14	Bone (Bison)	10435	25	12530	12110	-	-	Heintzman et al., 2016	Ultrafiltered Collagen
UCIAMS-11347	I	Charlie Lake, BC	56.2728	-120.9442	C14	Bone (Bison)	10430	30	12530	12110	-	-	Heintzman et al., 2016	Ultrafiltered Collagen
OxA-12084	I	Charlie Lake, BC	56.2728	-120.9442	C14	Bone (Bison)	10340	40	12390	12000	-	-	Shapiro et al., 2004	
UCIAMS 142219	I	Charlie Lake, BC	56.2728	-120.9442	C14	Bone (Bison)	10285	40	12380	11830	-	-	Heintzman et al., 2016	Ultrafiltered Collagen
UCIAMS 142220	I	Charlie Lake, BC	56.2728	-120.9442	C14	Bone (Bison)	10290	40	12380	11830	-	-	Heintzman et al., 2016	Ultrafiltered Collagen
UCIAMS 142222	I	Charlie Lake, BC	56.2728	-120.9442	C14	Bone (Bison)	10260	40	12160	11810	-	-	Heintzman et al., 2016	Ultrafiltered Collagen
OxA-10580	I	Charlie Lake, BC	56.2728	-120.9442	C14	Bone (Bison)	10230	55	12160	11710	-	-	Shapiro et al., 2004	
UCIAMS 142218	I	Charlie Lake, BC	56.2728	-120.9442	C14	Bone (Bison)	10170	40	12050	11640	-	-	Heintzman et al., 2016	Ultrafiltered Collagen
UCIAMS 142217	I	Charlie Lake, BC	56.2728	-120.9442	C14	Bone (Bison)	10060	35	11770	11360	-	-	Heintzman et al., 2016	Ultrafiltered Collagen
UCIAMS 142223	I	Charlie Lake, BC	56.2728	-120.9442	C14	Bone (Bison)	9980	40	11620	11260	-	-	Heintzman et al., 2016	Ultrafiltered Collagen
OxA-32206	I	Charlie Lake, BC	56.3370	-120.9950	C14	Plant (unidentified)	9230	40	10520	10260	-	-	Pederson et al., 2016	
OxA-31360	I	Charlie Lake, BC	56.3370	-120.9950	C14	Plant Seed (Cyperus sp. + Carex sp.)	7900	45	8980	8590	-	-	Pederson et al., 2016	regarded anomolous by author
OxA-31361	I	Charlie Lake, BC	56.3370	-120.9950	C14	Plant Seed (Caryx cf.)	7255	40	8170	7980	-	-	Pederson et al., 2016	
UCIAMS 117382	J	Smoky River, AB	54.7130	-118.5090	C14	Bone (Bison)	10410	30	12430	12090	-	-	Heintzman et al., 2016	Ultrafiltered Collagen
SFU-O-277	K	Grande Praire, AB	55.1098	-118.7348	OSL/IRSL	Sand	-	-	-	-	14,900	1,000	Wolfe et al., 2004	
SFU-O-278	K	Grande Praire, AB	55.1098	-118.7348	OSL/IRSL	Sand	-	-	-	-	14,200	900	Wolfe et al., 2004	
SFU-O-265	K	Grande Praire, AB	55.1098	-118.7348	OSL/IRSL	Sand	-	-	-	-	13,700	1,000	Wolfe et al., 2004	
SFU-O-266	K	Grande Praire, AB	55.0878	-118.8097	OSL/IRSL	Sand	-	-	-	-	13,500	1,000	Wolfe et al., 2004	
SFU-O-276	K	Grande Praire, AB	55.1098	-118.7348	OSL/IRSL	Sand	-	-	-	-	11,800	800	Wolfe et al., 2004	
GP02-OSL1	K	Grande Praire, AB	55.1098	-118.7348	OSL/IRSL	Sand	-	-	-	-	11,500	1,000	Munyikwa et al., 2017	
GP01-OSL2	K	Grande Praire, AB	55.1098	-118.7348	OSL/IRSL	Sand	-	-	-	-	10,500	800	Munyikwa et al., 2017	
SFU-O-279	L	Watino, AB	55.7233	-117.5367	OSL/IRSL	Sand	-	-	-	-	12,900	800	Wolfe et al., 2004	
WAT-408	M	Spring/ Boone Lake, AB	55.5750	-119.4250	C14	Gyttja	12650	320	16000	13940	-	-	White et al., 1979; cited in Dyke e I regard as anomolous BULK
SFU-223	M	Spring/ Boone Lake, AB	55.5750	-119.4250	C14	Wood (Populus)	11700	260	14230	13030	-	-	White et al., 1979; 1985; cited in DF regards as anomlous in papaer
SFU-210	M	Spring/ Boone Lake, AB	55.5100	-119.5830	C14	Gyttja	10800	180	13100	12180	-	-	White et al., 1979; cited in Dyke e I regard as anomloous BULK
OxA-31586	M	Spring/ Boone Lake, AB	55.5166	-119.5833	C14	Plant (unidentified)	10175	45	12060	11640	-	-	Pederson et al., 2016	
OxA-31354	M	Spring/ Boone Lake, AB	55.5166	-119.5833	C14	Plant (unidentified)	10105	50	11980	11400	-	-	Pederson et al., 2016	
OxA-31590	M	Spring/ Boone Lake, AB	55.5166	-119.5833	C14	Plant (unidentified)	10105	45	11980	11400	-	-	Pederson et al., 2016	
OxA-31355	M	Spring/ Boone Lake, AB	55.5166	-119.5833	C14	Plant (Sphagnaceae, cf. Sphagnum)	10080	55	11970	11350	-	-	Pederson et al., 2016	
OxA-31588	M	Spring/ Boone Lake, AB	55.5166	-119.5833	C14	Plant (unidentified)	10040	45	11770	11320	-	-	Pederson et al., 2016	
OxA-31589	M	Spring/ Boone Lake, AB	55.5166	-119.5833	C14	Plant (unidentified)	10045	45	11770	11320	-	-	Pederson et al., 2016	
OxA-31587	M	Spring/ Boone Lake, AB	55.5166	-119.5833	C14	Plant (unidentified)	10010	45	11720	11280	-	-	Pederson et al., 2016	
OxA-31898	M	Spring/ Boone Lake, AB	55.5166	-119.5833	C14	Plant (Grass)	7248	35	8170	7980	-	-	Pederson et al., 2016	
S-1964	N	Edmonton Region, AB	53.5833	-113.3250	C14	Bone (Mammuthus)	22750	1650	31300	23830	-	-	Burns, 1996; cited in Dyke et al., : Below till
AECV-538C	N	Edmonton Region, AB	53.5833	-113.3250	C14	Bone (Mammuthus)	22820	520	27940	26020	-	-	Burns, 1996; cited in Dyke et al., : Below till
AECV-1664C	N	Edmonton Region, AB	53.5833	-113.3250	C14	Bone (Equus sp.)	21330	340	26350	24790	-	-	Burns, 1996; cited in Dyke et al., : Below till
S-2385	N	Edmonton Region, AB	53.5000	-113.5000	C14	Bone (unidentified)	11345	420	14480	12240	-	-	Rains & Welch, 1988; cited in Dyke et al., 2003
AECV-1203C	N	Edmonton Region, AB	53.5000	-113.7500	C14	Bone (Bison)	11620	170	13780	13100	-	-	Burns, 1996; cited in Dyke et al., 2003
OxA-12900	N	Edmonton Region, AB	53.6417	-113.2830	C14	Bone (Panthra leo atrox)	11355	55	13300	13080	-	-	Barnett et al., 2009; Burns 2010 Ultrafiltered Collagen
UCIAMS 117399	N	Edmonton Region, AB	53.5960	-113.3500	C14	Bone (Bison)	11255	45	13220	13040	-	-	Heintzman et al., 2016	Ultrafiltered Collagen
UCIAMS 125537	N	Edmonton Region, AB	53.5960	-113.3500	C14	Bone (Bison)	11140	25	13100	12960	-	-	Heintzman et al., 2016	Ultrafiltered Collagen
UCIAMS 125527	N	Edmonton Region, AB	53.5960	-113.3500	C14	Bone (Bison)	11110	25	13090	12880	-	-	Heintzman et al., 2016	Ultrafiltered Collagen

Lab ID		Location	Lat	Long	Method	Material								Reference	Notes
UCIAMS 125531	N	Edmonton Region, AB	53.5960	-113.3500	C14	Bone (Bison)	11115	25	13090	12890	-	-		Heintzman et al., 2016	Ultrafiltered Collagen
UCIAMS 125526	N	Edmonton Region, AB	53.5960	-113.3500	C14	Bone (Bison)	11100	25	13080	12840	-	-		Heintzman et al., 2016	Ultrafiltered Collagen
UCIAMS 125532	N	Edmonton Region, AB	53.5960	-113.3500	C14	Bone (Bison)	11100	30	13080	12840	-	-		Heintzman et al., 2016	Ultrafiltered Collagen
UCIAMS 125533	N	Edmonton Region, AB	53.5960	-113.3500	C14	Bone (Bison)	11105	25	13080	12840	-	-		Heintzman et al., 2016	Ultrafiltered Collagen
UCIAMS 125541	N	Edmonton Region, AB	53.5960	-113.3500	C14	Bone (Bison)	11085	35	13070	12820	-	-		Heintzman et al., 2016	Ultrafiltered Collagen
UCIAMS 117388	N	Edmonton Region, AB	53.5960	-113.3500	C14	Bone (Bison)	11075	30	13060	12820	-	-		Heintzman et al., 2016	Ultrafiltered Collagen
UCIAMS 117391	N	Edmonton Region, AB	53.5960	-113.3500	C14	Bone (Bison)	11080	35	13060	12810	-	-		Heintzman et al., 2016	Ultrafiltered Collagen
UCIAMS 117392	N	Edmonton Region, AB	53.5960	-113.3500	C14	Bone (Bison)	11080	35	13060	12810	-	-		Heintzman et al., 2016	Ultrafiltered Collagen
UCIAMS 125528	N	Edmonton Region, AB	53.5960	-113.3500	C14	Bone (Bison)	11080	25	13060	12820	-	-		Heintzman et al., 2016	Ultrafiltered Collagen
UCIAMS 117390	N	Edmonton Region, AB	53.5960	-113.3500	C14	Bone (Bison)	11040	30	13020	12790	-	-		Heintzman et al., 2016	Ultrafiltered Collagen
UCIAMS 125544	N	Edmonton Region, AB	53.5960	-113.3500	C14	Bone (Bison)	11050	25	13020	12800	-	-		Heintzman et al., 2016	Ultrafiltered Collagen
UCIAMS 125529	N	Edmonton Region, AB	53.5960	-113.3500	C14	Bone (Bison)	11030	25	13010	12790	-	-		Heintzman et al., 2016	Ultrafiltered Collagen
UCIAMS 125540	N	Edmonton Region, AB	53.5960	-113.3500	C14	Bone (Bison)	11010	25	13000	12740	-	-		Heintzman et al., 2016	Ultrafiltered Collagen
UCIAMS 117384	N	Edmonton Region, AB	53.6310	-113.3050	C14	Bone (Bison)	10530	30	12580	12410	-	-		Heintzman et al., 2016	Ultrafiltered Collagen
UCIAMS 117400	N	Edmonton Region, AB	53.6310	-113.3050	C14	Bone (Bison)	10060	30	11760	11400	-	-		Heintzman et al., 2016	Ultrafiltered Collagen
HC1-OSL1	O	F. Assin./ H. Cross/ Windfall	54.2913	-114.8708	OSL/IRSL	Sand	-	-	-	-	18,300	1,200		Munyikwa et al., 2011	regarded anomolous by author
SFU-0-275	O	F. Assin./ H. Cross/ Windfall	54.1992	-114.8708	OSL/IRSL	Sand	-	-	-	-	15,700	1,600		Wolfe et al., 2004	
HC2-OSL1	O	F. Assin./ H. Cross/ Windfall	54.2913	-114.8708	OSL/IRSL	Sand	-	-	-	-	15,300	1,300		Munyikwa et al., 2011	
FA3-OSL1	O	F. Assin./ H. Cross/ Windfall	54.3695	-114.6393	OSL/IRSL	Sand	-	-	-	-	15,000	1,300		Munyikwa et al., 2011	
SFU-0-262	O	F. Assin./ H. Cross/ Windfall	54.2913	-114.8708	OSL/IRSL	Sand	-	-	-	-	14,900	1,000		Wolfe et al., 2004	
FA2-OSL1	O	F. Assin./ H. Cross/ Windfall	54.3695	-114.6393	OSL/IRSL	Sand	-	-	-	-	14,600	1,700		Munyikwa et al., 2011	
SFU-0-263	O	F. Assin./ H. Cross/ Windfall	54.3695	-114.6393	OSL/IRSL	Sand	-	-	-	-	14,500	1,000		Wolfe et al., 2004	
HC1-OSL3	O	F. Assin./ H. Cross/ Windfall	54.2913	-114.8708	OSL/IRSL	Sand	-	-	-	-	13,500	1,000		Munyikwa et al., 2011	
FA3-OSL4	O	F. Assin./ H. Cross/ Windfall	54.3695	-114.6393	OSL/IRSL	Sand	-	-	-	-	13,100	900		Munyikwa et al., 2011	
SFU-0-261	P	Nelson Lake, AB	54.4853	-112.2853	OSL/IRSL	Sand	-	-	-	-	14,500	900		Wolfe et al., 2004	
SM5-OSL3	Q	Chisholm/ Decrene/ Hondo, Al	55.1060	-114.0015	OSL/IRSL	Sand	-	-	-	-	20,300	1,800		Munyikwa et al., 2013	regarded anomolous by author
SM5-OSL1	Q	Chisholm/ Decrene/ Hondo, Al	55.1060	-114.0015	OSL/IRSL	Sand	-	-	-	-	18,200	1,200		Munyikwa et al., 2013	regarded anomolous by author
SM3-OSL1	Q	Chisholm/ Decrene/ Hondo, Al	55.1060	-114.0015	OSL/IRSL	Sand	-	-	-	-	15,400	1,100		Munyikwa et al., 2013	
SFU-0-260	Q	Chisholm/ Decrene/ Hondo, Al	54.8472	-114.2853	OSL/IRSL	Sand	-	-	-	-	15,300	800		Wolfe et al., 2004	
SM3-OSL3	Q	Chisholm/ Decrene/ Hondo, Al	55.1060	-114.0015	OSL/IRSL	Sand	-	-	-	-	14,900	1,100		Munyikwa et al., 2013	
DEC01-OSL4	Q	Chisholm/ Decrene/ Hondo, Al	55.1135	-114.1567	OSL/IRSL	Sand	-	-	-	-	14,800	1,600		Munyikwa et al., 2017	
SFU-0-259	Q	Chisholm/ Decrene/ Hondo, Al	55.1135	-114.1567	OSL/IRSL	Sand	-	-	-	-	14,800	900		Wolfe et al., 2004	
SM07-OSL8	Q	Chisholm/ Decrene/ Hondo, Al	55.1060	-114.0015	OSL/IRSL	Sand	-	-	-	-	14,300	1,000		Munyikwa et al., 2017	
SFU-0-258	Q	Chisholm/ Decrene/ Hondo, Al	55.1060	-114.0015	OSL/IRSL	Sand	-	-	-	-	14,200	700		Wolfe et al., 2004	
SM08-OSL3	Q	Chisholm/ Decrene/ Hondo, Al	55.1060	-114.0015	OSL/IRSL	Sand	-	-	-	-	13,800	1,000		Munyikwa et al., 2017	
SM5-OSL5	Q	Chisholm/ Decrene/ Hondo, Al	55.1060	-114.0015	OSL/IRSL	Sand	-	-	-	-	13,300	1,200		Munyikwa et al., 2013	
SM4-OSL1	Q	Chisholm/ Decrene/ Hondo, Al	55.1060	-114.0015	OSL/IRSL	Sand	-	-	-	-	13,200	1,100		Munyikwa et al., 2013	
SM14-OSL2	Q	Chisholm/ Decrene/ Hondo, Al	55.1060	-114.0015	OSL/IRSL	Sand	-	-	-	-	13,100	1,500		Munyikwa et al., 2017	
DEC02-OSL3	Q	Chisholm/ Decrene/ Hondo, Al	55.1135	-114.1567	OSL/IRSL	Sand	-	-	-	-	13,000	1,400		Munyikwa et al., 2017	
SM07-OSL4	Q	Chisholm/ Decrene/ Hondo, Al	55.1060	-114.0015	OSL/IRSL	Sand	-	-	-	-	12,900	1,300		Munyikwa et al., 2017	
SM08-OSL9	Q	Chisholm/ Decrene/ Hondo, Al	55.1060	-114.0015	OSL/IRSL	Sand	-	-	-	-	12,900	1,400		Munyikwa et al., 2017	
DEC03-OSL2	Q	Chisholm/ Decrene/ Hondo, Al	55.1135	-114.1567	OSL/IRSL	Sand	-	-	-	-	12,200	1,500		Munyikwa et al., 2017	
CH01-OSL2	Q	Chisholm/ Decrene/ Hondo, Al	54.8472	-114.2853	OSL/IRSL	Sand	-	-	-	-	12,100	1,000		Munyikwa et al., 2017	
LLB1-OSL2	R	Lac La Biche, AB	54.9905	-112.1533	OSL/IRSL	Sand	-	-	-	-	14,700	1,600		Munyikwa et al., 2013	
SFU-0-257	R	Lac La Biche, AB	54.9905	-112.1533	OSL/IRSL	Sand	-	-	-	-	12,600	600		Wolfe et al., 2004	
ETH-29215	S	Stony Mountain Region, AB	56.2079	-111.4276	C14	Wood	42540	780	47690	44520	-	-		Fisher et al., 2009	regarded anomolous by author
ETH-29216	S	Stony Mountain Region, AB	56.2079	-111.4276	C14	Wood	34980	390	40430	38660	-	-		Fisher et al., 2009	regarded anomolous by author
GSC-2038	S	Stony Mountain Region, AB	55.9500	-112.0170	C14	Gyttja	11300	110	13420	12940	-	-		Mott, 1974; cited in Dyke et al., 2	Minimum for glacial lake BULK
ETH-32167	S	Stony Mountain Region, AB	56.3178	-111.9293	C14	Peaty fragments	37820	520	42860	41400	-	-		Fisher et al., 2009	regarded anomolous by author

Lab ID		Location	Lat	Long	Method	Material	C14 age	±	Cal max	Cal min			Reference
ETH-32165	S	Stony Mountain Region, AB	55.9491	-112.0258	C14	Wood	10310	75	12420	11810	-	-	Fisher et al., 2009
ETH-30185	S	Stony Mountain Region, AB	56.1272	-111.3557	C14	Wood	9985	110	11960	11210	-	-	Fisher et al., 2009
Beta-200072	S	Stony Mountain Region, AB	56.1272	-111.3557	C14	Wood	10040	50	11800	11310	-	-	Fisher et al., 2009
Beta-200071	S	Stony Mountain Region, AB	56.1272	-111.3557	C14	Wood	10030	50	11770	11300	-	-	Fisher et al., 2009
ETH-30173	S	Stony Mountain Region, AB	56.1272	-111.3557	C14	Plant	9940	70	11710	11220	-	-	Fisher et al., 2009
ETH-30172	S	Stony Mountain Region, AB	56.1272	-111.3557	C14	Wood	9835	75	11610	11100	-	-	Fisher et al., 2009
ETH-28525	S	Stony Mountain Region, AB	56.1272	-111.3557	C14	Wood	9795	75	11410	10810	-	-	Fisher et al., 2009
ETH-28526	S	Stony Mountain Region, AB	56.1272	-111.3557	C14	Wood	9730	65	11260	10790	-	-	Fisher et al., 2009
ETH-29206	S	Stony Mountain Region, AB	56.1272	-111.3557	C14	Wood	9710	70	11250	10780	-	-	Fisher et al., 2009
ETH-29207	S	Stony Mountain Region, AB	56.1272	-111.3557	C14	Wood	9705	75	11250	10780	-	-	Fisher et al., 2009
ETH-28524	S	Stony Mountain Region, AB	56.2079	-111.4276	C14	Charcoal	9635	75	11200	10750	-	-	Fisher et al., 2009
ETH-30596	S	Stony Mountain Region, AB	56.2368	-111.4339	C14	Wood	9625	60	11190	10760	-	-	Fisher et al., 2009
ETH-30183	S	Stony Mountain Region, AB	56.2079	-111.4276	C14	Plant	8705	70	10110	9530	-	-	Fisher et al., 2009
GSC-4821	T	Gipsy Lake Region, AB	56.4078	-110.5500	C14	Gyttja	10600	120	12730	12140	-	-	Anderson and Lewis, 1992; cited in Dyke et al., 2003
Beta-194058	T	Gipsy Lake Region, AB	56.2953	-111.0422	C14	Wood	10270	50	12380	11810	-	-	Fisher et al., 2009
Beta-194059	T	Gipsy Lake Region, AB	56.2953	-111.0422	C14	Wood	10080	40	11940	11390	-	-	Fisher et al., 2009
ETH-30177	T	Gipsy Lake Region, AB	56.3255	-110.8572	C14	Wood	10030	75	11940	11250	-	-	Fisher et al., 2009
ETH-29219	T	Gipsy Lake Region, AB	56.3255	-110.8572	C14	Wood	10020	75	11920	11240	-	-	Fisher et al., 2009
UCIAMS 34698	T	Gipsy Lake Region, AB	56.4078	-110.5500	C14	Wood fragments	10000	35	11700	11280	-	-	Teller, 2007 (unpublished)
ETH-30187	T	Gipsy Lake Region, AB	56.2953	-111.0422	C14	Wood	9910	75	11700	11190	-	-	Fisher et al., 2009
ETH-28535	T	Gipsy Lake Region, AB	56.2953	-111.0422	C14	Wood	9820	70	11600	11090	-	-	Fisher et al., 2009
ETH-28536	T	Gipsy Lake Region, AB	56.2953	-111.0422	C14	Wood	9795	70	11400	10880	-	-	Fisher et al., 2009
ETH-30176	T	Gipsy Lake Region, AB	56.3255	-110.8572	C14	Wood	9375	70	11050	10300	-	-	Fisher et al., 2009
ETH-29221	T	Gipsy Lake Region, AB	56.3829	-110.2860	C14	Wood	8895	70	10210	9740	-	-	Fisher et al., 2009
ETH-28534	T	Gipsy Lake Region, AB	56.3829	-110.2860	C14	Wood	7760	65	8700	8400	-	-	Fisher et al., 2009
FMc01-OSL1	U	Fort McMurray, AB	56.6528	-111.7952	OSL/IRSL	Sand	-	-	-	-	14,000	1,000	Munyikwa et al., 2017
ETH-30586	V	Lower Athabasca Region, AB	57.2662	-112.5971	C14	Wood	10460	65	12570	12090	-	-	Fisher et al., 2009
GX-5301-II	V	Lower Athabasca Region, AB	57.1000	-111.7500	C14	Wood	10310	29	12380	11960	-	-	Smith and Fisher, 1993; cited in Dyke et al., 2003
ETH-30585	V	Lower Athabasca Region, AB	57.2662	-112.5971	C14	Wood	10210	65	12170	11610	-	-	Fisher et al., 2009
GX-5036-I	V	Lower Athabasca Region, AB	57.1000	-111.7500	C14	Wood	10015	32	11710	11320	-	-	Smith and Fisher, 1993; cited in Dyke et al., 2003
ETH-30590	V	Lower Athabasca Region, AB	57.2611	-112.2832	C14	Charcoal	9850	65	11600	11160	-	-	Fisher et al., 2009
GX-5031-I	V	Lower Athabasca Region, AB	57.1000	-111.7500	C14	Wood	9860	23	11310	11210	-	-	Smith and Fisher, 1993; cited in Dyke et al., 2003
ETH-30591	V	Lower Athabasca Region, AB	57.2611	-112.2832	C14	Wood	9730	65	11260	10790	-	-	Fisher et al., 2009
AECV-439C	W	Bushe River, AB	58.3000	-117.0000	C14	Bone (Bison)	10080	150	12380	11210	-	-	Beaudoin, 1988;; cited in Dyke et al., 2003
Beta-194061	X	Canadian Shield, SK	57.1590	-108.7518	C14	Wood	19250	80	23480	22930	-	-	Fisher et al., 2009
ETH-30175	X	Canadian Shield, SK	56.9275	-107.9701	C14	Wood	9665	75	11220	10770	-	-	Fisher et al., 2009
Beta-194055	X	Canadian Shield, SK	56.9275	-107.9701	C14	Wood	9520	40	11090	10680	-	-	Fisher et al., 2009
GSC-4832	X	Canadian Shield, SK	57.2144	-109.0567	C14	Wood	9230	120	10730	10190	-	-	Anderson, in GSC Paper 91; cited in Dyke et al., 2003
ETH-29211	X	Canadian Shield, SK	56.9275	-107.9701	C14	Wood	9000	70	10270	9900	-	-	Fisher et al., 2009
ETH-28529	X	Canadian Shield, SK	56.9275	-107.9701	C14	Wood	8975	60	10240	9910	-	-	Fisher et al., 2009
Beta-194057	X	Canadian Shield, SK	56.9275	-107.9701	C14	Wood	8850	40	10160	9740	-	-	Fisher et al., 2009
ETH-28530	X	Canadian Shield, SK	56.9275	-107.9701	C14	Wood	8660	70	9890	9520	-	-	Fisher et al., 2009
ETH-29220	X	Canadian Shield, SK	56.8227	-107.9386	C14	Wood	8345	70	9500	9130	-	-	Fisher et al., 2009
ETH-29222	X	Canadian Shield, SK	56.8227	-107.9386	C14	Wood	7800	65	8860	8410	-	-	Fisher et al., 2009
ETH-29223	X	Canadian Shield, SK	56.8227	-107.9386	C14	Wood	7730	65	8630	8400	-	-	Fisher et al., 2009

Sample	Group	Location	Lat	Lon	Method	Material					Age	Error	Reference	Notes
Quarry 1-60	Y	Clearwater Lower Athabasca	57.1957	-111.5345	OSL/IRSL	Fluvial sand	-	-	-	-	14.5	1.1	Woywitka et al., 2019	regarded anomolous by author
Quarry 1-98	Y	Clearwater Lower Athabasca	57.1957	-111.5345	OSL/IRSL	Fluvial sand	-	-	-	-	12.8	1.2	Woywitka et al., 2019	regarded anomolous by author
NWFH 3-125	Y	Clearwater Lower Athabasca	57.2858	-111.5232	OSL/IRSL	Eolian sand	-	-	-	-	12.3	1.4	Woywitka et al., 2019	
NWFH 3-55	Y	Clearwater Lower Athabasca	57.2858	-111.5232	OSL/IRSL	Eolian sand	-	-	-	-	12.2	1.3	Woywitka et al., 2019	
Quarry 1-25	Y	Clearwater Lower Athabasca	57.1957	-111.5345	OSL/IRSL	Eolian sand	-	-	-	-	12.2	1.1	Woywitka et al., 2019	
Shell 1-70	Y	Clearwater Lower Athabasca	57.2858	-111.5232	OSL/IRSL	Eolian sand	-	-	-	-	12	1	Woywitka et al., 2019	
UTS-1	Y	Clearwater Lower Athabasca	57.7842	-111.5586	OSL/IRSL	Eolian sand	-	-	-	-	11.1	1.3	Woywitka et al., 2019	
FHNW 1-100	Y	Clearwater Lower Athabasca	57.4923	-111.5325	OSL/IRSL	Eolian sand	-	-	-	-	10.1	1	Woywitka et al., 2019	
SAW05-01	Z	H. Level/ La Crete, AB	58.5183	-117.1255	OSL/IRSL	Sand	-	-	-	-	13,400	1,200	Wolfe et al., 2007	
HL01-OSL3	Z	H. Level/ La Crete, AB	58.5183	-117.1255	OSL/IRSL	Sand	-	-	-	-	11,900	900	Munyikwa et al., 2017	
SAW05-02	Z	H. Level/ La Crete, AB	58.5183	-117.1255	OSL/IRSL	Sand	-	-	-	-	11,700	1,000	Wolfe et al., 2007	
LC01-OSL-1	Z	H. Level/ La Crete, AB	58.1692	-116.5868	OSL/IRSL	Sand	-	-	-	-	11700	900	Munyikwa et al., 2017	
SAW05-04	Z	H. Level/ La Crete, AB	58.5183	-117.1255	OSL/IRSL	Sand	-	-	-	-	11,000	1,000	Wolfe et al., 2007	
SAW05-03	Z	H. Level/ La Crete, AB	58.5183	-117.1255	OSL/IRSL	Sand	-	-	-	-	10,300	1,000	Wolfe et al., 2007	
GSC-4302	AA	Athabasca Delta, AB	58.2500	-111.4167	C14	Wood	9910	190	12080	10760	-	-	Rhine and Smith, 1988; cited in Dyke et al., 2003	
GSC-3402	AA	Athabasca Delta, AB	58.2500	-111.4170	C14	Wood	9910	90	11750	11180	-	-	Smith and Fisher, 1993; cited in Dyke et al., 2003	
AECV-1183C	AA	Athabasca Delta, AB	58.2500	-111.4167	C14	Wood	9710	130	11600	10650	-	-	Smith and Fisher, 1993; cited in Dyke et al., 2003	

References

Anderson, T.W., and Lewis, C.F.M., 1992, Evidence for ice margin retreat and proglacial lake (Agassiz?) drainage by about 11 ka, Clearwater River spillway area, Saskatch- ewan, in Current research, Part B: Geological Survey of Canada Paper 92-1B, p. 7-11.

Barnett, Ross, Beth Shapiro, I. A. N. Barnes, Simon YW Ho, Joachim Burger, Nobuyuki Yamaguchi, Thomas FG Higham et al. 2009 Phylogeography of lions (Panthera leo ssp.) reveals three distinct taxa and a late Pleistocene reduction in genetic diversity. Molecular ecology 18(8):1668-1677.

Blake, W., Jr (1986). Geological Survey of Canada Radiocarbon Dates XXV. Geological Survey of Canada, Paper 85-7, 32 pp.

Burns, James A. 1996 Vertebrate paleontology and the alleged ice-free corridor: the meat of the matter.Quaternary International 32: 107-112

Burns, James A. 2010 Mammalian faunal dynamics in late Pleistocene Alberta, Canada. Quaternary International217(1): 37-42

Dyke, A.S., Moore, A., Robertson, L., 2003. Deglaciation ofNorth America. Geological Survey of Canada, Ottawa

Fisher, T.G., Waterson, N., Lowell, T. V., Hajdas, I., 2009. Deglaciation ages and meltwater routing in the Fort McMurray region, northeastern Alberta and northwestern Saskatchewan, Canada. Quat. Sci. Rev. 28, 1608–1624. https://doi.org/10.1016/j.quascirev.2009.02.003

Hall, D. 1999 Alberta Scientists Track Mammoths Across recently Exposed Landscape. Mammoth Trumpet 14(4):1-6

Hebda, Richard J., James A. Burns, Marten Geertsema, and AJ Timothy Jull. 2008 AMS-dated late 2008 Pleistocene taiga vole (Rodentia: Microtus xanthognathus) from northeast British Columbia, Canada: a cautionary lesson in chronology. Canadian Journal of Earth Sciences 45(5): 611-618.

Heintzman, P.D., Froese, D., Ives, J.W., Soares, A.E.R., Zazula, G.D., Letts, B., Andrews, T.D., et al., 2016. Bison phy- logeography constrains dispersal and viability of the Ice Free Cor- ridor in western Canada. Proceedings ofthe National Academy of Sciences USA 113, 8057–8063

Margold, Martin, John C. Gosse, Alan J. Hidy, Robin J. Woywitka, Joseph M Young, and Duane Froese. 2019. Beryllium-10 dating of the foothills Erratics Train in Alberta, Canada, indicated detachment of the Laurentide Ice Sheet from the Rocky Mountains at ~15 ka BP. Quaternary Research, in press

Mott, R.J., 1973. Palynological Studies in Central Saskatchewan: Pollen Stratigraphy from Lake Sediment Sequences. Geological Survey of Canada, Ottawa.

Munyikwa, K., Feathers, J.K., Rittenour, T.M., Shrimpton, H.K., 2011. Constraining the late Wisconsinan retreat of the Laurentide ice sheet fromwestern Canada using luminescence ages from post- glacial aeolian dunes. Quaternary Geochronology 6, 407–422

Munyikwa, K., Rittenour, T.M., Feathers, J.K., 2017. Temporal con- straints for the late Wisconsinan deglaciation of western Canada using eolian dune luminescence chronologies fromAlberta. Palae- ogeography, Palaeoclimatology, Palaeoecology 470, 147–16

Pedersen, Mikkel W., Anthony Ruter, Charles Schweger, Harvey Friebe, Richard A. Staff, Kristian K. Kjeldsen, Marie LZ Mendoza et al. 2016 Postglacial viability and colonization in North America's ice-free corridor. Nature 537(7618): 45-49.

Rhine, J.L., and Smith, D.G., 1988, Sedimentol- ogy and paraglacial eolian influence of the late Pleistocene Athabasca fan-delta, northeast Alberta, Canada, in Nemec, W., and Steel, R., eds., Fan-deltas, sedimentology and tec- tonic settings: London, Blackie, p. 158-169.

Shapiro, Beth, Alexei J. Drummond, Andrew Rambaut, Michael C. Wilson, Paul E. Matheus, Andrei V. Sher, Oliver G. Pybus et al.2004 Rise and fall of the Beringian steppe bison. Science 306(5701): 1561-1565

Smith, D.G., Fisher, T.G., 1993. Glacial Lake Agassiz: The northwest outlet and paleoflood. Geol. 21. 9–12.

Stalker, A. M. (1968) Identification of Saskatchewan Gravels and Sands. Canadian Journal of Earth Sciences. 5: 155-163.

Waters, Michael R., Thomas W. Stafford, Brian Kooyman, and L. V. Hills. 2015 Late Pleistocene horse and camel hunting at the southern margin of the ice-free corridor: Reassessing the age of Wally's Beach, Canada. Proceedings of the National Academy of Sciences 112(14): 4263-4267.

White, James M., Rolf W. Mathewes, and William H. Mathews. 1985 Late Pleistocene chronology and environment of the "Ice-Free Corridor" of northwestern Alberta. Quaternary Research 249(2): 173-186.

White, J.M., Mathewes, R.W., Mathews, W.H., 1979. Radiocarbon dates from Boone Lake and their relation to the 'ice-free corridor' in the Peace River District of Alberta, Canada. Canadian Journal ofEarth

Wilson, M.C. (1983). Once upon a river: archaeology and geology of the Bow River valley at Calgary, Alberta, Canada. Ottawa, National Museum of Man Mercury Series. Archaeological Survey of Canada Paper, 114.

Wilson, Michael, and Charles S. Churcher. 1978 Late Pleistocene Camelops from the Gallelli pit, Calgary, Alberta: morphology and geologic setting. Canadian Journal of Earth Sciences 15(5): 729-740.

Wilson, Michael C., Leonard V. Hills, and Beth Shapiro. 2008. Late Pleistocene northward-dispersing Bison antiquus from the Bighill Creek Formation, Gallelli gravel pit, Alberta, Canada, and the fate of Bison occidentalis. Canadian Journal of Earth Sciences 45(7): 827-859.

Wolfe, S., Huntley, D., Ollerhead, J., 2004. Relict late Wisconsinan dune fields ofthe northern Great Plains, Canada. Géographie phy- sique et Quaternaire 58, 323–336.

Wolfe, S.A., Paulen, R.C., Smith, I.E.R., Lamothe, M., 2007. Age and palaeoenvironmental significance of Late Wisconsinan dune fields in the Mount Watt and Fontas River map areas, northern Alberta and British Columbia. Geol. Surv. Can. Curr. Res. 2007-B4.

Woywitka et al., 20XX.

APPENDIX C: SUPPORTING INFORMATION FOR CHAPTER 4

SC1: Glacial landforms of northeast Alberta and northwest Saskatchewan.

Supplementary Data references

Balco, G., Stone, J. O., Lifton, N. A., and Dunai, T. J. 2008: A complete and easily accessible means of calculating surface exposure ages or erosion rates from 10Be and 26Al measurements. *Quaternary geochronology*, *3*(3), 174-195.

Borchers, B., Marrero, S., Balco, G., Caffee, M., Goehring, B., Lifton, N., Nishiizumi, K., Phillips, F., Schaefer, J. and Stone, J. 2016: Geological calibration of spallation production rates in the CRONUS-Earth project. *Quaternary Geochronology 31,* 188–198.

Gowan, E. J., Tregoning, P., Purcell, A., Montillet, J. P. and McClusky, S. 2016: A model of the western Laurentide Ice Sheet, using observations of glacial isostatic adjustment. *Quaternary Science Reviews*, *139*, 1-16.

Kohl, C. P., & Nishiizumi, K. 1992: Chemical isolation of quartz for measurement of in-situ-produced cosmogenic nuclides. *Geochimica et Cosmochimica Acta*, *56*(9), 3583-3587.

Lal, D. 1991: Cosmic ray labeling of erosion surfaces: in siiu nuclide production. *Earth and Planetary Science Letters*, *104*, 424-439.

Lambeck, K., Purcell, A., and Zhao, S. 2017: The North American Late Wisconsin ice sheet and mantle viscosity from glacial rebound analyses. *Quaternary Science Reviews*, *158*, 172-210.

Lifton, N., Sato, T., and Dunai, T. J. 2014: Scaling in situ cosmogenic nuclide production rates using analytical approximations to atmospheric cosmic-ray fluxes. *Earth and Planetary Science Letters*, *386*, 149-160.

Munyikwa, K., Feathers, J. K., Rittenour, T. M., and Shrimpton, H. K. 2011: Constraining the Late Wisconsinan retreat of the Laurentide ice sheet from western Canada using luminescence ages from postglacial aeolian dunes. *Quaternary Geochronology*, *6*(3-4), 407-422.

Munyikwa, K., Rittenour, T. M., and Feathers, J. K. 2017: Temporal constraints for the Late Wisconsinan deglaciation of western Canada using eolian dune luminescence chronologies from Alberta. *Palaeogeography, palaeoclimatology, palaeoecology*, *470*, 147-165.

Nishiizumi, K., Imamura, M., Caffee, M. W., Southon, J. R., Finkel, R. C., and McAninch, J. 2007: Absolute calibration of 10Be AMS standards. *Nuclear Instruments and Methods in Physics Research Section B: Beam Interactions with Materials and Atoms*, *258*(2), 403-413.

Peltier, W.R., Argus, D.F. and Drummond, R. 2015: Space geodesy constrains ice-age terminal deglaciation: the global ICE-6G_C (VM5a) model. *Journal of Geophysical Research, 120,* 450-487.

Reimer, P. J., Bard, E., Bayliss, A., Beck, J. W., Blackwell, P. G., Ramsey, C. B., and Grootes, P. M. 2013: IntCal13 and Marine13 radiocarbon age calibration curves 0–50,000 years cal BP. *Radiocarbon*, *55*(4), 1869-1887.

Stone, J. O. 2000: Air pressure and cosmogenic isotope production. *Journal of Geophysical Research: Solid Earth*, *105*(B10), 23753-23759.

Wolfe, S., Huntley, D., and Ollerhead, J. 2004: Relict late Wisconsinan dune fields of the northern Great Plains, Canada. *Géographie physique et Quaternaire*, *58*(2-3), 323-336.